1971

Gamma-ray decay schemes for 92Kr, 92Rb, and 92Sr

Richard John Olson
Iowa State University

Gamma-ray decay schemes for ^{92}Kr, ^{92}Rb, and ^{92}Sr

by

Richard John Olson

A Dissertation Submitted to the

Graduate Faculty in Partial Fulfillment of

The Requirements for the Degree of

DOCTOR OF PHILOSOPHY

Major Subject: Nuclear Physics

Approved:

Signature was redacted for privacy.

In Charge of Major Work

Signature was redacted for privacy.

For the Major Department

Signature was redacted for privacy.

For the Graduate College

Iowa State University
Ames, Iowa
1971

TABLE OF CONTENTS

I. INTRODUCTION

The underlying quest behind nuclear structure studies is the search for knowledge of the basic inter-nucleon force. The properties of the deuteron and experimental results from p-n, p-p (and n-n) scattering have yielded a great deal of information concerning the two-body character of this force up to high energies. The characteristics of the nuclear force have also been observed in many-body circumstances in the form of properties of a variety of nuclei which tend to lie near the valley of beta-stability. In these many-body situations, various physical pictures have been used to relate the measured variables to the constants and parameters of the nuclear force, itself formalized by physical models. There has not yet been discovered a formulation of the nuclear force which can be considered "tidy" in the same sense as electromagnetic interaction theory. This lack of success is traceable in part to the difficulty in expanding terms in the nuclear interaction using a nuclear structure constant which is more than two orders of magnitude larger than the electromagnetic fine structure constant (about 1/137), and in part to the lack of sufficiently interpretive models relating the nuclear properties to the nuclear force.

It cannot be determined *a priori* which areas of the nuclidic chart will present all the information necessary to develop a comprehensive nuclear theory. Past experience and the prophecies of nuclear theorists can suggest some regions which will probably be productive but there will remain those areas which will provide unexpected phenomena. It is known *a posteriori* that maximum benefit will be derived from knowledge of the

dependence of nuclear properties on atomic mass number, A, atomic number Z, and neutron number, N. For these reasons, all nuclear structure studies which are possible (physically and financially) should be made in a systematic manner. The results of the measurements for one nuclide ought then to be scrutinized for contrast to and comparison with other similar nuclei. By such means additional light may be shed upon the remaining obscurity of the nuclear force.

There are approximately 300 nuclei occurring naturally on earth (Z = 1-92). In the past 30 years, there have been about 1300 additional nuclei created by man. (There are probably at least 900 more producible by present bombardment techniques). Of these 1600 nuclei about 450 are very poorly known, primarily because of short half-lives. Figure 1 gives a version of the nuclidic chart which shows the stable nuclides, the radioactive nuclides, and the approximate limits of particle binding. Extensive information on nuclides exists in general only near the beta stability valley. Knowledge of the properties of short-lived nuclides (that is, those farther from beta stability) is required to provide a broader picture of the variation of nuclear phenomena with N and Z.

A. Fission

In order to study these short-lived nuclei some technique is necessary which will allow their production in sufficient quantity with subsequent processing rapid enough to enable spectroscopic investigation before the majority of the nuclei undergo beta decay. The first part of this problem may be solved by obtaining short-lived nuclei as the by-products of thermal

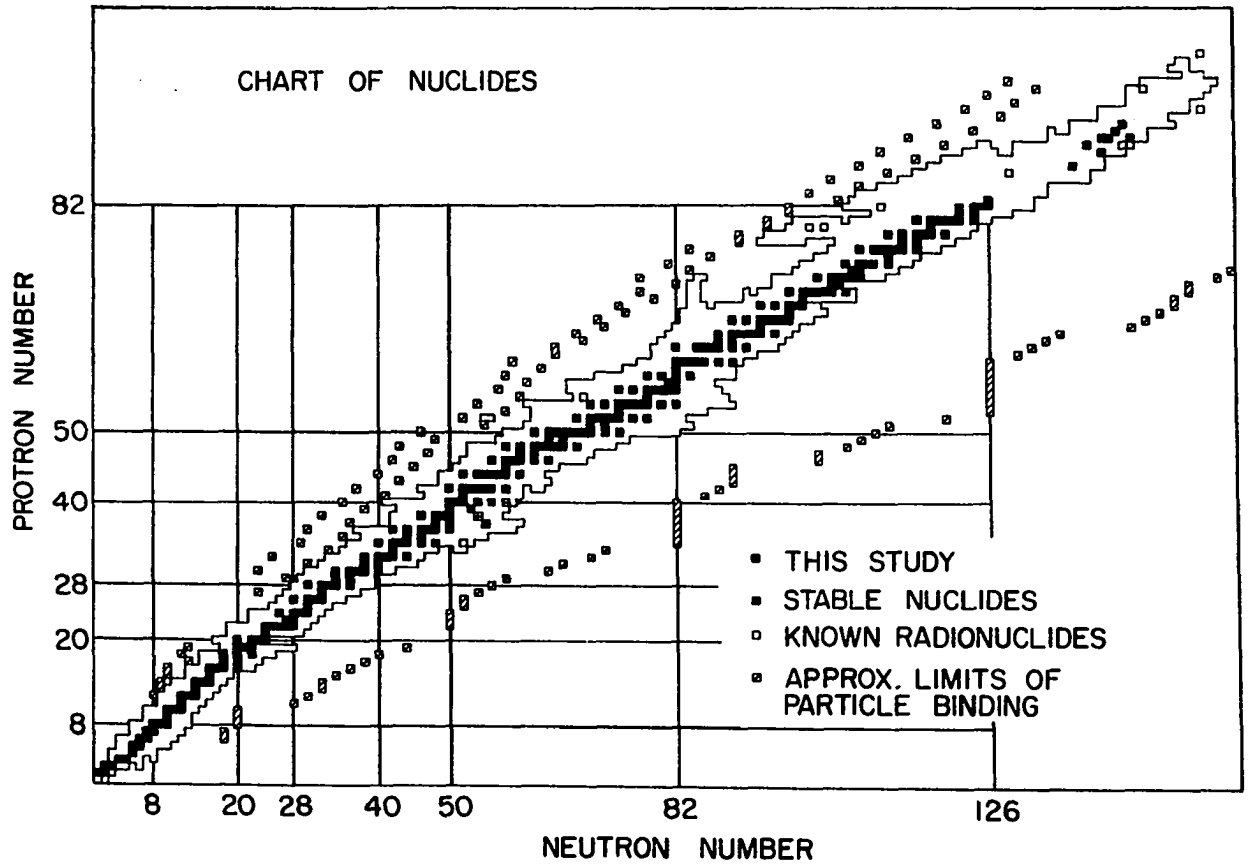

Figure 1. Chart of the nuclides showing stable nuclides and known radionuclides

induced fission of ^{235}U. These nuclei will be neutron-enriched and the study of them will extend the knowledge of nuclear properties away from the beta stability valley in Figure 1 towards the right. In fact, the fission process is the most efficient way to reach neutron-rich nuclides in the region of Z = 35 or Z = 54.

Standard gamma-ray spectroscopy will allow the establishment of level schemes for these short-lived fission product nuclides. Further, since many of these products constitute part of a long beta series of isotopes and isobars, such data improves the possibility of studying the variation of nuclear properties with N and Z. An added benefit from looking at neutron-enriched nuclides is that the beta decay energy available is usually large which enables the study of excited levels to high energies. This feature will tell us more about nuclear correlations, for example. Finally, it is expected that we may contribute to the studies of the process of fission itself by studying the characteristics of the fission products.

Once the choice has been made to obtain neutron-enriched nuclides from the fission process, the second part of the experimental problem of conducting spectroscopic studies assumes the following perspective: many different nuclides are produced simultaneously from $^{235}U + n$ as shown in Figure 2. It thus becomes necessary to have some means of isolating one or a very few of the nuclides produced in order that the subsequent spectroscopy be kept as simple as possible. Mass separation provides a convenient method of selecting a single A value for further study. For the

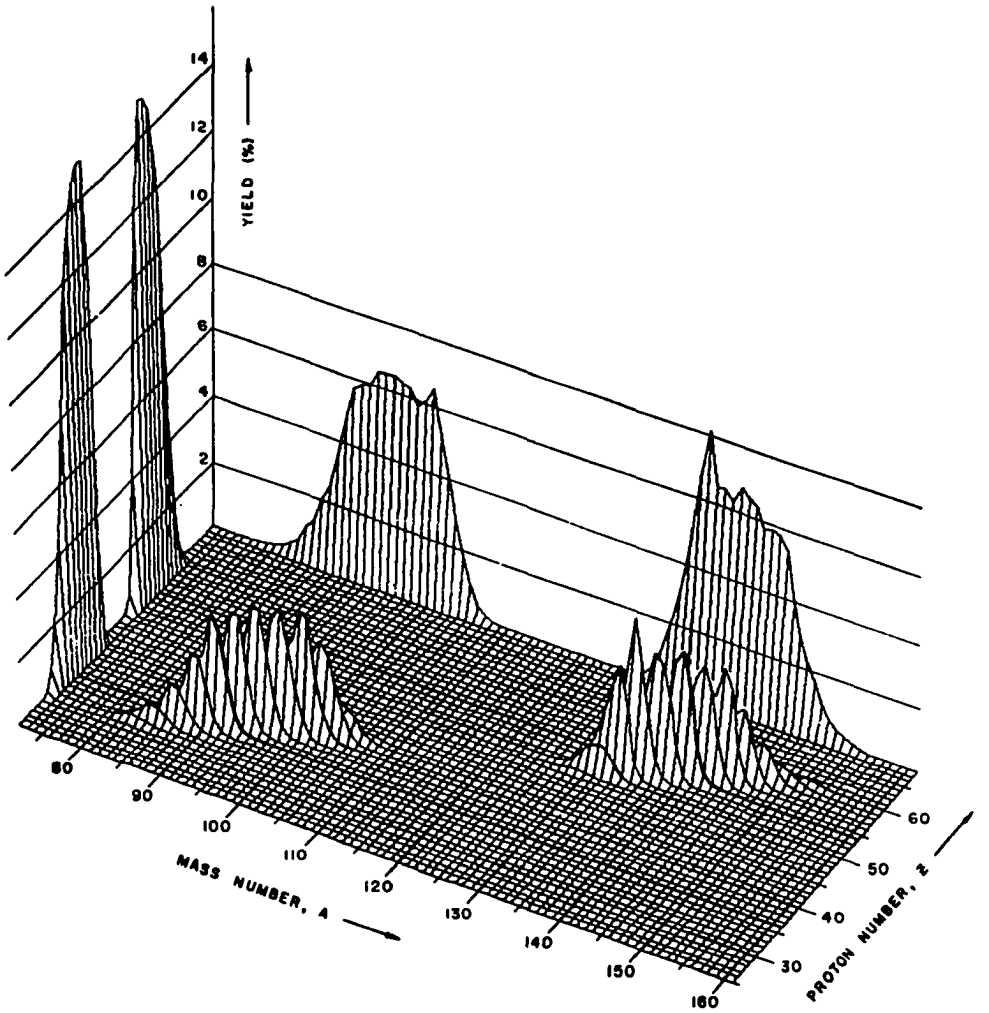

Figure 2. Fission yield of ^{235}U as a function of A and Z

case of short-lived nuclides under consideration here, it is necessary also to consider this mass separation as taking place in an on-line sense, with a sample of the desired radioactive nuclide being continuously collected and spectroscopic studies made on its decay simultaneously.

B. On-line Mass Separation

The first experimenters to operate a mass separator on-line were O. Kofoed-Hansen and K. O. Nielsen at the Institute for Theoretical Physics, University of Copenhagen, Denmark, in 1951 (1). Using a magnetic-type ion source, Kofoed-Hansen and Nielsen connected their separator on-line to a cyclotron which accelerated deuterons into a beryllium target to provide neutrons. The neutrons were moderated and allowed to induce fission in a sample of uranium mixed with a small amount of ammonium carbonate. The dissociation products from this latter compound provided a carrier gas for the radioactive rare gases being studied. A cold trap placed in front of the ion source allowed the passage of only the rare gases to the mass separator. Stable krypton was added as a sweep between the cold trap and the ion source to aid in isotope identification. The separated beam was then collected on a stationary foil.

This brief description illustrates that the experiment was quite sophisticated in modern-day terms in the features of production and separation of the desired radioactive isotopes. In contrast, the nuclear spectroscopic detection equipment available in 1951 was very crude by modern standards. The counting apparatus severely limited the capabilities for on-line studies in this experiment.

Kofoed-Hansen and Nielsen observed activities at many mass positions.

The amount obtained for mass 92, for example, was small and the decay curve measured found to be complex. Improvements in experimental technique were needed before mass 92 could be studied further. Quoting from the close of the 1951 paper: "At present the work is interrupted because of some rearrangements of the equipment of the Institute, but it is hoped to resume the study of these isotopes." Unfortunately, as is often the case for such interruptions, this continuation of on-line studies did not occur at the Institute. But while the work of Kofoed-Hansen and Nielsen had been hampered by the crudeness of the detection apparatus, it had shown the power of the on-line mass separation technique and blazed a path for future work in this area.

It was not until 1964 that G. Holm and co-workers at Stockholm carried out further experiments with a similar setup (2). Their on-line operation started as a natural extension of studies in progress. The experiences of Holm *et al.* led them to use on-line experimental techniques to study single-closed-shell and neighboring nuclei (3). The separator in this experiment was connected at times by a 40 meter transit line to a cyclotron and at other times to a neutron generator through a 5 meter transit line. Transit times of the radioactive atoms from the uranyl stearate "generator" of fission products to the ion source were measured as 140 seconds for the cyclotron connection and 13 seconds for that with the neutron generator. ^{91}Kr, with a 10 second half-life, was the shortest-lived nucleus observed to decay.

Holm *et al.* used a uranyl stearate sample such as that later adopted with much success by the TRISTAN group at Iowa State University. This ISOL

(Isotope Separator On-Line) system also incorporated a moveable tape collector for beam deposit. For gamma-ray studies, a 1.5 cm^3 Ge(Li) detector was used for singles and two NaI detectors were used for coincidence measurements. In each case a 1600 channel analyzer was used, operating in the 1 x 1600 mode for singles and in the 40 x 40 mode for coincidence.

With the advent of solid state detectors and their application by Holm et al., on-line isotope separation came of age and began to fulfill the promise shown in the work of Kofoed-Hansen and Nielsen. As of late 1970, nine true ISOL facilities had reported results with more groups expected in the field shortly (4). The TRISTAN project represents one of these efforts directed toward expanding the limits of detailed studies of nuclear structure.

C. Classification of Nuclei

One of the earliest physical pictures developed to correlate observed nuclear phenomena was the liquid drop model. It was the basis for the semi-empirical mass formula of Weizsäcker (5). This model recognized the approximate independence of mass number A of the binding energy per nucleon and the density of nuclear matter as analogous to the independence of drop size of the heat of vaporization and the liquid density for a liquid droplet. This crude model was able to reproduce many properties of the nucleus as, for example, the nuclear mass as a function of A and Z.

The drop model of the nucleus as constituted of incompressible, irrotational nuclear "fluid" (neutrons and protons), may be invested

further with gross shape properties which have proven useful in understanding many features of low energy nuclear spectra. By shape, the nuclides can be divided into three general classes:

1) spherical

2) deformed

3) intermediate.

There is a clear-cut distinction between the first two classes but the third class represents the rather gray in-between region. Class 1 nuclei are found at the limits of harmonic vibration of the spherical liquid drop nucleus whereas Class 2 nuclei are stably deformed drops which undergo rigid rotation. Spherical nuclei are thus found in regions not too far from the closed shells of the independent-particle shell model of Mayer and Jensen (6,7). Deformed nuclei are found in the regions farthest from closed shells and have been interpreted by Bohr and Mottelson (8,9) by an adiabatic separation of the nuclear wave function into a rotational part and an intrinsic part. Experimentally, spherical nuclei are found near ^{16}O, ^{40}Ca, ^{88}Sr and ^{208}Pb. Stably deformed nuclei have been observed in the rare earth and actinide regions.

The existence of two such distinct types of nuclei is attributable to two different types of correlation in the individual nucleonic motion. Residual forces in the nucleus tend to correlate the nucleons into a state with a spherically symmetric mass distribution. Long-range correlations tend to align the orbits of the nucleons with respect to a deformed field. These two correlations are in competition: when the residual forces dominate, spherical nuclei result; when the long-range correlations are

stronger, the nuclei become stably deformed in their ground states.

For the intermediate class of nuclei which display a shape transition such as spherical to deformed or vice versa, the residual forces and long-range correlations tend to have about the same strength. On the one hand this makes a theoretical understanding of these intermediate nuclei more difficult but on the other hand these nuclei represent potentially the best region to obtain information on the interplay between the collective effects of, for example, rotational motion in the deformed region and the individual-particle effects of, say, single particle levels in singly-closed shell nuclei. Thus the study of the intermediate class of nuclei offers an opportunity to discover, for example, where and how the transition from a spherical to a deformed shape takes place.

D. A New Deformed Region

As mentioned in the previous section, stably-deformed nuclei have been found in the actinide region ($Z > 82$, $N > 126$) and in the rare earth region ($50 < Z < 82$, $82 < N < 126$). Recently, evidence has been uncovered which points to the existence of a new deformed region for $28 < Z < 50$, $50 < N < 82$. There is some disagreement on exactly which nuclides have stably deformed ground states but there is general accord that they will be located somewhere near $A = 100$.

S. A. E. Johansson was the first to see evidence for such a deformed region when he measured the characteristics of delayed (10 to 90 nsec) gamma emission from ^{235}U + n fission fragments in 1965 (10). Maienschein et al. (11) had earlier looked at delayed gamma radiation associated with

fission and found that it had an intensity of 5.7% of the prompt component. Johansson added the feature of detection of the delayed gamma radiation with some degree of mass selection. In doing so he discovered that gamma emission from some fragments in the mass range 92 - 110 had the same characteristics as emission from deformed fragments in the rare earth region. The radiation of some of these light fragments was found to have a rotational-type spectrum similar to the spectrum of the rare earth elements. Of course, the energy level spacings do not directly determine the existence of a static deformation but the systematic behavior of such spacings can be indicative of a nuclear softness towards deformation.

Johansson also used a straightforward addition of the single-particle energies to get an estimate of the total nucleonic energy which gave a theoretical estimate of the deformation [cf. Mottelson and Nilsson (12)]. He found that nuclei with Z = 36 and Z = 38 were most likely to be stably deformed. Z = 44 and possibly also Z = 46 could also be expected to be deformed on the basis of this calculation. Johansson considered that semi-magic properties of Z = 40 would prevent Zr from showing static deformation. A more recent paper by Arseniev et al. (13) claimed that the Z = 38, 40 subshells have almost no effect on the deformation of nuclei with neutron number somewhere in the middle of the shell $50 < N < 82$. Arseniev calculated that the regions of strongest deformation should be in the heavier isotopes of Sr (A = 98 - 102) and of Kr (96 - 102) with the largest deformation possibility being obtained for ^{102}Kr. Arseniev further predicted that the oblate shape would be preferred for all nuclei in the A = 100 deformed region.

Ragnarsson (14) extrapolated parameters into the Z = 40 - 60 region of elements and concluded that the isotopes from ^{100}Zr, ^{104}Mo (possibly ^{102}Mo) and ^{108}Ru (possibly ^{106}Ru) and on were permanently deformed. Finally, Cheifetz et al. (15) found from experimental evidence from the first excited 2+ state in even-even nuclei that a region of deformation existed for about A = 100 with ^{102}Zr as the most likely candidate. The change in the energy of the first excited 2+ state between ^{98}Zr (1223 keV) and ^{100}Zr (212.7 keV) was noted to be very extreme and larger than even the well-noted discontinuity between ^{150}Sm and ^{152}Sm.

It is thus seen that new experimental data is needed for nuclei in the A = 100 region to determine exactly which nuclei are deformed. In addition, the nuclei intermediate between this new deformed region and the spherical region of ^{88}Sr, ^{90}Zr should be studied to observe the properties of the transition between spherical and deformed as a function of N and Z. It is expected that the behavior of this intermediate region will be somewhat different from others in that there are fewer protons in the case of atomic mass number approximately equal to 100 which means that Coulombic effects will be less. This should lead to a better understanding of the effect of the Coulomb forces on intermediate nuclei in general. As new theories are developed to explain new phenomena, the older phenomena are usually found to be better understood as a result.

The TRISTAN ISOL system at Iowa State University can be used to probe into the neutron-enriched region in the direction of A = 100, with particular emphasis on the lower mass intermediate nuclei. Because the current separation process used by TRISTAN hinders the collection of all but the

rare gases resulting from fission, the beta chains studied in this region will necessarily begin with krypton.

Although TRISTAN is not used to study delayed gammas associated with fission per se, it does in some sense represent an extension of Johansson's investigations by using a much cleaner mass separation and in addition an isobaric separation. The continuing improvement of detectors and associated electronic instrumentation has increased the quality and quantity of information which can be obtained from nuclear spectroscopy on intermediate nuclei in this region.

E. Present Work

This present work incorporated nuclear spectroscopic research into the decay of those neutron-rich mass 92 nuclides, ^{92}Kr, ^{92}Rb and ^{92}Sr, which were obtainable using the TRISTAN on-line isotope separator system and which had not yet been extensively studied. ^{92}Kr, which begins the beta chain studied (see Figure 3) is one of the gaseous isotopes released in thermal-neutron-induced fission of ^{235}U. The gases krypton and xenon are formed in amounts corresponding to about 0.25 noble gas atom per ^{235}U nucleus fission (16). The fission yield contour map (Figure 2) shows that the fission fragments with atomic mass number 92 constitute 5.9% of the total fission yield. Twenty-five percent of this A = 92 fission material is krypton with Z = 36 (17).

The investigation involved direct observation of de-excitation gamma rays only, following the three beta decays. Solid state detectors and state-of-the-art nuclear instrumentation were used. Singles and

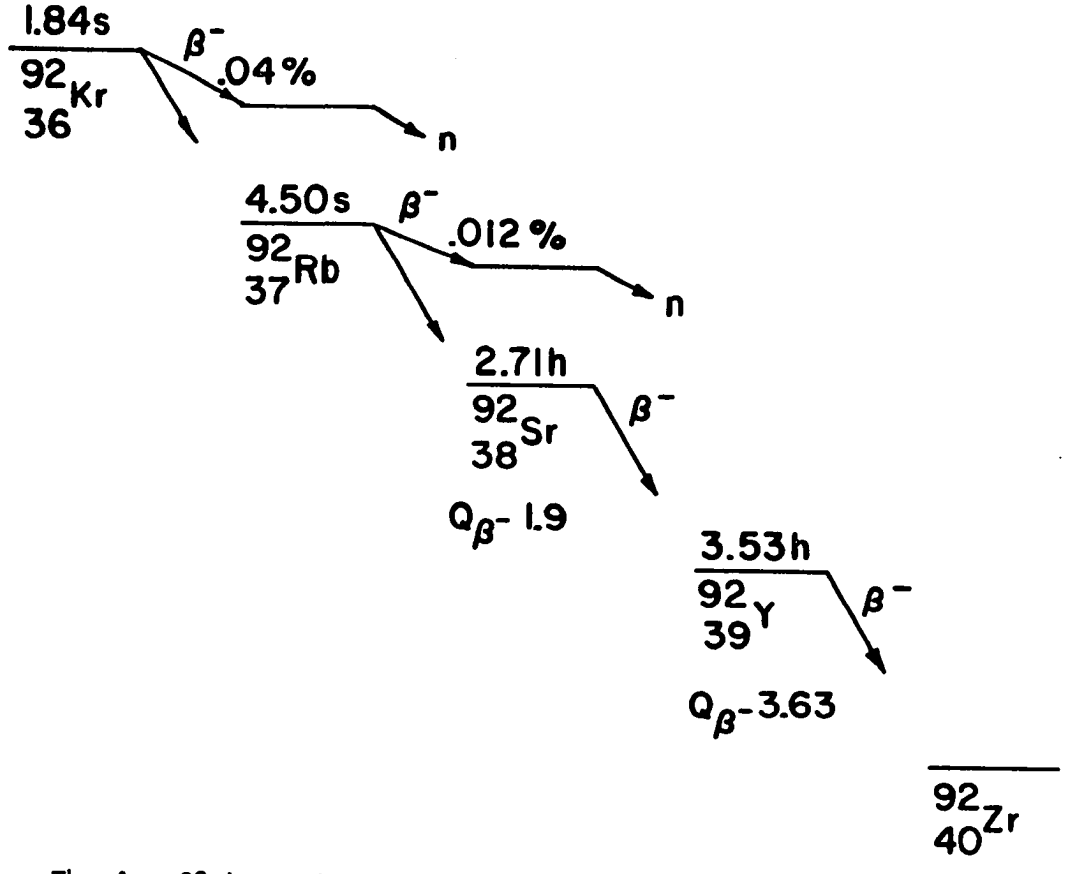

Figure 3. The A = 92 beta decay chain studied with the TRISTAN ISOL system

coincidence spectra were taken and the data analyzed by computer. The resultant transition energies, relative intensities and coincidence information for the three decays were combined into partial level schemes for ^{92}Rb, ^{92}Sr and ^{92}Y. From these level schemes, beta-feed percentages and associated beta-decay log ft's were determined for those levels considered beta fed. Finally, an attempt was made to interpret some of the levels found by comparing the nuclides studied with those nearby or those expected to be similar on the basis of shell model theory.

F. Previous Work: Neutron-Enriched Mass 92

The earliest report of an observation of neutron-enriched Sr and Y nuclei was made by Hahn and Strassmann in 1939. At first (18) they hesitantly suggested fission giving rise to Ba and La but soon they reported a more thorough experiment showing Ba, La, Sr and Y (19). Finally Hahn and Strassmann reported what probably was the first observation of mass 92 neutron-enriched nuclei (20). The half-life they gave for the Rb beta decay was more than an order of magnitude too large, the Sr half-life more than twice too big, but the Y decay half-life was correct. The following year Götte definitely observed the mass 92 chain (21), obtaining the correct half-life for both the ^{92}Sr and ^{92}Y decays although the ^{92}Rb half-life remained over an order of magnitude too large.

There were other papers in the 1940's in which neutron-enriched mass 92 nuclei were reported but since the counting equipment available at the time did not allow any more than the rough measurement of the half-life against beta-decay, these are chiefly interesting only in the historical

context of early researchers slowly developing a picture of the products of uranium fission and they will not be listed here. More than a decade later the methods of detection of radiation had improved greatly and Herrmann and Strassmann reported on ^{92}Sr and ^{92}Y decay in 1956 (22). Unfortunately, there was some problem with contamination in this beta measurement as Herrmann and Strassmann reported a beta group in the Sr decay not seen by Heath (23) in 1957 or by Clifford in 1971 (24). Heath found gamma rays of energy 0.23, 0.44, and 1.37 MeV following the beta decay of ^{92}Sr, with relative intensities of 0.039, 0.045 and 1.00, respectively. Using beta-gamma coincidence techniques, Heath measured a beta endpoint energy of 1.93 MeV, since verified by Clifford. Finally, Heath used 4-pi beta measurements to find a branching ratio of 90 $\pm$ 10% leading to the 1.37 MeV gamma ray. From his work, Heath postulated levels at 1.37, 0.44 and 0.23 MeV.

The best half-life measurement for the beta decays of ^{92}Kr and ^{92}Rb was done by Carlson *et al.* (25). The results are included in the beta decay scheme shown in Figure 3. No level schemes existed previously for ^{92}Kr or ^{92}Rb decay. A complete gamma spectroscopy study has been done by Talbert *et al.* for the decay of ^{92}Y (26) with the results being shown in the level scheme in Figure 4.

In summary, prior to this work the level scheme of ^{92}Zr was well-known, some information was available for ^{92}Y levels, and no information had been published on ^{92}Rb and ^{92}Sr levels.

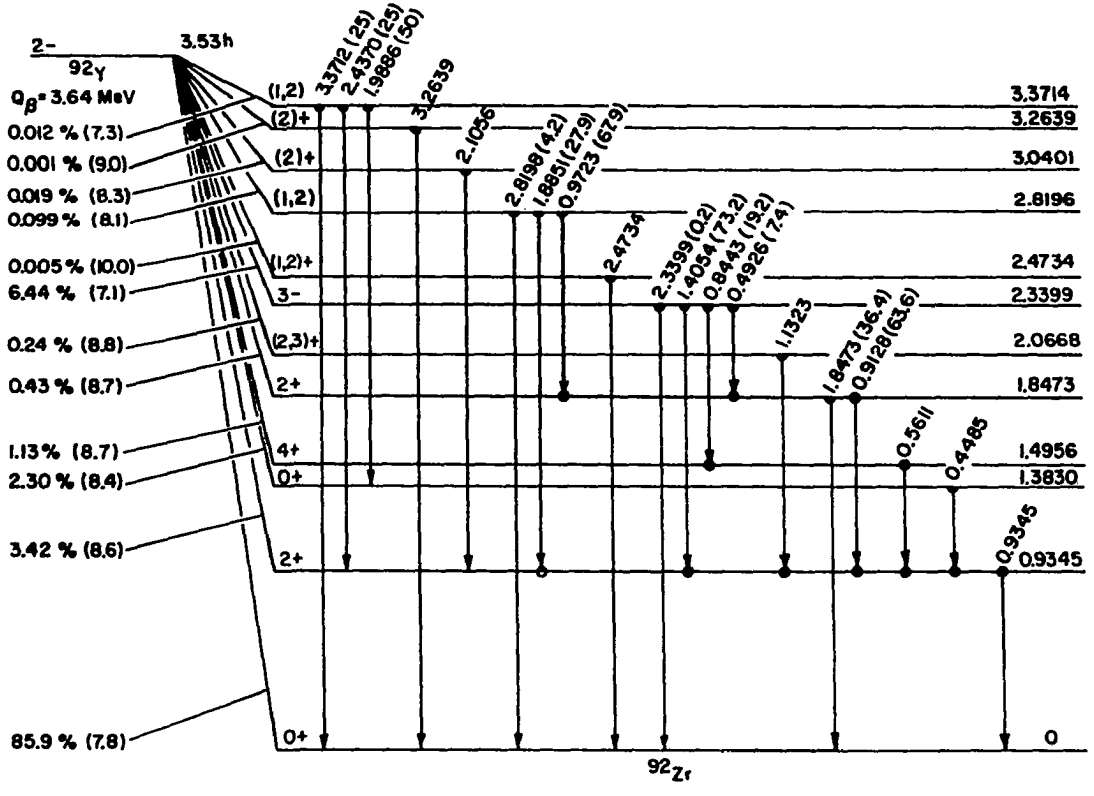

Figure 4. Level structure of ^{92}Zr following the beta decay of ^{92}Y

II. SAMPLE PRODUCTION

Standard spectroscopic methods were used to detect and analyze the gamma rays from the beta decays of ^{92}Kr, ^{92}Rb and ^{92}Sr. The mass separator facility TRISTAN used for these studies was the first of its type to be connected on-line to a reactor, on October 25, 1966 (27). TRISTAN was constructed using a "Scandinavian-type" separator, a term which has arisen because this form of machine was developed mainly in the Scandinavian countries (28). It is a 1.6 meter, 90° sector-type mass separator in which the ion beam is focused and controlled by electrostatic lenses.

The components of TRISTAN which are of interest for this work are shown in Figure 5. Several changes have been made in the system configuration since the beginning and this figure shows an outline of the apparatus as it existed at the conclusion of this experiment.

A. Production and Transport of Gaseous Fission Products

The rare gas ^{92}Kr atoms which begin the beta chain studied were produced by two different means over the course of the investigation. Both methods required the use of the Ames Laboratory Research Reactor, a CP-5 type pile with 5 Megawatts maximum thermal power, as a source of neutrons. During the experimental runs made prior to the summer of 1969, the fission fragments were obtained by placing a sample of fully enriched UO_2 containing approximately 200 mg of ^{235}U near the core by inserting it in a beam tube in Face 7 of the reactor. The neutron flux at this point is nearly 10^{13} neutrons/cm^2/sec. Since this location provided more activity than needed at some of the mass numbers and also led to early degeneration of the UO_2

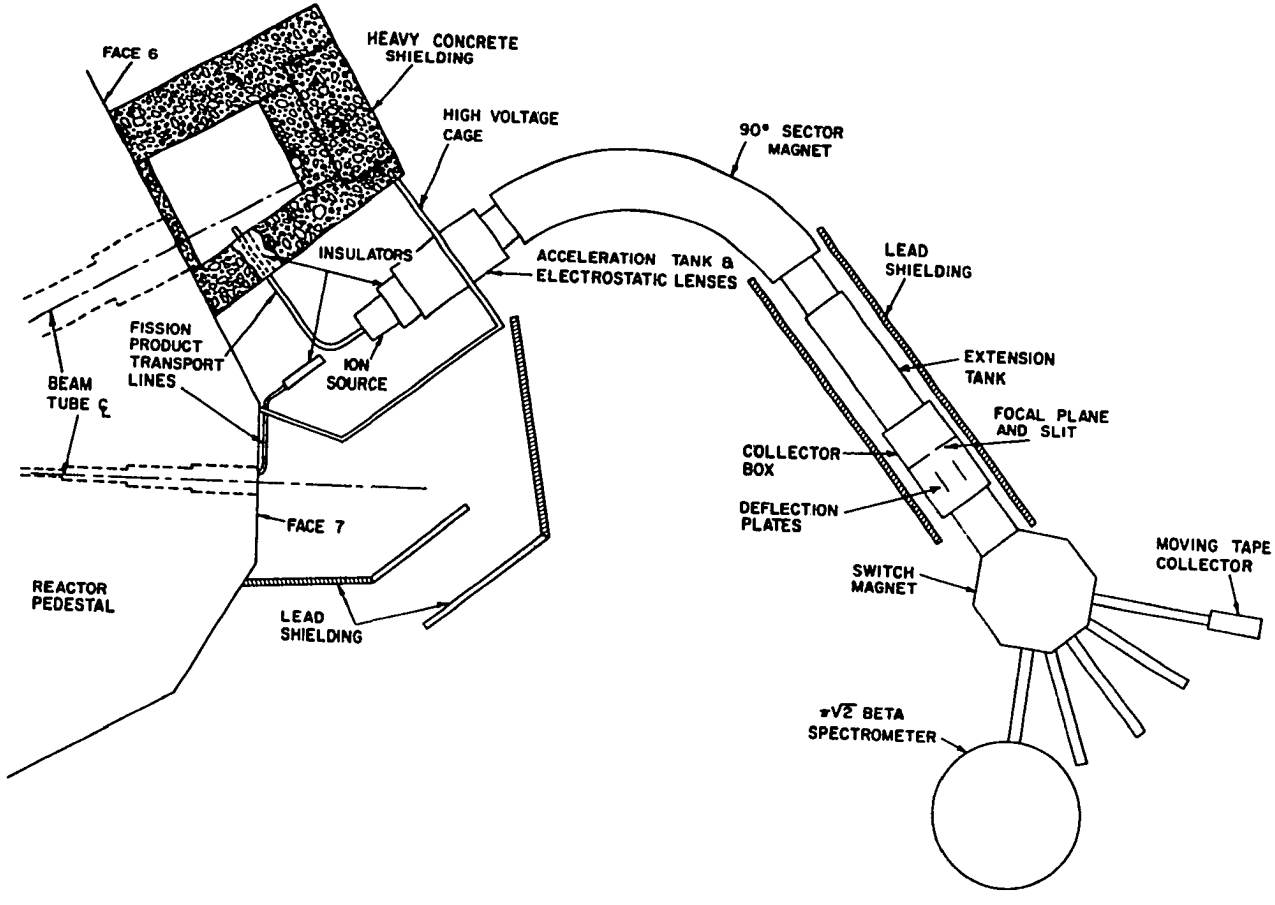

Figure 5. Layout of the TRISTAN ISOL system at the Ames Laboratory Research Reactor

sample from the standpoint of gaseous fission product generation, provision was made to allow for operation with the distance from the core to the sample as a variable to be adjusted as the need arose. Withdrawing the fuel sample partially from its point of deepest penetration rather than running the reactor at lower power enabled other users of the reactor facility to retain full power operation at all times for their own particular experimental needs. This flexibility also allowed the sample to be withdrawn from regions of high neutron and gamma flux and high temperature during periods when the separator was idle, which extended greatly the useful lifetime of any given fuel sample. With an internal sample it was found empirically that continuous running of the system for a period of more than eight to ten hours appreciably accelerated the degeneration of the fuel sample, leading to a greater and greater reduction in emanation of fission products until finally a sample replacement was dictated. It is believed by the TRISTAN group that this degeneration of the sample can be traced to a change in the crystal structure of the UO_2 when it experiences high temperatures under vacuum. This high temperature is caused by fission and gamma heating. Such an effect has been observed for U_3O_8 (29). Because the old samples are highly radioactive, it has not been possible to perform a post-mortem examination to determine possible causes of the degeneration.

For the internal sample the UO_2 powder was sandwiched between two sintered stainless steel discs, each about 0.71 mm thick with nominal pore sizes of 3 microns. The uranium dioxide powder had a particle size of 2 microns. This arrangement allowed the release of the rare gases of interest

while still providing containment for the UO_2 powder. This feature was important in preventing the spillage of any contaminated sample material when the sample was moved back and forth in the beam tube and particularly when it was removed during a replacement operation. Some old samples have shown an activity of over 50 Roentgens/hour at a distance of one inch so that even a minute leakage of irradiated powder would have represented a major contamination problem.

After diffusing out of the internal sample, the fission product material was pumped through a stainless steel line to the ion source. This transport line was maintained at ambient temperature which, during a run, varied from above 650 ^{o}C at the deep end of the fission product generator to about 22 ^{o}C for that portion of the line which was external to the reactor. The rare gases traveled easily from the generator to the ion source because they remained gases at these temperatures while almost all of the remaining fission products deposited out somewhere along the walls of the transport line if they even left the generator at all.

One of the major obstacles to the collection of short-lived activities using TRISTAN was the 5.48 meter length of the transport line from the internal fission product generator to the ion source. Transit time studies made on a simulated transport line have shown that a krypton gas atom in a xenon gas sweep will take on the order of 12 seconds to make the trip along a tube of this length (27). (In these studies "transit time" was defined as the most probable time of arrival of a gas atom in a pulse.) This delay led to a great reduction in the number of short-lived atoms successfully completing the trip. For this reason it was decided to build

another fission product generator to be placed in the external neutron beam available at Face 6 of the reactor. With this external beam it was possible to reduce the length of the transport line to 1.8 meters.

Since the flux available in the external neutron beam was found to be down a factor of some 3000 from that obtainable in the internal beam plug, additional enhancement of some form was needed in the production of the rare gases. The answer was found in changing the chemical composition of the uranium fuel sample. UO_2, the compound used in the internal sample, is also commonly used as a material in fuel rods for reactors. One of its advantages for such use is that in the event of a fuel element cladding failure, it will not release appreciable amounts of uranium or fission products into the coolant system. This characteristic, so desirable for a nuclear fuel, is a hindrance to the operation of an efficient gaseous fission product generator.

In a study made on the determination of the diffusion constant of fission products in UO_2 crystals (30) it was found that the fraction of the rare gas ^{133}Xe which emanated from the material at a constant temperature obeyed the approximate relation

$$f \propto 6/a\sqrt{Dt/\pi} \quad .$$

In this relation, a represents the radius of the particle, D the diffusion constant, and t the time. The approximation requires that only a small fraction of the initial amount of gas diffuses out of the spherical particle, a good assumption in the case of UO_2. The sample investigated was formed by powdering a lump consisting of large crystals which had been made by

fusing a quantity of uranium dioxide. After powdering, the particle radius was about 28 microns. It was also found in this investigation that the effects of temperature could be incorporated into the above relation through the diffusion constant, D, through an equation of the form

$$D = D_o e^{-E/RT}$$

where T is the absolute temperature, R is the gas constant, and D_o and E are constants. Experimentally it was found that at 1400 ^oC less than 0.3% of the ^{133}Xe formed was released after one minute. Assuming that krypton would behave roughly the same as xenon, changing the particle radius from 28 microns to the 2 micron case of TRISTAN would enhance the release by a factor of 14. The temperature of the fuel holder had been measured during a run to be on the order of 650 ^oC. This cannot be considered to be an accurate measure of the temperature of the fuel powder grains. Using the (probably unrealistically) high temperature of 1300 ^oC will give an optimistic value for the rate of emission.

In calculating the effect of the new radius and temperature on the fractional emanation the values proposed by B. Lustman (16) for the constants were for Xe

$$D_o = 6.6 \times 10^{-6} \text{ cm}^2/\text{sec}$$

and

$$E = 71,700 \text{ cal/mole.}$$

Other workers have found that there is either no significant difference between the release rates of the krypton and xeonon isotopes (30) or that the release rate for the kryptons is only slightly greater than that of the xenons (31). This was the basis for using the Xe constants in a calculation

of the diffusion rate for Kr. The result for the TRISTAN fuel sample is that about 2.1% of the rare gas krypton formed would be released after one minute. The percentage released after a few seconds would be still smaller. This slow emanation clearly represented an area for improvement.

It was known that in the case of diffusion of gases from solids some long-chain fatty acid salts of heavy metals have a strong emanation property (32). In fact, O. Hahn had based separation techniques on this property (33). Hahn defined the concept of an "emanating power," the fraction of the inert gas nuclide formed in the salt that escapes under the conditions of irradiation. In the case of the rare gases formed during fission, this power of emanation is complicated by being composed of a recoil contribution and a diffusion contribution. Wahl *et al.* (34) found the emanating power of uranyl stearate $[UO_2(CO_2C_{17}H_{35})_2]$ for ^{92}Kr to be greater than 0.95. This emanating power follows from a relationship given by

$$E = e^{-\lambda\delta}$$

where E is the emanating power, λ is the decay constant of the inert gas and δ is the effective time spent by the inert gas in the stearate salt. Wahl calculated that for an emanating power of greater than 0.95 the effective time spent by the krypton gas in the salt was less than 0.22 sec. For the half-life of ^{92}Kr he used a value of 3 seconds, which was the commonly accepted measurement at the time. Using the more recent value of 1.84 seconds (25) this effective time is reduced to less than 0.14 sec. This great increase in the emanation of fission product gases was achieved at the expense of the stability of the UO_2 against the conditions of radiation and heat. The stearate salt could never be used under the

conditions existing near the center of the reactor.

The preceding calculations, incorporating many assumptions and approximations, indicated that there might be enough radioactive material generated and released to compensate for the reduced fission rate due to the decrease in neutron flux for the external beam and allow a continuation of the gamma ray spectroscopy. Although there was no guarantee of success, enough hope had been generated to try the system on-line. Much of the shielding needed for use of the external beam of neutrons was already in existence, having been constructed during an attempt to generate halogen fission products for study using the separator.

The method used was to replace the UO_2 powder sample of the internal sample with approximately 650 mg of ^{235}U in the form of uranyl stearate (25.44% ^{235}U) which was spread on trays placed in a piece of apparatus designed by Jon Larsen, at the time a member of the TRISTAN group. This apparatus was an evacuated vessel called the "ham can" because its shape remarkably resembled that of a canned ham. A more recent version of the ham can is shown in Figure 6. The gaseous fission products are pumped out through the top of the ham can directly into the transport line. The entire ham can except for the O-ring which provides the vacuum seal is constructed of aluminum since it operates in a region of high radiation level. The ham can and its transport line are shown in the airbrush drawing reproduced in Figure 7. Also shown is the electrostatic lens box of the separator system.

The ham can is provided with an inlet for sweep gas to assist in moving the rare gases along to the ion source more quickly. In addition this sweep

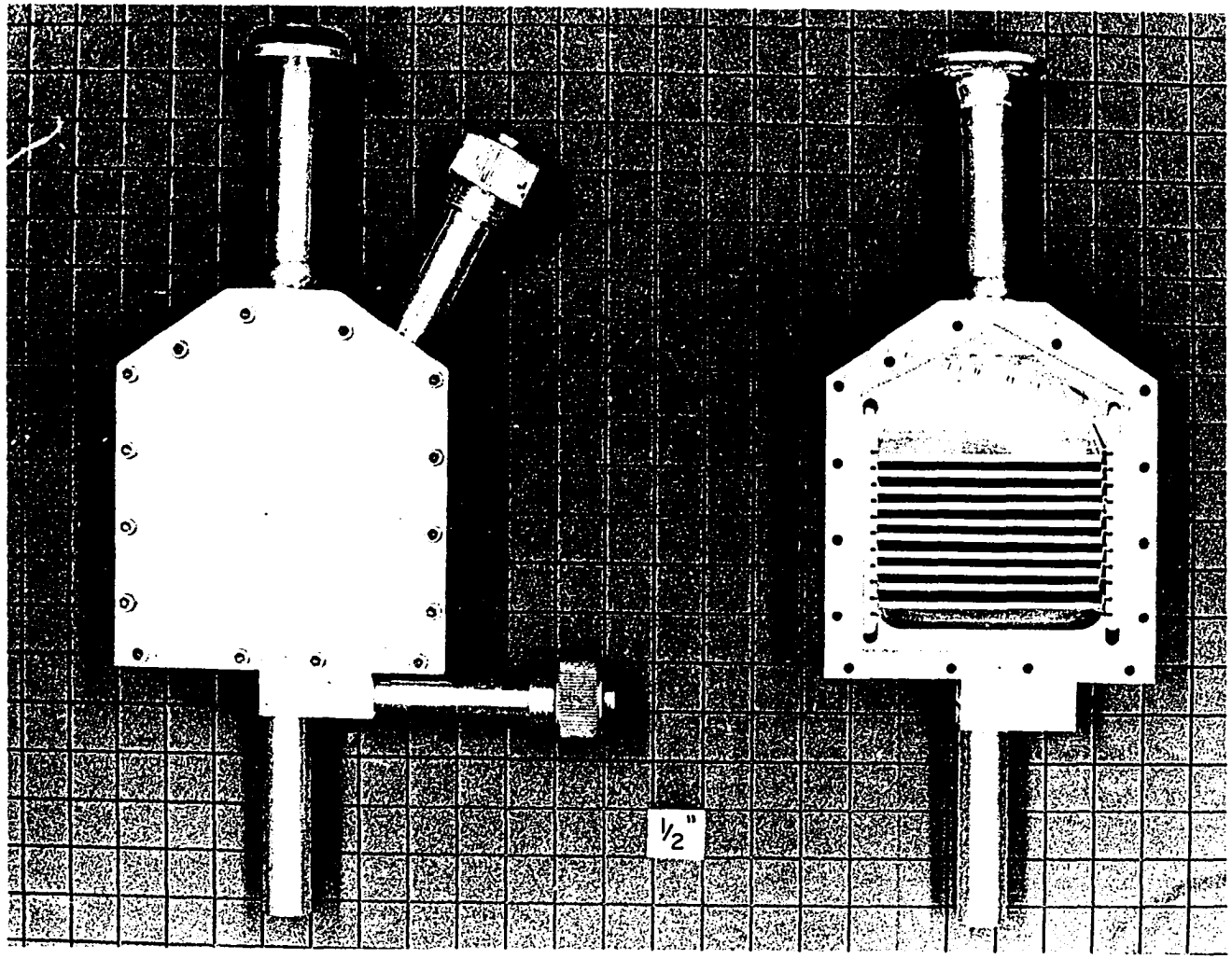

Figure 6. External fission product generator

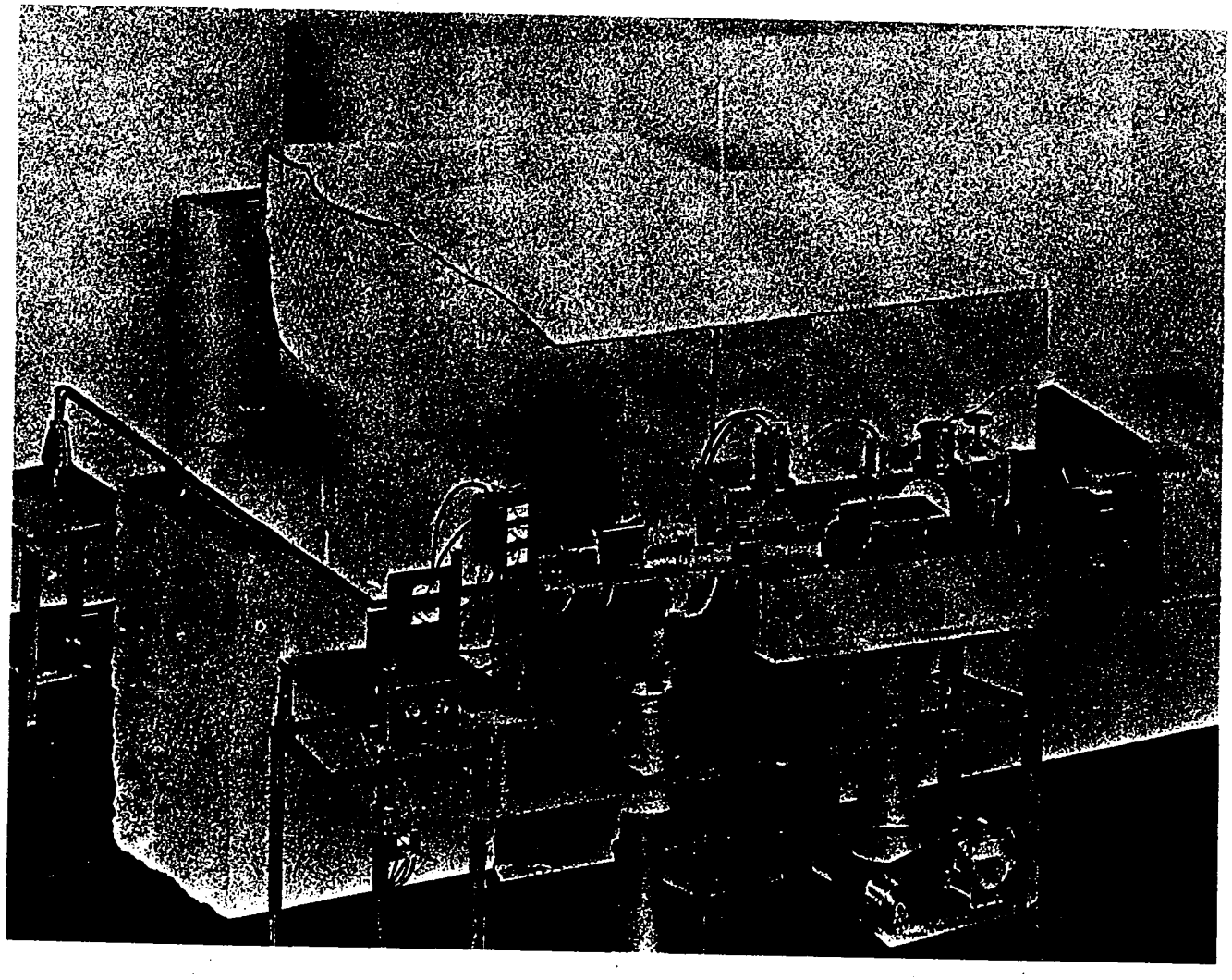

Figure 7. Ham can, transport line, ion source and electrostatic lens section of TRISTAN

gas provides a support for maintaining a discharge in the ion source. The sweep is made up of a small amount of krypton gas, an approximately equal amount of xenon gas, and a large amount of helium gas. The rare gases are used for "mass markers" and separator beam tuning purposes. The helium is used for the bulk of the sweep because of its low mass and associated high mobility and because its presence is believed to enhance the operation of the ion source.

A shutter is provided for the Face 6 neutron beam which can be opened or closed within a period of about one second. Using this shutter, it was possible to obtain an approximate value for the transit time of between one and two seconds for the rare gas fission products from the ham can generator to the separator ion source.

A survey was taken of the activity available at the various mass positions being studied with TRISTAN. As expected with the new system there was much less activity available for the longer-lived isotopes. Here the transit time had not been a problem and the reduction in the available flux was the dominant factor. At the other end of the spectrum, there was more activity available for the shorter-lived isotopes. In the short-lived cases the better transit time and the emanation power increase more than made up for the reduced flux. It was observed during the runs made using the original ham can that there was roughly 50-100% more activity collectible for mass 92 on the average than there had been for the internal plug source. Other mass numbers, for example 142, showed a much larger increase. But the 50-100% increase for mass 92 was useful, particularly for the coincidence runs where the coincidence rate goes approximately as the square of the

activity, neglecting dead time losses and assuming approximately equal detection efficiencies in the two detection systems.

There is one other major difference between the internal source and the ham can. The former, operating in the interior of the reactor, was most conveniently designed to run at ground potential while the ion source operated at a potential of about 60 kV. An insulating section was placed in the transport line to connect these two regions of differing potential. Since the ham can itself is run at the acceleration potential (along with the entire transport line) no insulating section is necessary. However the ham can and the transport line have to be insulated from the reactor face and the shielding through which the line passes. Despite much effort, it has been found impossible to operate the separator with an acceleration potential much higher than 50 kV without causing excessive sparking. This is a drawback because as the accelerating voltage is decreased the cross section for scattering of the beam by residual gas in the vacuum system increases (35) leading to more cross contamination of the beam. There is more mass 91 material showing up at the mass 92 position in the focal plane of the separator after mass separation. The problem of low accelerating voltage is fortunately minimized by providing a second degree of separation with a switching magnet after the first mass separation.

B. Principles of Operation of the Mass Separator

The sweep gas and fission product gases from the ham can pass into an electron plasma ion source with an efficiency of ionization of about 10%. All the gases leave the ion source through an exit hole and pass through an

electric field set up by an extractor lens about 5 mm from the end of the ion source. This field directs the ionized atoms through a hole in the center of the extractor and on into the electrostatic lens box. The neutral gaseous material is differentially pumped away by a six-inch diffusion pump.

The electrostatic lens section focuses the ion beam into a suitable shape. This shaped beam next passes through the 90^{o} magnet which provides the mass separation. The magnetic field also acts as a cylindrical lens and provides a beam profile of vertical lines in a plane some distance from the end of the magnet. A collector box is located in the region of the focal plane of the separator. This box contains a pair of aluminum plates with edges separated by about 3 mm to form a gap which allows the desired mass through but collects the neighboring masses. When the experiment was run on mass 92, masses 85-99 reached the collector box. Blockage of all the other activities besides mass 92 reaching the collector box quickly built up large amounts of activity on the aluminum plates when the internal fission product generator was being used. It was necessary to add additional lead shielding between the collector box and the moving tape collector to reduce the background activity seen by the Ge(Li) detectors.

The collector box has a screen coated with potassium bromide which can be dropped in front of the slit to allow observation of those mass numbers with beam currents greater than about 0.1 microampere. Viewing this screen through a lexan view-port, the operator may tune the separator to give the beam a sharp focus and reduce cross-contamination.

A small pin is swept periodically through the beam just in front of the potassium bromide screen. The small portion of the beam current picked up by this pin is amplified and displayed on an oscilloscope to give a visual indication of the beam current profile in the horizontal direction for separator tuning purposes. Signals from a magnet field flux probe and the accelerator voltage are combined by a mass meter system to give the ratio of B^2/V and an identification of the mass number currently being sent through the slit is displayed on a digital voltmeter. This device is extremely useful for setting the magnet current "in the ball park" for a given mass prior to fine tuning.

Once mass 92 is set to pass through the slit, it is necessary to compensate for any beam shifts which could interrupt the beam collection. For this purpose a pair of copper pins are placed in front of the aluminum plates and set to bracket another mass as close as possible to mass 92. The position of the copper pins is adjusted so that they pick up the same amount of current from the mass tails on either side of the peak being sensed. Then any drift in the position of mass 92 will be accompanied by a similar drift in the neighboring bracketed mass which causes more current to be collected by one pin than the other. This inequality is detected by electronic circuitry and a correction is automatically applied to the accelerating voltage to return the masses to their initial positions.

The collector box also contains a pair of high voltage deflection plates behind the slit. When 1200 volts is applied to these plates, the beam is deflected and kept from reaching the detection station. This feature allows easy interruption of the beam current for the daughter analysis

mode of operation of the moving tape collector.

The beam next passes through a compression lens section and then into a switching magnet which for this experiment usually directed the beam through an angle of 45° (45 cm mean radius) to reach the moving tape collector. The switching magnet also provides a second mass separation with a dispersion at mass 92 of somewhat more than 5 mm. This second separation is useful in reducing the cross-contamination at the moving tape collector.

For some runs on mass 92 the field in the switching magnet was controlled by monitoring the position of the mass 92 beam between two stabilizer pins before it entered the tape collector. This stabilizer operates similarly to the one in the collector box except that in this case the perturbative correction is applied to the current in the switching magnet rather than to the separator acceleration voltage.

C. Separation of the ^{92}Sr Activity

^{92}Sr activity was obtained by collecting ^{92}Kr ions on a thin copper foil (0.025 mm thickness) in the shape of a disk with diameter 4.45 cm for a period of two to three hours. The foil was mounted on a printed circuit board positioned in the beam tube leading toward the beta-ray spectrometer. Copper was chosen as the collection material because tests had shown it to combine good retention properties for krypton with ease of solubility for later chemical treatment. Immediately after the collection was ended the copper foil held atomic mass number 92 activity in the form of Kr, Rb, Sr, and Y. In addition there was a small amount of atomic mass number 91

activity caused by the presence of ^{91}Kr, in the form of the molecular ion "krypton hydride" (35,36). This hydride activity was subsequently identified by referring to the results of an investigation of the decay of ^{91}Sr (37).

Since it always took at least several minutes to remove the sample from the beam tube and transport it to the chemistry room there was no need to be concerned with the activities due either to ^{92}Kr (half-life = 1.840 $\pm$ 0.008 sec) or to ^{92}Rb (half-life = 4.50 $\pm$ 0.03 sec) (25). All that remained to be considered besides the desired ^{92}Sr activity was that from the decay of the ^{92}Y and of course that resulting from the hydride (^{91}Sr). For a collection time of two hours and a delay of five minutes, 87.4% of the activity could be attributed to ^{92}Sr while 12.6% was due to the ^{92}Y (here the contribution of the hydride products to the total activity has been taken to be negligible to simplify the calculation). It was desirable to undertake chemical separation as soon as possible because the fraction of the activity which was due to the Y would continue to increase as time elapsed. With the same two hour collection but with a one-half hour delay, 82.7% of the activity would have been due to the Sr while 17.3% would have come from the Y.

The copper foil was treated chemically to separate the Sr activity from that of the Y for subsequent gamma spectroscopy. The following steps were used:

1) The foil was dissolved in as little 6 Normal HNO_3 as possible with the mixture warmed in a hot water bath to speed the process.

2) The solution was placed in a 40 ml centrifuge tube. Five mg of Sr

(as a carrier) and water solution were added to bring to a total amount of 20 ml.

3) 6 Normal H_2SO_4 was added, heating was continued and the solution allowed to digest.

4) The mixture was then placed in an ice bath and allowed to cool.

5) The cooled solution was centrifuged and the supernate discarded. (Note: It was necessary at this point to retain the supernate for further processing in case the Sr failed to "come down" in the first treatment).

6) The sample was washed with dilute sulfuric acid (about 1/2 to 1 Normal) and then transferred to a 5 ml centrifuge tube.

7) The solution was centrifuged and the supernate discarded. If all had worked well, the remaining precipitate was the Sr sample ready for gamma ray spectroscopy. If the sample proved to be weaker than expected, then the supernate from step 5 was taken through additional treatment to recover more of the activity.

The sample that was prepared in the above manner was initially "clean," that is, free of Y contamination. As the observation of gamma rays resulting from the decay of ^{92}Sr proceeded, there was a build-up of ^{92}Y activity which appeared as contaminant peaks in the strontium spectra. In all of the Sr runs a clean-up chemical separation was performed quickly on the sample to remove the Y activity during the measurement. The procedure was to wash the sample with dilute (about 1 Normal) sulfuric acid containing about 2 or 3 mg Y carrier. This process was facilitated by having previously placed the Sr sample in a test tube which had a hole in its bottom. The hole had been plugged with a cotton wad to retain the

sample material. The sulfuric acid and the Y solution were then slowly poured through the Sr and Y sample and the Y which had grown in was flushed away. This method was not 100% effective but did remove a large amount of the Y contaminant. In principle it would have been possible to flush the Sr sample continuously to remove the Y as soon as it grew in, but this was never tried.

Since the Sr had a half-life of 2.71 hours and data collection usually extended over a period greater than eight hours, it was necessary to make more than one collection for a given series of runs. The usual number of collections was three. As each new sample was being readied, the sample being counted was taken back to the chemistry room for a clean-up and then brought back and added to the newer sample.

D. ^{92}Kr and ^{92}Rb Activity Separation by Use of a Moving Tape Collector

The decays of ^{92}Kr and ^{92}Rb were both studied on-line using a moving tape collector. The first version of the moving tape collector is documented in an Ames Laboratory Research and Development Report (38) and will not be described here. All specifications will apply to the second version of the moving tape collector (MTC) which was installed early in 1970.

The MTC represents the final step in the experimental preparation of samples for on-line gamma-ray spectroscopy. The collector performs a "mechanical chemistry" by providing an isobaric separation discriminating between two different chemical elements (unlike Z) with the same atomic mass number. In the particular case of the mass 92 chain the MTC was used to differentiate between the "parent" activity of the Kr collected on the

tape and the "daughter" Rb activity. The MTC is an open-loop system such as that used by Sidenius et al. (39). Figure 8 shows a schematic of the collector with the features of interest to this experiment indicated. Figure 9 is a photo of the collector with its side plate removed, showing the tape supply and take-up reels as the most prominent features.

The MTC is constructed mainly from aluminum. An idea of the overall size may be obtained from the scale in Figure 8. All the lead shielding for this collector was external at the time of this experiment and may be seen in Figures 10 and 11 which show 30 cc Ge(Li) detectors positioned for gamma-ray detection on either side at port number one. This external shielding reduced cross-talk between activity on different parts of the tape.

For each side of port one there are 2.54 cm thick lead collimators with tapered holes for use in enhancing the parent decay. It was found that the moving tape operation led to an enhancement of the intensities of the higher-energy gamma rays over those of the lower-energy gamma rays. As a given portion of the sample was moved along with the tape to a position behind the shielding, the edge of the shielding appeared "softer" to the higher-energy gammas than to the lower-energy gammas. The latter were absorbed easily by a small amount of lead in their path while the former had to pass farther behind the shielding before their contribution to the activity seen by the detector was reduced to a negligible amount. For the mass 92 experimental results shown in a later section the lead collimators were used with the narrow side of the taper facing the activity on the tape. This was the same configuration that had been used in the old moving tape

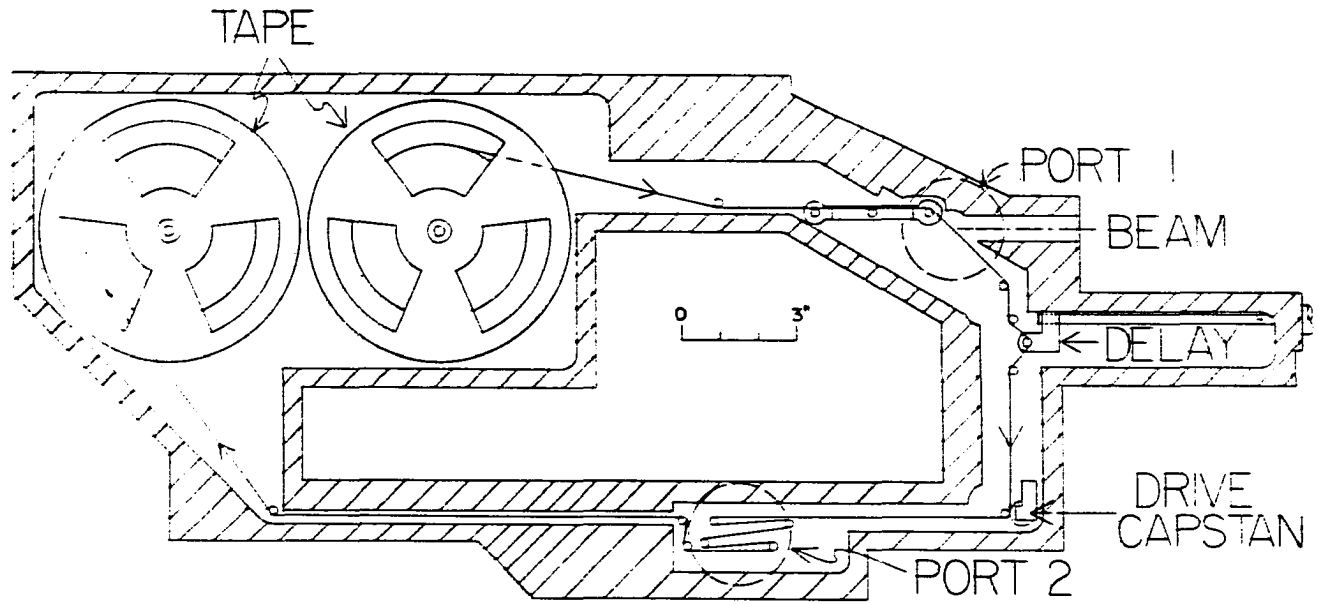

Figure 8. Moving Tape Collector schematic

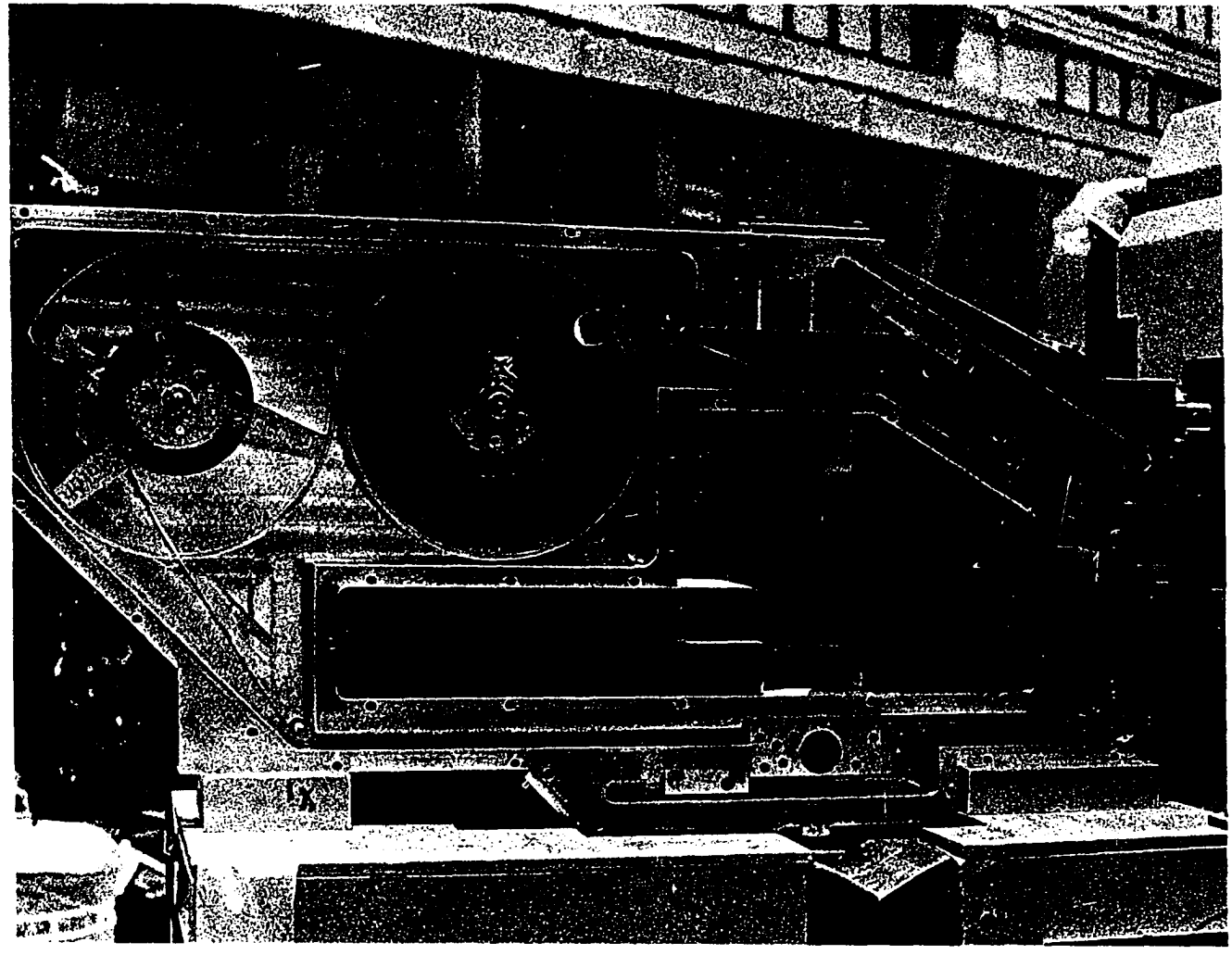

Figure 9. Moving Tape Collector with side plate removed

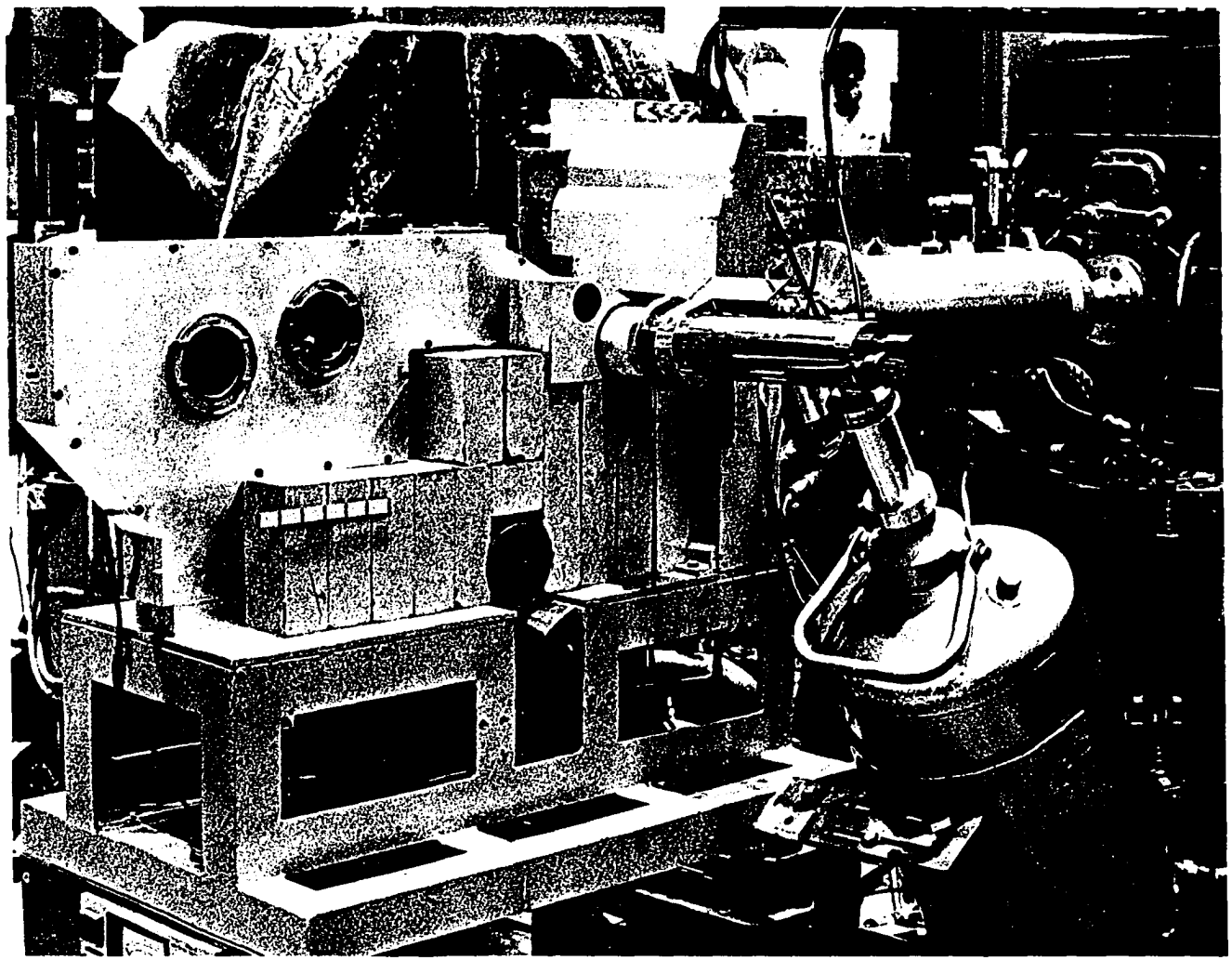

Figure 10. Moving Tape Collector with Ge(Li) detector in position at port one

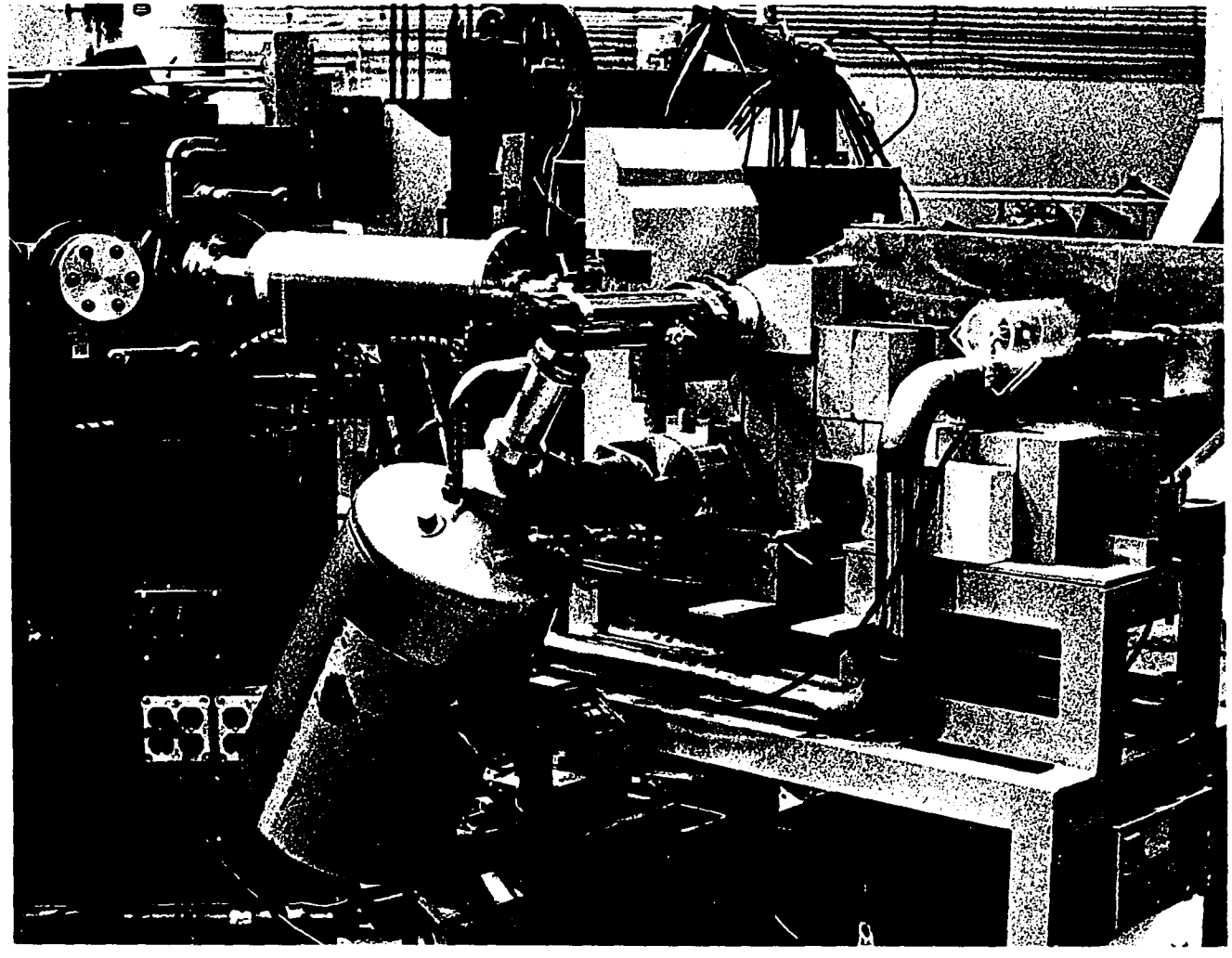

Figure 11. Moving Tape Collector with Ge(Li) detector in position at port one on motor side

collector. But since the collimators in the new MTC were less than half as thick as the ones in the old, the result was about a factor of two enhancement in the relative intensity at 1 MeV compared to 100 keV. A correction run was necessary to compensate for this effect.

The moving tape was aluminized mylar of width 1.27 cm which was obtained from type MF-150 CABELTAPE made by the Lamart Corporation, 16 Richmond Street, Clifton, New Jersey. The CABELTAPE has a 0.0254 mm mylar base bonded to a 0.0089 mm aluminum layer. The primary use of this material is as a wrap for the protection of electrical cables but the manufacturer was willing to slice it to meet the MTC requirements.

The beam from the separator hits the aluminized side of the CABELTAPE in a spot which is focused to be nominally 6 to 9 mm high and roughly 1 mm wide. The amount of beam striking the stationary tape at any instant can be be monitored by a current pickup. The end of the tape is fastened to the insulated bearing holding the supply tape reel, providing a path for the current to get outside the vacuum. The resistance of a full reel of tape is only about 50 ohms and presents no problem. It is not possible to measure the current when the tape is being moved because of the low beam currents and the large amount of signal noise generated by the tape motion. It is necessary to ground the tape during operation to prevent the tape from building up a charge, with subsequent effects on the amount and quality of beam deposition on the tape.

For mass 92 the beam current is of the order of a few nanoamps. Most of this current is due to stable ions other than ^{92}Kr which have the same m/e value. This stable part of the beam does not contribute to the activity

and makes handling and controlling the beam possible. Monitoring the current with the tape fixed serves as a useful device in fine-tuning the separator and the field strength in the switching magnet although the final criterion is always maximization of the activity. In some runs it was found that the maximum activity was obtained on a side hump of the main current peak. In such cases it was not possible to operate with the switching magnet stabilization circuitry in use.

The MTC drive mechanism consists of a two-phase induction motor controlled by a tachometer feedback system and a transmission with reduction ratios of 20:1 and 10:1. The drive is transmitted to the tape via a capstan. Slack in the tape is prevented from developing by a motor on the take-up reel. The tape position is monitored by a photocell driving a scaler (shown in Figure 12) which allows a predetermined tape movement to be made. Controlled motion of the tape is available at any speed from 0 to 2 inches/sec.

Enhancement of the parent decay in the mass 92 beta chain is in principle quite simple. The activity separation between Kr and Rb decay will be greater as the tape is run faster. This is shown in Table I which lists the fractional integrated activity ratio R as calculated by computer program ISOBAR (38) for each of the isotopes for various speeds of the tape past the detector. The relation between tape speed and dial setting is linear with Speed = (0.006364 x Dial - 0.036) cm/sec. The integrated activity ratio, R, is the ratio of counts for the particular isobaric decay detected during the tape movement across the collimator slot to the total number of counts detected in the same interval.

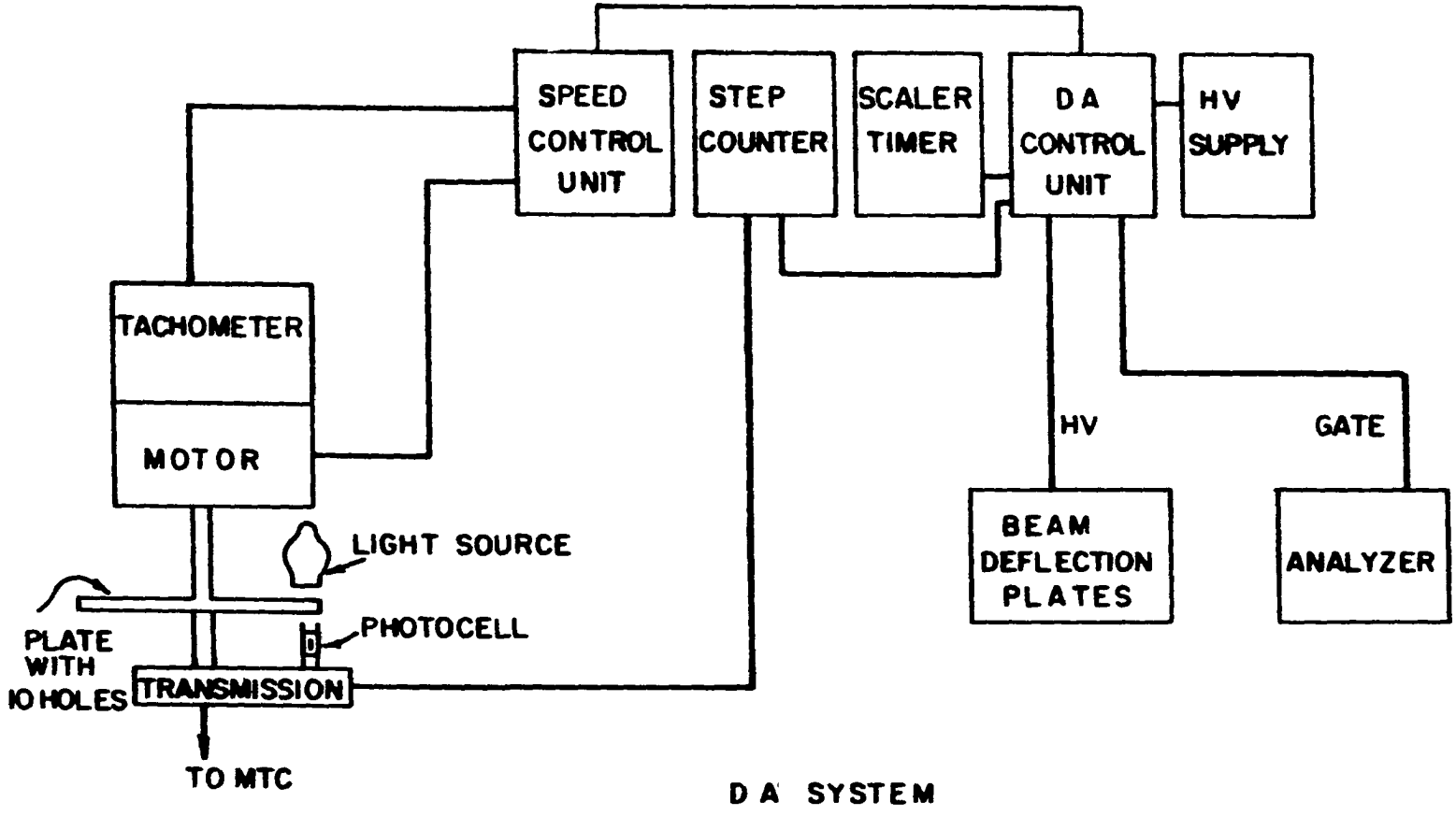

Figure 12. Block diagram of daughter analysis system

Table 1. Integrated activity ratio R for various tape speeds

Dial	^{92}Kr	^{92}Rb	^{92}Sr	^{92}Y
840.0	.981891E00	.18109E-01	.11644E-06	---
700.0	.978332E00	.21668E-01	.16774E-06	---
600.0	.974794E00	.25206E-01	.22839E-06	---
500.0	.969876E00	.30123E-01	.32904E-06	---
400.0	.962576E00	.37423E-01	.51446E-06	---
300.0	.950614E00	.49386E-01	.91556E-06	.79560E-11
250.0	.941227E00	.58772E-01	.13195E-05	.12563E-10
200.0	.927450E00	.72548E-01	.20640E-05	.23193E-10
150.0	.905291E00	.94705E-01	.36755E-05	.58194E-10
130.0	.892147E00	.107848E00	.48979E-05	.90596E-10
100.0	.863922E00	.136069E00	.82925E-05	.20534E-09
80.0	.835398E00	.164589E00	.12978E-04	.41303E-09
60.0	.792379E00	.207598E00	.23118E-04	.10282E-08
50.0	.761786E00	.238181E00	.33331E-04	.18469E-08
30.0	.668319E00	.331588E00	.93007E-04	.10004E-07
20.0	.598924E00	.400863E00	.21220E-03	.41639E-07
10.0	.524860E00	.474111E00	.10291E-02	.78548E-06

In practice there are two other factors which also determine how fast the tape is run. First, the supply of tape in the MTC is not limitless. At two inches/sec a reel of tape will be exhausted in three hours. The external shielding must then be removed and the tape collector vented to atmospheric pressure, opened and a new tape installed. The system is then closed up and pumped back down to the microtorr range, a time-consuming procedure. For this reason the MTC was seldom run at top speed.

The second consideration is the counting rate. For a given deposition rate of Kr on the tape, the count rate will be less as the tape is moved faster and the parent activity does not build up as far toward saturation. Table 2 shows the percent saturation and count rate calculated by ISOBAR (with a 10^7 counts/sec rate as a hypothetical maximum for an equilibrium run) versus the same tape speeds as in the previous table. For mass 92, the activity available from the system is limited by fission yield combined with transport loss and this limitation on the counting rate requires a compromise to be made in setting the tape speed. Also, since the amount of activity collectible varied from run to run, this compromise had to be made just as a run was being started. The moving tape series of runs shown in the spectra plots in the data section were made at a dial setting of 300.0 or a speed of 1.87 cm/sec.

Runs to enhance the Rb decay were made using the daughter analysis (DA) system shown schematically in Figure 12. Collection of the beam is interrupted after a fixed period of time by sending a high voltage signal to the pair of beam deflection plates located in the collector box. After a fixed delay the analyzer is gated on and the sample is counted for

Table 2. Count rate and % saturation for various tape speeds

Dial	Kr cts/sec	Rb cts/sec	% Kr sat.	% Rb sat.
840.0	.1586E06	.5706E04	15.86	0.57
700.0	.1873E06	.8108E04	18.73	0.81
600.0	.2152E06	.1089E05	21.52	1.09
500.0	.2528E06	.1539E05	25.28	1.54
400.0	.3060E06	.2338E05	30.60	2.34
300.0	.3870E06	.3967E05	38.70	3.97
250.0	.4454E06	.5503E05	44.54	5.50
200.0	.5235E06	.8133E05	52.35	8.13
150.0	.6314E06	.1318E06	63.14	13.18
130.0	.6861E06	.1659E06	68.61	16.59
100.0	.7829E06	.2472E06	78.29	24.72
80.0	.8561E06	.3375E06	85.61	33.75
60.0	.9295E06	.4815E06	92.95	48.15
50.0	.9613E06	.5841E06	96.13	58.41
30.0	.9973E06	.8559E06	99.73	85.59
20.0	.1000E07	.9739E06	100.00	97.39
10.0	.1000E07	.1000E07	100.00	100.00

another fixed period either at port 1 or port 2 of the MTC. If port 2 is used, the time of travel of the tape from port 1 to port 2 provides all or part of the delay time. For this experiment the variable delay in the tape was set to zero and the distance from the point of beam collection to the center position of port 2 along the tape path was 20.6 inches.

The DA control unit has four timers which may be used in two operational modes. In the sequential mode the following relations hold:

$$\text{Collect} = T_1$$

$$\text{Delay} = T_2$$

$$\text{Accum.} = T_3$$

$$\text{Move} = T_4 \ .$$

This mode is used when it is desired to use the detector at port 1. Table 3 shows the relative activity ratios calculated by ISOBAR (integrated over the counting period) for Kr and Rb for various $(T_{collect}, T_{delay}, T_{count})$. Also shown are the percentage Rb saturation at the beginning of the counting period and a figure of merit, F, which gives an indication of the relative count rate for Rb decay per unit time for the different time settings. F is obtained from

$$F = \frac{(\%\ \text{Rb sat.}) \left[\sum_{n=1}^{T_{acc}/5} (1/2)^n \right]}{(T_{cycle})}$$

where an approximation has been made in using 5 seconds instead of 4.48 seconds for the half-life of Rb.

A high duty factor mode (HDF) was also included in the control unit

Table 3. Isobar results for daughter analysis

(T_{col}, T_d, T_{ct})	% Rb sat.	R_A(Kr)	R_A(Rb)	F
(5,5,5)	33.1866	.189682E00	.809592E00	5.53
(5,5,10)	33.1866	.151625E00	.847225E00	6.22
(5,10,5)	18.1599	.66122E-01	.931772E00	2.27
(5,10,10)	18.1599	.52429E-01	.944519E00	2.72
(5,15,5)	8.8201	.22457E-01	.972420E00	0.88
(5,15,10)	8.8201	.17740E-01	.975090E00	1.10
(10,5,5)	51.3466	.151625E00	.847225E00	6.42
(10,5,10)	51.3466	.120900E00	.877360E00	7.70
(10,10,5)	26.9801	.52429E-01	.944519E00	2.70
(10,10,10)	26.9801	.41523E-01	.954130E00	3.37
(10,15,5)	12.9579	.17740E-01	.975090E00	1.08
(10,15,10)	12.9579	.13998E-01	.976040E00	1.39
(15,5,5)	60.1667	.135691E00	.862668E00	6.02
(15,5,10)	60.1667	.108070E00	.889515E00	7.52
(15,5,15)	60.1667	.96542E-01	.900157E00	7.52
(15,10,5)	31.1178	.46744E-01	.949121E00	2.59
(15,10,10)	31.1178	.36993E-01	.957180E00	3.33
(15,15,5)	14.8775	.15779E-01	.974711E00	1.06
(15,15,10)	14.8775	12439E-01	.974417E00	1.39
(15,15,15)	14.8775	.11042E-01	.971677E00	1.45

for gamma detection at port 2. For the HDF mode:

$$T_1 = 1/2\ (T_{col} + T_{delay} - T_{acc} - T_{move})$$
$$T_2 = 1/2\ (T_{col} - T_{delay} + T_{acc} + T_{move})$$
$$T_3 = 1/2\ (-T_{col} + T_{delay} + T_{acc} - T_{move})$$
$$T_4 = T_{move}$$

and so

$$T_{col} = T_1 + T_2$$
$$T_{del} = T_1 + T_3 + T_4$$
$$T_{acc} = T_2 + T_3$$
$$T_{move} = T_4 .$$

Because the HDF mode allows data accumulation at the second port simultaneously with beam collection at port 1, it is possible to have the analyzer gated on 50% of the time. The general timing case and the particular case of $T_1 = T_3 = 0$ used for this experiment are shown in Figure 13.

The DA runs shown in the spectra in the data results section were made using the HDF mode with $T_2 = T_4 = 10.3$ seconds. This represented the lower limit on T_4 since the fastest controlled tape speed was two inches/sec. For these settings the percentage saturation of Rb at the beginning of the counting period was 26.19% and the activity ratios integrated over the counting period as calculated by ISOBAR for Kr and Rb were .38178E-01 and .957068E00 respectively. As Figure 14 shows, the choice of $T_1 = T_3 = 0$ and $T_2 = T_4$ provided close to the maximum possible integrated activity ratio for Rb with the constraint that $T_4 = 10.3$ sec. The figure of merit, F, assuming $T_2 = T_4 = 10$ sec is 4.91 for this HDF mode. This is nearly a

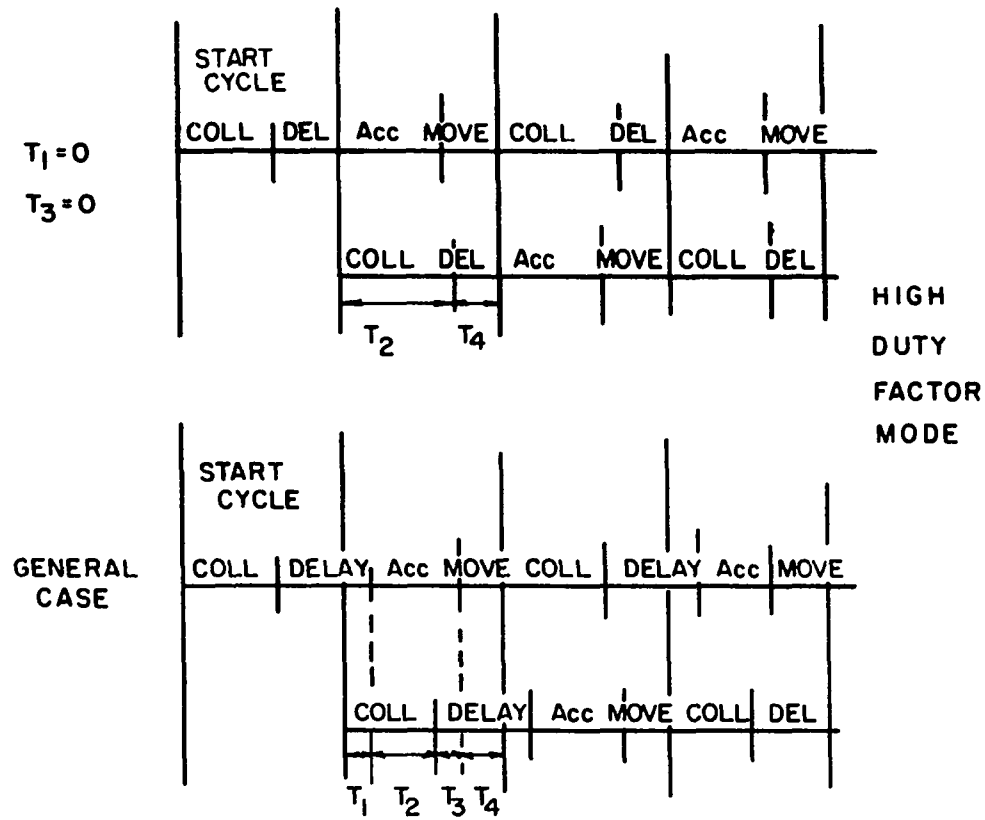

Figure 13. Daughter analysis timing parameters in high duty factor mode

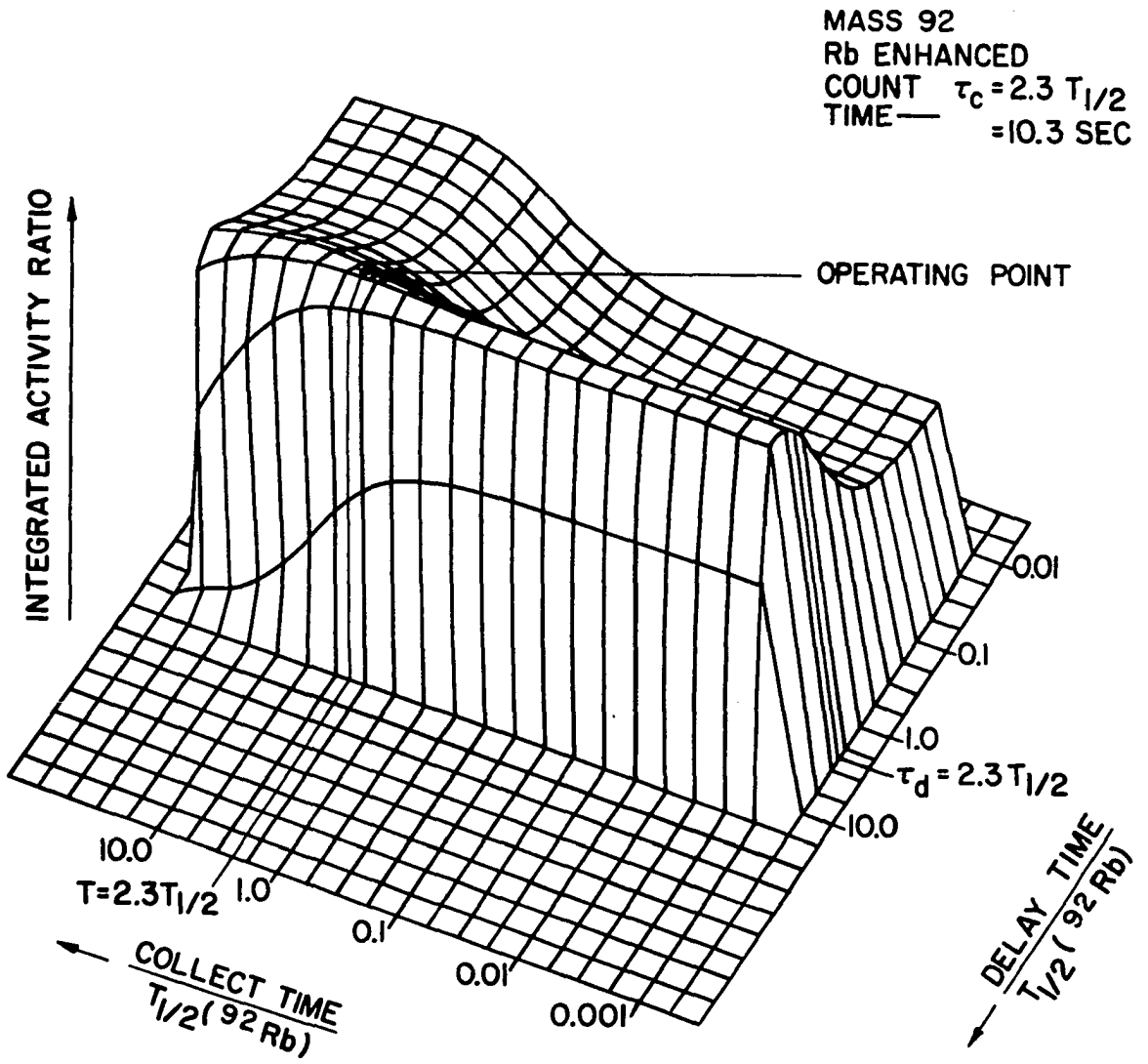

Figure 14. ISOBAR optimization plot for ^{92}Rb decay

50% improvement over the sequential mode of operation where F for a similar R_A(Rb) is 3.37. In fact this latter figure is somewhat high as the figure of merit calculations did not include the amount of time necessary to move the tape from in front of the detector at port 1 to a point behind the shielding (about an additional 2 seconds which would reduce $F_{sequential}$ from 3.37 to 3.16).

With the use of the new MTC, a significant number of Rb decay lines were seen for the first time due to greatly improved statistics. The reasons for this improvement were several. The new MTC allowed the detector to be placed closer to the sample on the tape, increasing the count rate for a given sample strength because of solid-angle considerations. The HDF mode of operation allowed about 50% more counts to be taken per unit time. The ham can system was producing about 50% more mass 92 activity than had the old fission product generator. A better ADC with a much smaller dead time for a given count rate was being used which probably increased the effective count rate by 25%. Finally the DA run was preceded by a three-week period of intensive debugging of the entire detection chain from the preamp to the ADC. This resulted in better integral linearity for gamma-ray energy versus channel number, less system noise (especially 60 Hz) and much improved gain stability. This last factor allowed longer runs to be made with very little shift in peak locations. Seven reels of MTC tape were used in the MT-DA series of runs and the unknown portion of the DA series alone represented 24 hours of data collection.

III. DATA ACQUISITION

With the exception of some early coincidence work for which a 3 x 3" NaI(Tl) crystal was used in one detection chain, all gamma-ray data was taken using Ge(Li) detectors. During the past approximately seven years they have been available, these solid state detectors have revolutionized the science of nuclear spectroscopy. The detailed experimental work reported here would not have been possible without the fine resolution afforded by these crystals.

A Ge(Li) detector is a solid state ionization device in which gamma rays interact with electrons through the mechanism of the photoelectric effect, Compton scattering or pair production. The resultant high-energy electrons create, by ionization, electron-hole pairs which are then collected by an electric field maintained across the detector. The amount of charge collected in a detector operating properly is linearly dependent upon the amount of energy left in the form of high-energy electrons in the intrinsic region of the germanium crystal by the gamma ray. There are a number of good review articles on the fabrication, operation and general characteristics of Ge(Li) detectors (40,41,42,43) and these features will not be discussed here.

The detectors used for this work, along with their relative efficiencies, resolution in the form of the full width at half maximum (FWHM) in keV and the Peak-to-Compton (P/C) ratio for a gamma ray of energy 1.332 MeV (^{60}Co) are listed in Table 4.

The efficiency of a Ge(Li) detector is defined to be that percentage

Table 4. Detectors used

Number	Type	Volume	Relative Efficiency	FWHM	P/C
1	Planar	6 cc	(not available)	1.6 at 122	(n.a.)
2	Trapezoidal Coax	20 cc	1.7%	4.3	8/1
3	Trap. Coax A	27 cc	3.75%	2.82	14/1
4	Trap. Coax B	25.2 cc	3.5%	2.58	16/1
5	True Coax	58.2 cc	9 %	2.24	28/1

of ^{60}Co gamma rays that lose all their energy in the detector compared to the percentage that lose all their energy in a 3 x 3" NaI(Tl) crystal with measurements being made with the front face of the detector being 25 cm from the source in each case. The Peak-to-Compton ratio is the ratio of the height of the 1.332 MeV gamma ray to the height of the highest point of the Compton spectrum just below the Compton edge, with both heights measured from zero counts per channel.

A block diagram of a typical experiment for counting gamma singles data is shown in Figure 15. For the Kr and Rb decay data shown in the results section, the following equipment was used:

Detector: Number 3

Bias: -2000 volts from a Nuclear Data High Voltage Source Model 537

Preamp power: Canberra Industries bin Model 1400

Amplifier: Tennelec TC203BLR linear amplifier with 4 microsec time constants and bipolar pulse

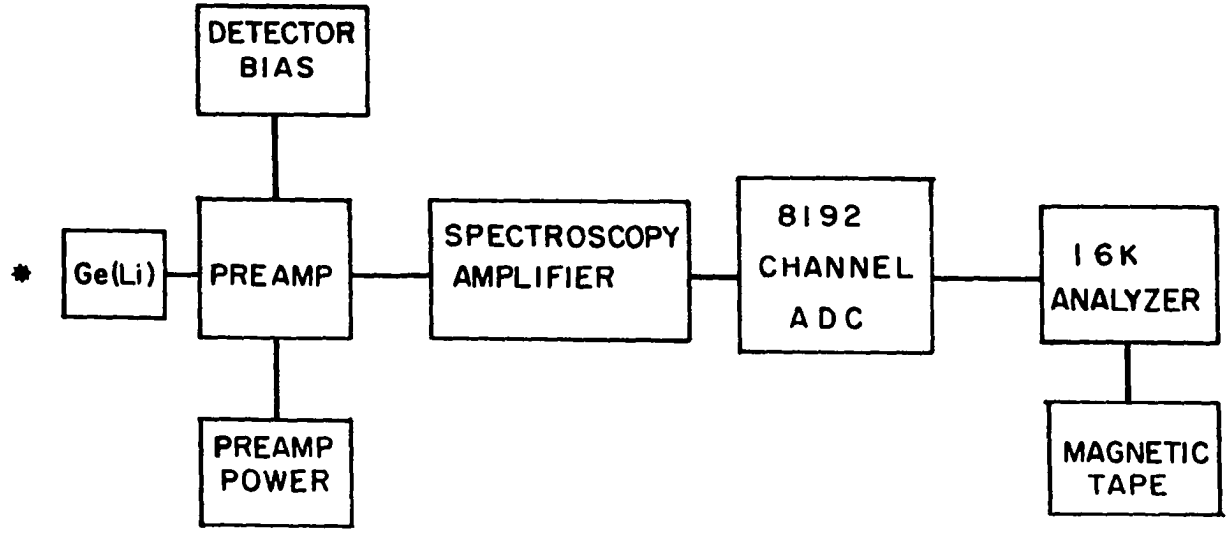

Figure 15. Block diagram of singles detection system

A D C: Geoscience Nuclear Model 8050 using full 8192 channel capacity

Analyzer: Technical Measurement Corporation 16384 channel

Mag Tape: Hewlett-Packard Digital Tape Unit 2020.

For these runs there was 1/4" of plexiglas between the detector and the source at all times as a beta absorber in addition to the 1/16" aluminum window which served as the port in the tape collector.

In the preparation period immediately preceding these Kr and Rb decay runs the detector head preamplifier was remounted from its original BNC connection to the detector to a rigid mechanical connection with the detector housing. This mechanical stability provided a more constant physical configuration which improved the constancy of the preamplifier gain. Prior to this modification, any movement of the head preamp such as a slight rotation of the BNC connector resulted in gain changes of 0.2% (16 channels out of 8192) and more. After the change was made there was long term stability (assuming no major mechanical shocks) of better than 0.01%.

During the preparation period a ground loop problem was diagnosed and alleviated. Because of the large amount of electronic equipment involved in the gamma spectroscopy, the preamplifier power supply and the ADC were mounted in different relay bin racks. When these racks were connected by the ground shield of the signal coax being attached to the ADC, a 60 Hz ripple was observed to appear in the preamp power supply voltages. This ripple was successfully minimized by connecting the equipment bays involved with 4/0 gauge copper wire. As a precautionary measure, grounding

strap was run between all the pieces of detection equipment, including the shell of the moving tape collector.

All singles experiments from which gamma-ray energy information was desired involved four classes of runs:

1) A background run was made before and/or after all the other runs. Where possible the background run was made after the other runs because running the separator would build up long-lived fission product decay chain members in the separator and on the take-up reel in the moving tape collector. All background runs were taken with the reactor in operation at full power.

The background runs were taken with the Ge(Li) detector in the same physical configuration as for the unknown or unknown plus calibration runs. All shielding in place for these latter runs was also used for the background run. The live time of the analyzer system was carefully recorded for the background runs so that they might be compared in an absolute sense with the unknown runs which were of different length (usually longer).

2) A linearity run was made before and/or after the two classes of unknown runs. The linearity run was used to measure the integral non-linearity in the relation between the energy of a gamma ray and the channel number of the corresponding peak in the singles spectrum. An effort was made to keep the dead-time in the ADC (a measure of the count rate) the same for the linearity run as for the unknown runs. Table 5 lists the various isotopes used at one time or another for the linearity runs. The energies listed are those in use by the TRISTAN group. The errors shown in the table were used to help determine the errors in the integral

Table 5. Gamma ray transitions used as standards

Energy (keV)	Delta (E) (eV)	Isotope
59.536	1	^{241}Am
121.779	6	^{152}Eu
145.450	5	^{141}Ce
205.782	14	^{192}Ir
244.68	20	^{152}Eu
279.179	10	^{203}Hg
295.938	10	^{192}Ir
308.440	10	^{192}Ir
316.490	10	^{192}Ir
344.27	30	^{152}Eu
367.77	50	^{152}Eu
411.10	50	^{152}Eu
416.435	30	^{192}Ir
443.96	50	^{152}Eu
468.060	10	^{192}Ir
511.003	2	$m_e c^2 (^{22}Na)$
569.690	30	^{207}Bi
588.557	20	^{192}Ir
604.378	20	^{192}Ir
612.430	20	^{192}Ir
661.615	30	^{137}Cs

Table 5. (Continued)

Energy (keV)	Delta (E) (eV)	Isotope
(688.65)	(50)	(^{152}Eu)
778.90	50	^{152}Eu
814.115 DE[a]	50	^{88}Y
834.840	50	^{54}Mn
846.782	60	^{56}Co
867.38	50	^{152}Eu
898.023	65	^{88}Y
964.05	50	^{152}Eu
1037.851	60	^{56}Co
1063.655	40	^{207}Bi
1085.84	50	^{152}Eu
(1089.74)	(100)	(^{152}Eu)
1112.05	50	^{152}Eu
1173.231	30	^{60}Co
1175.085	70	^{56}Co
1212.95	50	^{152}Eu
1238.290	40	^{56}Co
1274.550	40	^{22}Na
1299.14	50	^{152}Eu
1332.508	15	^{60}Co
1360.219	40	^{56}Co

[a]DE denotes double escape peak.

Table 5. (Continued)

Energy (keV)	Delta (E) (eV)	Isotope
1368.526	44	^{24}Na
1408.01	50	^{152}Eu
1576.561 DE	50	^{56}Co
1732.13 DE	60	^{24}Na
(1770.13)	(100)	(^{207}Bi)
1771.33	60	^{56}Co
1836.127	50	^{88}Y
2015.33	70	^{56}Co
2034.90	60	^{56}Co
2180.17 DE	70	^{56}Co
2231.60 DE	60	^{56}Co
2243.136 SE[b]	60	^{24}Na
2251.15 DE	70	^{56}Co
2429.28 DE	100	^{56}Co
2598.52	50	^{56}Co
2691.17 SE	70	^{56}Co
2742.60 SE	60	^{56}Co
2754.142	60	^{24}Na
2762.15 SE	70	^{56}Co
2940.28 SE	100	^{56}Co

[b]SE denotes single escape peak.

Table 5. (Continued)

Energy (keV)	Delta (E) (eV)	Isotope
3009.62 SP[c]	70	^{56}Co 1771 plus 1238
3202.18	70	^{56}Co
3253.61	60	^{56}Co
3273.16	70	^{56}Co
3445.302 SP	80	^{56}Co 2598 plus 846
3451.29	100	^{56}Co
3589.382 SP	90	^{56}Co 2742 plus 846
4048.962 SP	90	^{56}Co 3202 plus 846
4100.392 SP	90	^{56}Co 3253 plus 846
4119.942 SP	90	^{56}Co 3273 plus 846
4298.072 SP	120	^{56}Co 3451 plus 846

[c] SP denotes sum peak.

non-linearity as a function of the energy.

Not all of the sources listed were used in each linearity run. For example, the linearity runs for the Kr-Rb series shown in the spectra in the results section involved the use of the calibration sources ^{56}Co, ^{60}Co, ^{152}Eu, ^{54}Mn, ^{137}Cs, ^{241}Am and ^{24}Na. The particular choice of sources for a linearity run was dictated by the energy interval being studied in the unknown runs.

3) A run was made with the detector counting simultaneously both the unknown sample and some of the same sources used in the linearity run. Here again an attempt was made to have the dead time be the same as in the run on the unknown alone. These calibration sources were used to provide a gain calibration enabling the energies of some of the stronger unknown lines to be determined as accurately as possible. These strong unknown lines themselves would then serve to provide an internal gain calibration for the unknown alone run. The method by which this gain-calibrating was done is covered in the Data Analysis section.

4) Finally a run was made with the detector counting only on the unknown sample. This run was usually much longer than the others because it was desired to have as good statistics as possible in order to observe the very weak lines.

As each of these runs was completed, the information would be read out from the analyzer onto 7 track magnetic tape for later transport to the computer. During the early experimental work a back-up data set was created on punched paper tape. As faith in the magnetic tape system grew and the stacks of oily paper tape mounted ever higher, this practice was

discontinued and only the magnetic record was made. Each data set was recorded several times on the tape and no time was lost in transferring the records to more permanent form on a disk pack at the Iowa State University Computation Center.

The other type of runs made were Ge(Li)-Ge(Li) coincidence runs. The block diagram in Figure 16 shows the setup for such an experiment where the buffer tape system of data storage during a run was used. This buffer tape system was designed by C. H. Weber of the Reactor Instrumentation Staff. The buffer system format selector is shown in Figure 17.

Earlier coincidence runs had been made using a band sorter on the 16384 channel analyzer. This device allowed up to eight regions to be selected in one side of the coincidence chain. In practice, the bands were set around four gamma rays and correspondingly-sized regions in the Compton background above each of these lines. Then each coincidence was examined and if the channel number in the band side was in one of the bands, the channel number from the other side was incremented in the portion of the memory reserved for that particular band. This allowed eight 1024 spectra to be taken at one time.

The buffer tape system allows all coincidences in a 4096 x 4096 mode to be recorded as they occur. Coincidences are stored in a buffer until 2048 pairs are obtained and then this 4096-number record is written on a magnetic tape. Afterwards, using the format selector shown in Figure 17, bands are selected and the tape(s) replayed through the buffer system. Four regions can be examined at one time when one looks at 4096 channel

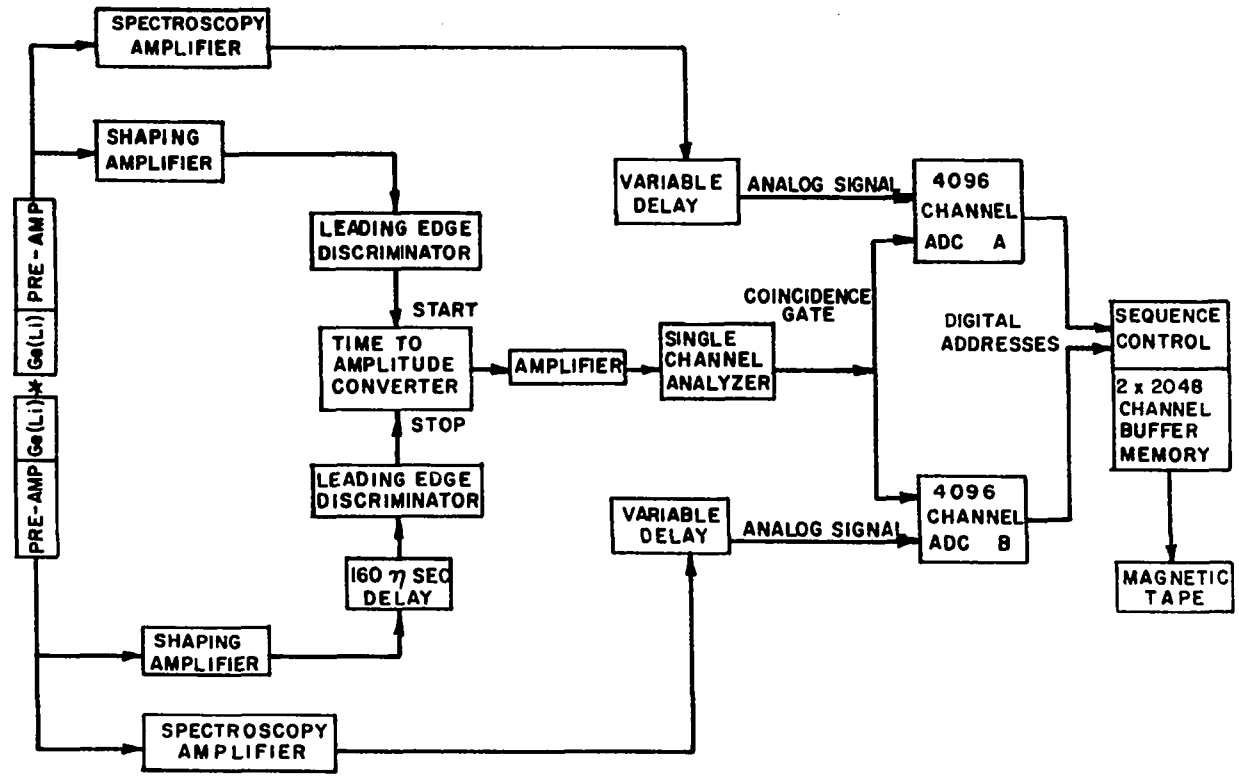

Figure 16. Block diagram of coincidence detection system with buffer system

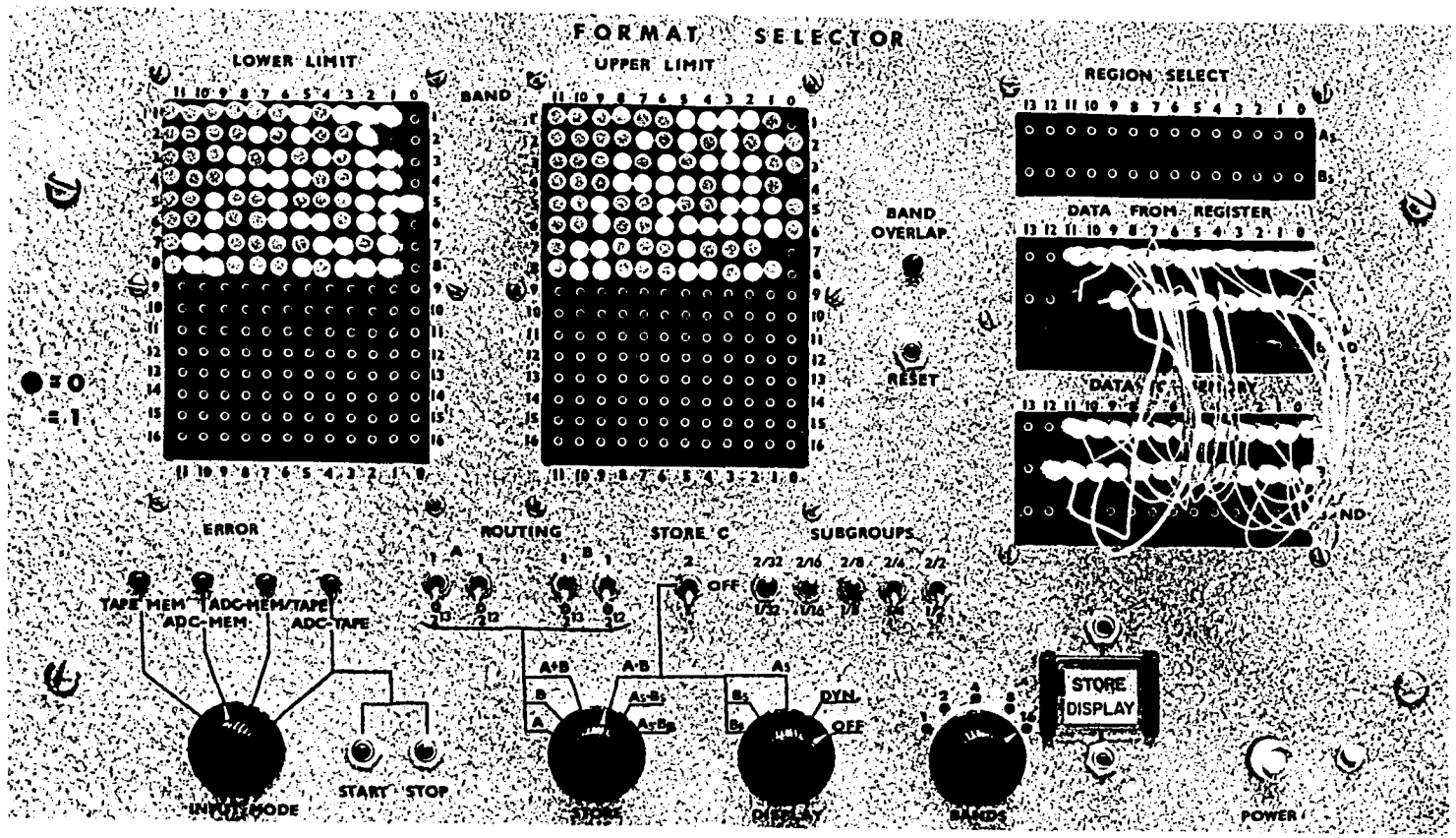

Figure 17. Buffer system format selector

spectra. In effect, each pass of the tape through the buffer system is a repeat of the entire actual experiment but this time with the gates set on the energy on one side. (Only the actual coincidence events are being repeated.) In this manner a coincidence run (consisting of about 3.7×10^6 coincidence events per tape) can be repeated as often as desired, with only about 12-1/2 minutes being required for each tape pass (even though the actual experiment may have required as long as three days to fill one tape). This represents a great savings in experimental time and makes possible gating on peaks which probably would have been ignored had a separate 8×1024 channel run been required for each set of four lines.

For the coincidence run with the buffer system the following equipment was used:

Detectors: Numbers 3 and 4

Bias, preamp power, preamps and analyzer: as before

Amplifiers: Nuclear Data 524 in one chain and Tennelec TC200 in the other

Shaping Amplifiers: Canberra Instruments 1410

Leading Edge Discriminators: Mech-Tronics Nuclear Corp. Pile-up Rejector 904 modified to give LE timing output

Time-to-Amplitude Converter: LeCroy Research Systems Corp. Model 108H-A

Coinc Single Amplifier: Nuclear Data 524

Single Channel Analyzer: Canberra Industries 1430

Variable Delay: Mech-Tronics Nuclear Corp. Model 506

ADC's: Technical Measurement Corp. Model 217A

Magnetic Tape: Precision Instrument PI1200 (for buffer)
Hewlett-Packard 2020 for 7 track tape.

The 4096 spectra resulting from the various passes of the buffer tape with different gate settings were recorded on the 7 track tape unit and transferred to the disk pack to await analysis.

All coincidence runs made were of the form of unknown source alone. The spectra were well-known enough to allow the use of the strong unknown peaks for internal gain calibration.

IV. DATA ANALYSIS

Data analysis was undertaken with the aid of the following computational hardware:

1) Wang calculator Model 360K

2) Wang calculator Model 360KT

3) Hewlett-Packard calculator Model 9100A

4) IBM 360/65 computer system.

Each of these was programmable to some degree. This chapter discusses the specific software and methods used to reduce the raw singles and coincidence data taken to the final results reported in the following chapter. A few of the methods and most of the programs used were in a state of constant change during the course of the experiment and only the final form of each will be described.

Singles data were taken and analyzed first. They yielded gamma ray energies, intensities, and possible gamma level placements. These tentative level placements then provided a starting point for a series of coincidence studies which provided more level scheme information.

Basically the quantities required from each singles spectrum are the following for each peak of interest:

1) Peak "centroid," X_o (strictly speaking not the centroid but the point at which the number of counts per channel is maximum)

2) Peak area, A (and in practice also the peak height)

3) The error in both of the above.

The introduction of Ge(Li) detectors with their excellent resolution has resulted in the observation of increased fine detail in gamma spectra. So many lines are now observed in the average spectra that it has been necessary to automate much of the analysis. Computer programs have been designed to fit the peaks in the spectra to yield the three types of information listed above to the greatest precision possible. The programs used for this work on the singles analysis are known as UPLT, PEAKFIND, SKEWGAUS and DRUDGE. They were all run on the IBM 360/65.

A. UPLT

This program is a utility plot routine which was run on the data first to provide a hard copy of the spectra as they existed on the disk storage at the computation center. These plots were carefully checked for any problems in the data before the time-consuming analysis proceeded. UPLT was written around a Fortran IV routine known as SIMPLOTTER. The actual plotting was done on a Cal-Comp Digital Incremental Plotter at the Iowa State University Computation Center. UPLT is versatile enough to provide for almost any requirements but was usually run in a default mode which could provide the type of plot generally desired (semi-logarithmic) with a minimum of input control data. The plot of each spectrum was then used for the data overview and also as a check on the output from PEAKFIND.

B. PEAKFIND

This is a program which provides automatic identification of peaks in a spectrum in the presence of background. Its operation is similar to that of the method reported by Mariscotti (44).

Because gamma spectroscopy data is discrete in form, the program calculates essentially the second difference of the number of counts as a function of channel number. This difference is averaged over neighboring points to reduce the effect of statistical fluctuations in order that weaker peaks might be identified. This averaged second difference (ASD) tends to vanish everywhere except near a peak. PEAKFIND identifies a peak whenever there is a group of channels with ASD lying at least one standard deviation above zero followed by a group of channels with negative ASD. The ASD's are also checked to see if they have the characteristics of the ASD of a Gaussian with the expected FWHM for the region being tested. This allows Compton edges to be rejected in most cases. PEAKFIND is also capable of determining the presence of a doublet if the two lines are somewhat resolved. Detection of weak peaks and detection of doublets are antipodal in that more smoothing aids in the separation of the ASD of a weak peak from background but tends to wash out the signature of a doublet.

PEAKFIND provides fits and graphs of the fits for those peaks with relative intensity greater than a specified limit, usually two percent of the intensity of the strongest peak found in the search. For the fitting, use is made of the same skewed Gaussian function that is described under SKEWGAUS. In addition to the fits for the stronger peaks, the program punches out, for all peaks found, computer cards which can be used as input for the more detailed fitting program SKEWGAUS. These cards are compared with the plot of the spectra previously obtained from UPLT. Any necessary changes, deletions or additions can then be made and the cards submitted under SKEWGAUS. In this manner the peaks of interest were found and the

effort of punching cards for the next step in the computer analysis was minimized.

C. SKEWGAUS

This is a peak-fitting routine which has three major parts: a subroutine NLLS (45) which does the non-linear least-squares fitting using the Gaussian iteration method; a main subroutine which handles the stream of program execution; and FUNCT which defines the function used for the fitting. The program searches for a best fit to a user-specified portion of the gamma spectra containing up to nine overlapping lines by attempting to minimize $x^2 \equiv Q$ with

$$Q = \sum_i \left(y_{exp}(i) - y_{calc}(i)\right)^2 \cdot W_i$$

where the summation is over the i channels in the fit and y(i) represents the number of counts in channel i. W_i is a weighting factor which takes into account the experimental uncertainty in the number of counts in channel i in the following way:

$$W_i = \left[y(i) + \left(y(i) \cdot (DIFLIN)\right)^2 + CONST \cdot \left(y_{max} - y(i)\right)\right]^{-1}$$

DIFLIN represents the contribution to the uncertainty by the differential non-linearity of the system (all of the channels do not have exactly the same "bin-width"). The CONST term accounts for the fact that the fit is not as good at the base of the peak as it is at the top.

Assuming that Q is a function of the variables a_j which represent such factors as peak location, X_o, peak height, y_o, background terms and peak

shape parameters, SKEWGAUS searches for the a_j which will satisfy

$$\frac{\partial Q}{\partial a_j} = 0.$$

The program takes $a_j = a_{oj} + \Delta a_j$, expands Q in a Taylor's series, discarding all terms of second order and higher in the Δa_j, and solves for the Δa_j with the a_{oj} set equal to the initial approximations for the parameters. The process is then continued with $a_{oj}' = a_{oj} + \Delta a_j$ until Q reaches a minimum or changes by less than a predetermined amount during one iteration, or the error matrix becomes singular (indicating some problem with the fit), or the number of iterations reaches a preset value. If any variable changes by less than a certain small amount specified by the user during an iteration, SKEWGAUS considers that variable to be a constant for the remaining iterations.

After each fit is completed, SKEWGAUS prints out information on the fit, prepares a plot of the fit and the data, and punches for each peak in the fit an input card for DRUDGE which contains the peak location, X_o, the error in X_o, the peak height and its associated error, and peak area computed as a numerical integration over the channels in the fit. The printout contains Q as well as the variance $(Q_{final}/(n-m)$, where n is the number of channels in the fit and m is the number of free parameters in the fit and thus (n-m) is the number of degrees of freedom) which indicates the quality of the fit. The plot of the fit is another good indicator of the success of the fitting method and is usually made with the ordinate in terms of the square root of the number of counts per channel to make it

easier to determine the agreement between the y_{calc} curve and the y_{exp} points in the tail regions. A square root rather than a log plot is used to emphasize the tails because the statistical error bars for points in the former are all one size and are easily plotted.

Errors in the variable parameters are listed in the printout along with the final parameter values and are obtained from

$$\text{Error}(a_j) = [\text{Variance} \cdot A_{jj}]^{1/2}$$

where A_{jj} is the diagonal element of the inverse of the final matrix used to solve the set of linearized equations for the Δa_j.

The fitting function in SKEWGAUS was designed for gamma-ray spectra which are skewed away from a normal distribution by small-angle Compton scattering in beta absorbers placed between the source and the detector crystal (46) and by the non-Gaussian response functions of large Ge(Li) spectrometer systems. This skewness is generally observed on the low-energy side of the gamma line but under some run conditions can be present to a lesser extent on the high side. SKEWGAUS can handle either or both of these skewnesses with a fit function with three regional forms. The fit function form on the low side was derived from an observation that the low-energy tails of gamma peaks appeared quite linear when plotted in a semi-logarithmic form.

In addition to background terms (constant, linear or quadratic) the function contains:

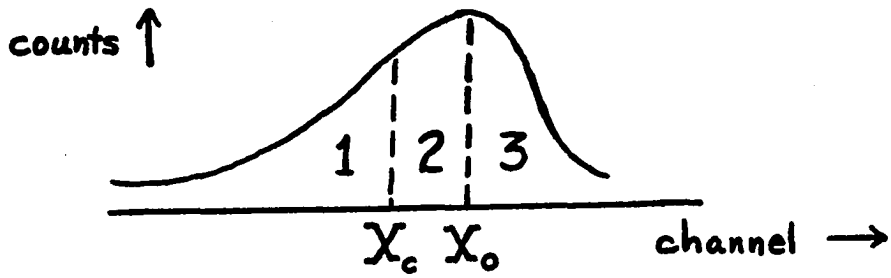

Region 1: an exponential decay and a skewness term (parameter A)

Region 2: a pure Gaussian

Region 3: a pure Gaussian and a skewness term (parameter B).

The analytical expressions in the three regions are:

Region 1: $y = y_o e^{-z_c(2z-z_c)} (1 + A \cdot (z-z_c)^4)$

Region 2: $y = y_o e^{-z^2}$

Region 3: $y = y_o e^{-z^2} (1 + B \cdot (-z)^5)$

where y_o is the height of the fit function at the "centroid" location, X_o,

$$z = \frac{2\sqrt{\ln 2}}{W_o} (x-X_o) \quad ,$$

the "crossover" distance, TAU, is

$$TAU = X_o - X_c \quad ,$$

and W_o is the FWHM at X_o. The exponents of the $(z-z_c)$ term in Region 1 and the $(-z)$ term in Region 3 have been determined empirically for the spectra that have been fit.

In practice the skewness features were not used in all runs. It was found that setting A = B = 0 did not appreciably change the results for X_o and the peak height. The skewnesses were used mainly where it was desired to fit a peak very carefully in order that another much smaller peak present in the tail of the first might be examined more accurately. Good statistics and several strong and isolated peaks were necessary in these cases in order to establish the dependence of the skewness factors A and B on energy. A and B were always found to be small compared to unity and were usually less than zero.

Initial approximations for the parameters in SKEWGAUS were obtained from the output of PEAKFIND. Using results of early SKEWGAUS and PEAKFIND runs on a spectra, the variables FWHM(E) and TAU(E) were linearized as a function of energy. Peaks with a FWHM larger than the value expected were considered likely candidates for doublets and were investigated more closely. Final fits were then obtained for all the peaks desired with FWHM(E) and TAU(E) fixed as a function of energy. A typical SKEWGAUS fit with four gamma rays is shown in Figure 18.

D. DRUDGE

This is a "secretary" routine which performs bookkeeping chores to transform SKEWGAUS output information into transition energies, intensities and concomitant errors. In addition, information is provided concerning possible Compton edges and escape-related peaks. DRUDGE was originally written to provide a release from the tedium of much of the conversion work which was previously done by hand and with desk calculator. It also removed the possibility of errors entering when many numerical quantities

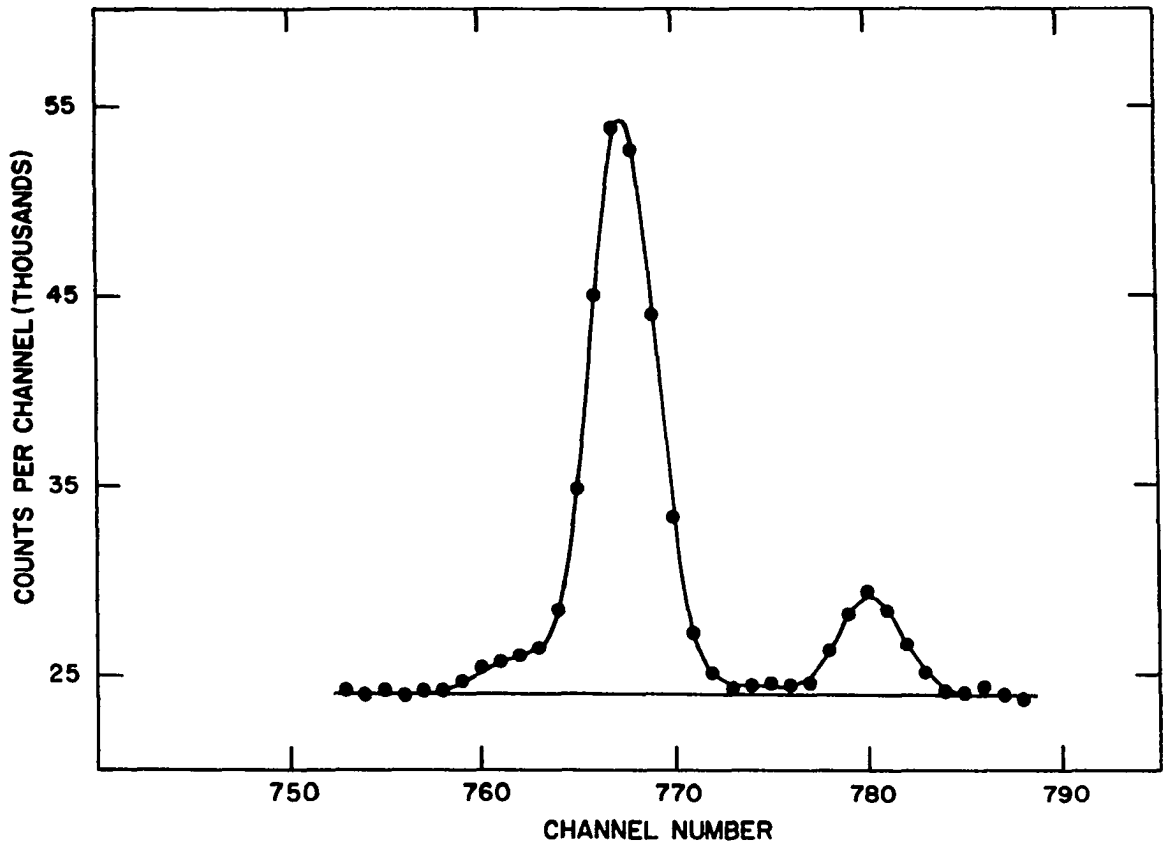

Figure 18. Typical SKEWGAUS fit to gamma-ray multiplet region

were being manipulated and transposed by hand. Finally, it made possible the easy repetition of tedious calculations very quickly if an error was discovered in the early stages of the analysis or if some change was desired, say, for example, in the line chosen for intensity normalization. This last feature came to be a most useful asset.

The use of DRUDGE required the existence of data from three gamma runs: a linearity calibration (I), an unknown plus calibration run (II), and an unknown alone (III). Also required were tables of the energy dependence of the relative efficiency of the detector, of the relative attenuation of the gamma rays from the unknown source due to absorption external to the detector window, and of the ratios of the intensities of the single- and double-escape peaks to the intensity of the associated photopeak (calculated for practical reasons using escape peak intensities that are corrected for the relative efficiency of the detector at their apparent energy).

The relative efficiency of one of the trapezoidal coax detectors used for this work was determined using the calibration sources ^{133}Ba, ^{152}Eu and ^{56}Co. The resulting curve is shown in Figure 19. The errors shown on the points are $\pm$ 5%.

The absorption table was prepared using the National Bureau of Standards X-ray attenuation coefficients (47,48). For the spectra shown in the results section, the table incorporated the total experimental attenuation (less coherent scattering) of the 1.59 mm aluminum window in the MTC and 6.35 mm plexiglass beta absorber taped to the front of the Ge(Li) housing.

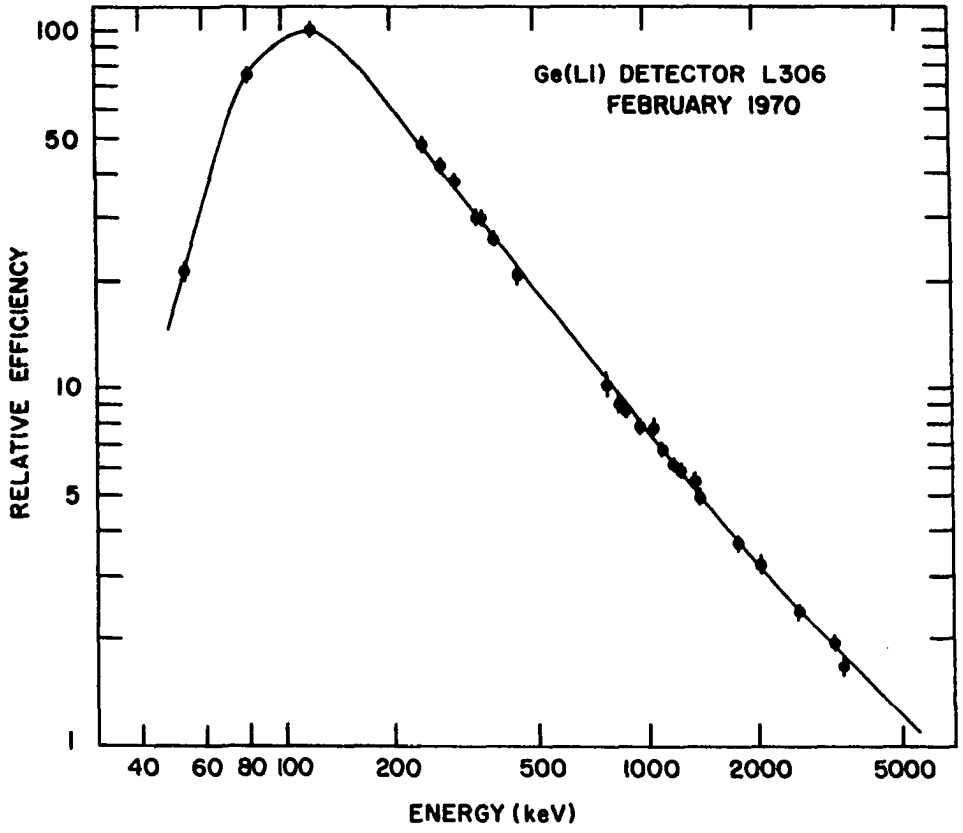

Figure 19. Relative efficiency curve for detector No. 3

The ratios of the single- and double-escape intensities to the photopeak intensities were determined from several sources with known escape peaks and extended with lines from several experimenters' work. Figure 20 shows the resultant curves used for DRUDGE with some of the experimental points indicated.

The operation of DRUDGE in converting channel numbers into energies is based on the relation

$$E_i = aX_i + b + c_i \quad .$$

E_i is the gamma-ray energy associated with channel number X_i. $\underline{a}$ is the overall system gain in keV/channel and $\underline{b}$ is the energy intercept for channel number zero (both $\underline{a}$ and $\underline{b}$ are determined for each run). The integral non-linearity in the relation between the energy and channel number is taken into account by the c_i term. It is assumed that drifts in the system calibration from run to run are small and that their effects can be contained in the a and b. Since c_i is a small term, any correction to it is of second order and is neglected. The c_i are determined only once (actually as a function of energy rather than channel number) for a series of runs using the linearity calibration run I.

The correction for the integral non-linearity was derived manually. Several "convenient" pairs of data (E_{true}, X_I) were chosen and a straight line fit to them was found by a least squares method with one of the desk calculators. This line was then used to determine a new set of pairs (E_{LSQ}, E_{true}). A graph of $\Delta E = E_{LSQ} - E_{true}$ versus E_{LSQ} was drawn (see Figure 21 for an example) and used to construct a tabulation suitable for

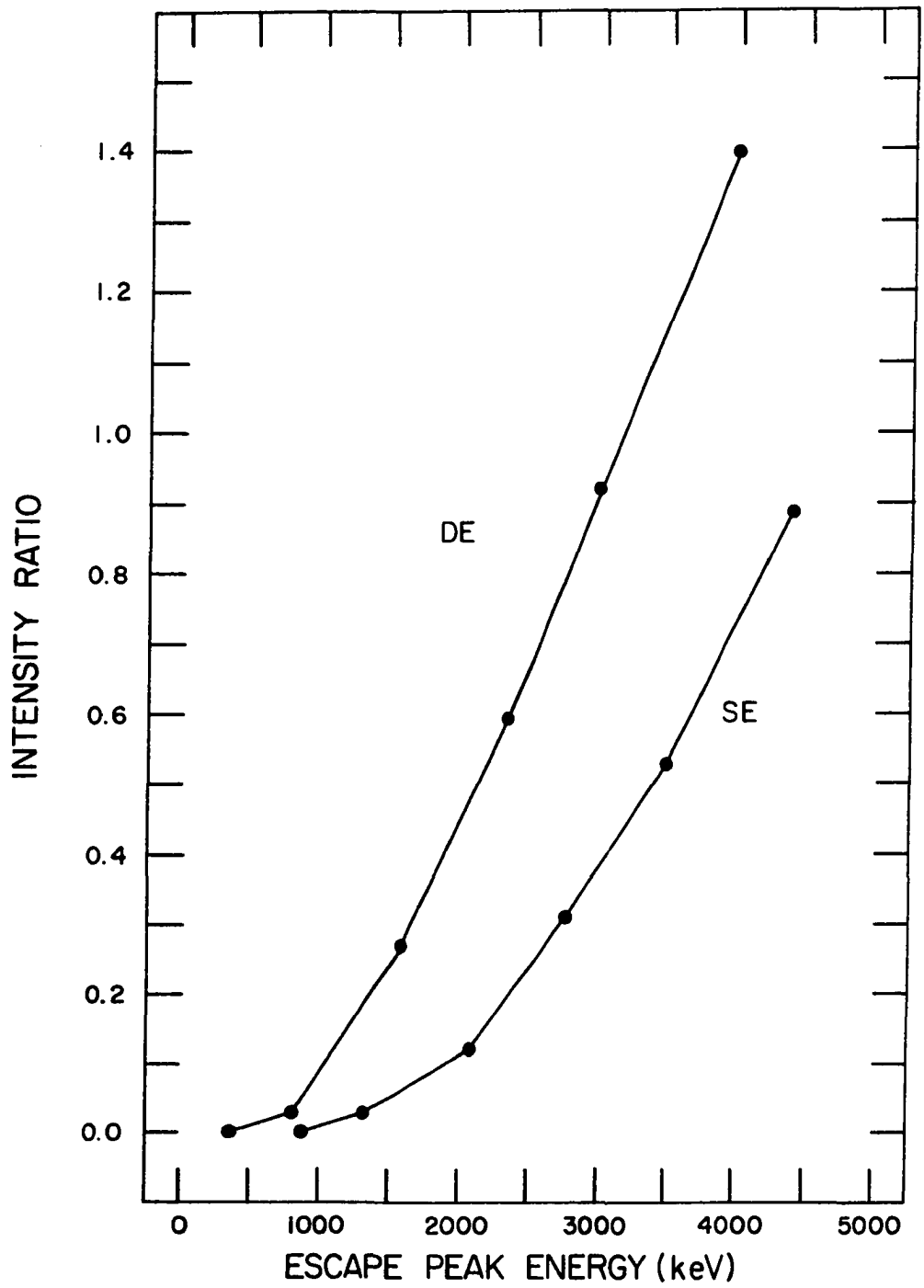

Figure 20. Ratios of single and double escape peak intensities to photopeak intensities versus escape peak energy for detector No. 3

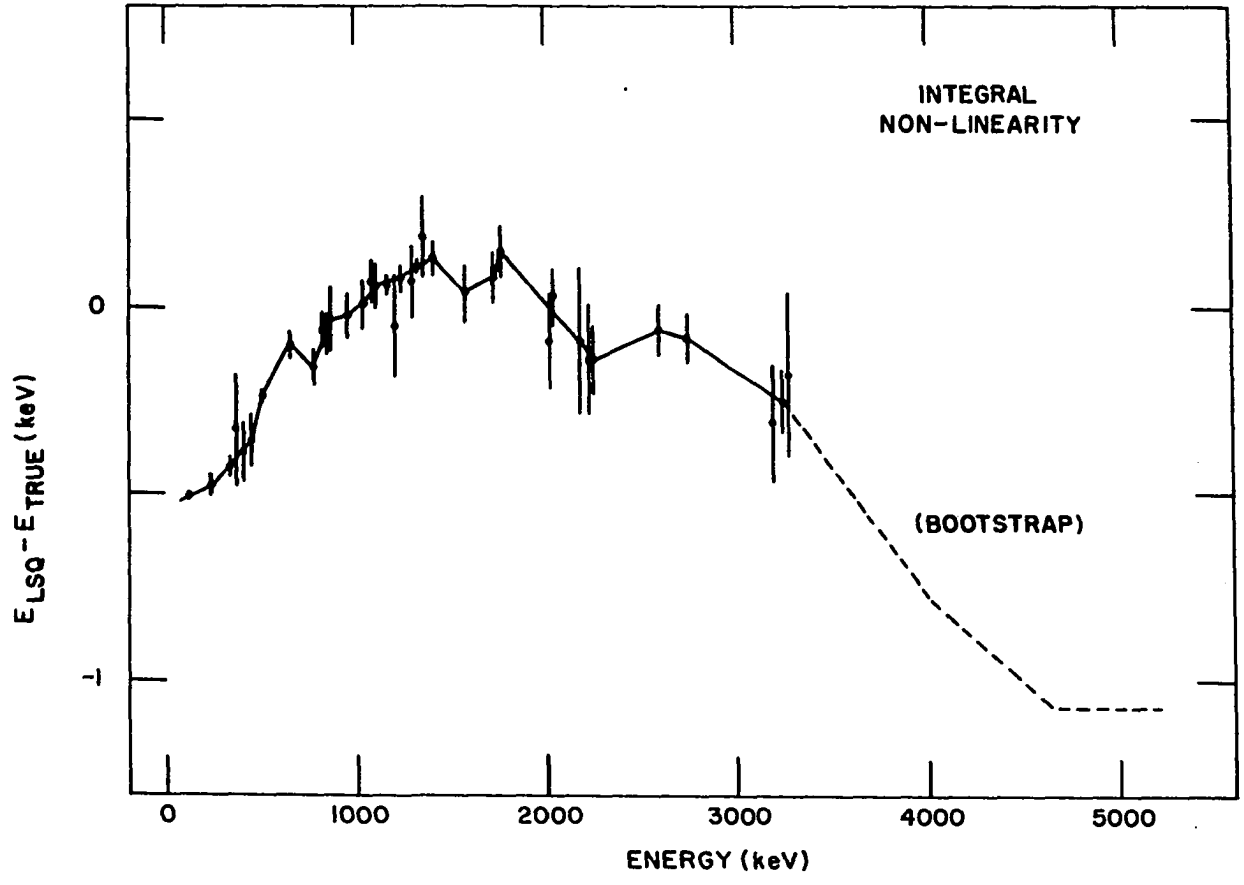

Figure 21. Typical detection system integral non-linearity as a function of energy

linear interpolation to be input to DRUDGE. (As indicated in Figure 21, after escape peaks had been identified, they were used to "bootstrap" the integral non-linearity out beyond the region where calibration source lines were available.) At this point the errors in the integral non-linearity were also determined to be used by the program in finding the overall error in the gamma-ray energies calculated.

The use of DRUDGE then began on data set II with the input quantities mentioned above. The calibration lines in II to be used were identified to the program which then determined a_{II} and b_{II} by first correcting the E_{true} of these lines to E_{LSQ} values and then finding the least squares straight line through the latter quantities. E_{LSQ}, ΔE and then $E = E_{LSQ} - \Delta E$ were then calculated for all the channel numbers input from II. Errors in the energies were calculated as the geometrical sum of two standard deviations of the error from SKEWGAUS and the estimated error in the non-linearity.

DRUDGE was then run on the data of run III with several strong unknown lines whose energies were determined from II being used to find the system gain a_{III} and intercept b_{III}. The energies and errors of all input channel numbers were found as in II. Run III allowed the close examination of weak unknown lines which may have been obscured by calibration lines or Compton background in II.

Relative intensities were calculated with DRUDGE using log-log interpolation on the relative efficiency and absorption tables. Intensities were normalized with a chosen transition set equal to 1000. Errors in the intensities were calculated as the geometrical sum of twice the error

(Δ height/height) as determined by SKEWGAUS and an estimated 5% uncertainty in the efficiency calibration.

The program prints out the input and the results of calculations for energies, intensities and errors. Any Compton edges which might disturb a peak are listed. Finally, DRUDGE lists possible escape-related peaks along with their expected intensity ratios for comparison.

Any peaks found to be disturbed in intensity by more than 10% by Compton edges or escape peaks were refit using SKEWGAUS. When all fits were considered complete, a final DRUDGE run was made.

When the results from DRUDGE for the Kr decay run shown in the results section were compared with other Kr decay runs, the higher-energy lines were found to have enhanced intensities. This is the "collimator effect" described in an earlier section.

Extensive calculations were undertaken to try to find the exact mechanism by which the higher-energy lines were being enhanced. A numerical integration of the "shadow effect" (performed on the Hewlett-Packard calculator) was the last method tried. It reproduced the effect qualitatively (the levelling off of the effect at low and high energies and the rapid change from about 300 keV to about 1200 keV) but did not predict the magnitude of the effect correctly. Instead it was found necessary to correct for the collimator effect by taking another singles run at Port 1 of the MTC in the following mode: the beam was deposited on the fixed tape for three seconds while the analyzer was gated on, then the beam was deflected and the analyzer gated off while the collection point on the tape was moved to a spot well behind the external shielding. The

deposition and counting were then started again. Approximately 2500 cycles were taken to obtain good statistics. The intensities of the strong gammas from the MTC run with the enhanced lines were then compared with the same gammas in the "fixed-tape parent enhancement" run and the collimator effect found (as a function of energy) is shown in Figure 22.

At this point the value of DRUDGE as a time-saver became apparent. The correction to the intensities due to the collimator effect was "folded" into the efficiency table used previously. Another quick run of DRUDGE with this new table then yielded the final intensities.

E. Isotopic Assignment of Transitions

After gamma energies and intensities were obtained from singles runs and the single- and double-escape peaks were removed, isotopic identification of the lines had to be made before continuing with level scheme work. First, lines which could be attributed to background were removed with the aid of the background spectra that had been taken. Contributions from other isotopes were then identified and removed.

Reduction of the ^{92}Sr decay lines was easy because other workers had previously found both the ^{92}Y decay lines (26) and the lines from the $^{91}KrH^{+}$ daughter ^{91}Sr (37). Work done on the ^{91}Kr and ^{91}Rb decays by others using TRISTAN (49) made possible the removal of these hydride contaminant lines from the ^{92}Kr and ^{92}Rb decays.

^{92}Rb decay lines in the ^{92}Kr decay runs and <u>vice versa</u> were identified by comparing pairs of runs, one of which had the parent Kr decay enhanced and the other of which had the daughter Rb decay enhanced. Such a Kr-Rb

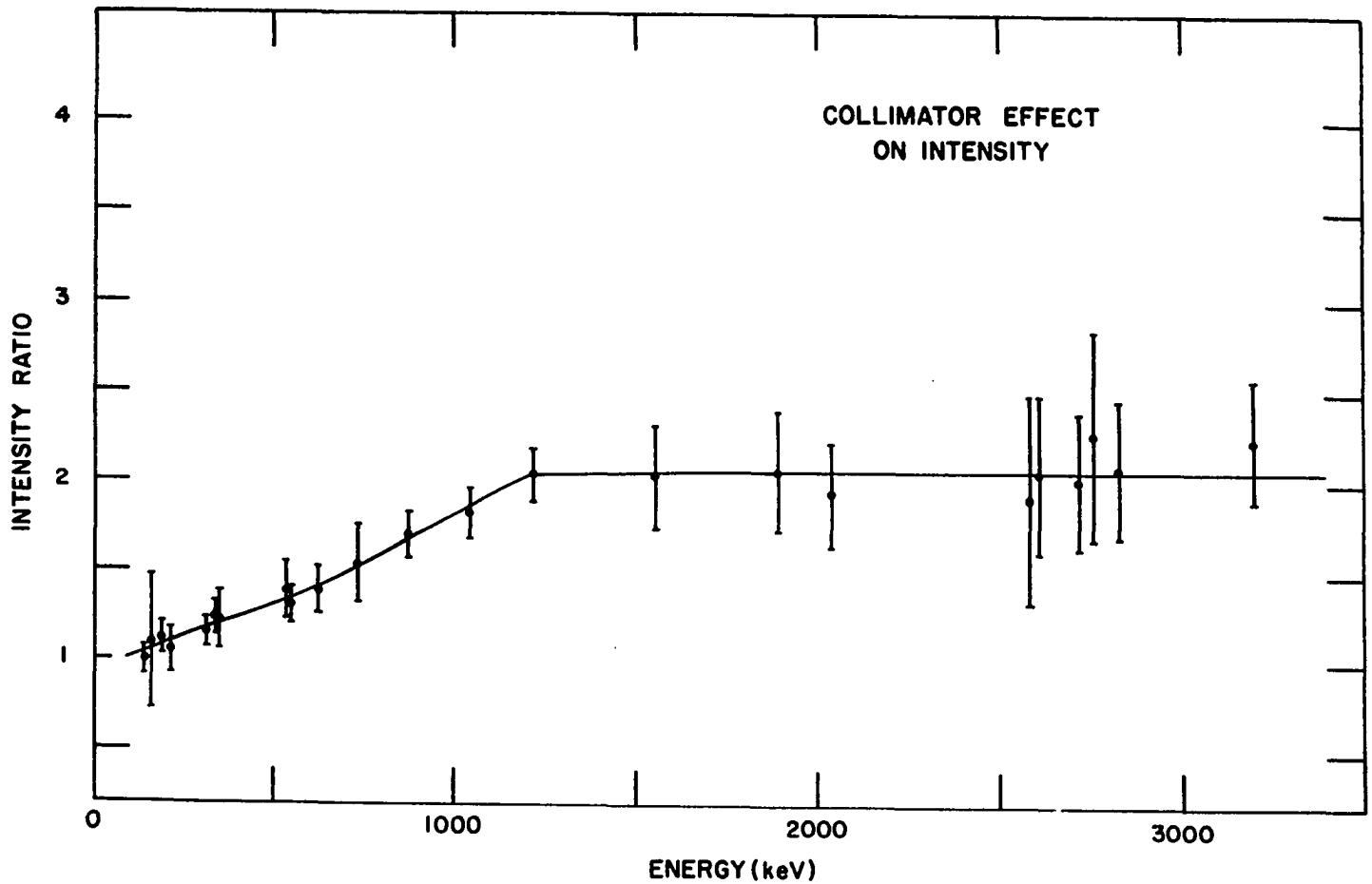

Figure 22. Collimator effect for ^{92}Kr decay as a function of energy

series is shown in the spectra in the results section. For this series an intensity ratio map (plot of the ratio of the intensity of a gamma in the Rb enhanced run to the intensity of the same line in the Kr enhanced run) was made and is shown in Figure 23. The identities of some of the strong Kr lines and of one of the Rb lines were known from previous half-life measurements (25) and this allowed the demarcation of the regions of Kr and Rb decay lines on the plot. Some background lines (such as the two from ^{60}Co) enabled the background region to be fixed.

Because of the way the runs were normalized, the Kr line ratios cluster around unity, fairly independent of the energy. The intensity of the Rb lines in the Kr run had been corrected along with the intensity of the Kr lines when the collimator effect was removed. Since the Kr and Rb decays have different half-lives and the collimator effect is half-life dependent (the greater the percentage of activity left on the tape as it passes through the "shadow region," the greater will be the effect) the intensities of the Rb decay lines were not quite right and there is a slight downward trend of these latter points on the graph as a result.

The average enhancement shown for the Rb lines over the Kr lines between the two runs is about a factor of 110 to 120. ISOBAR was used to calculate an expected enhancement factor between the daughter analysis run of (10.3, 10.3, 10.3) and the moving tape run with a dial setting of 300. The result was an enhancement factor of 130 which is quite good agreement with the experimental enhancement.

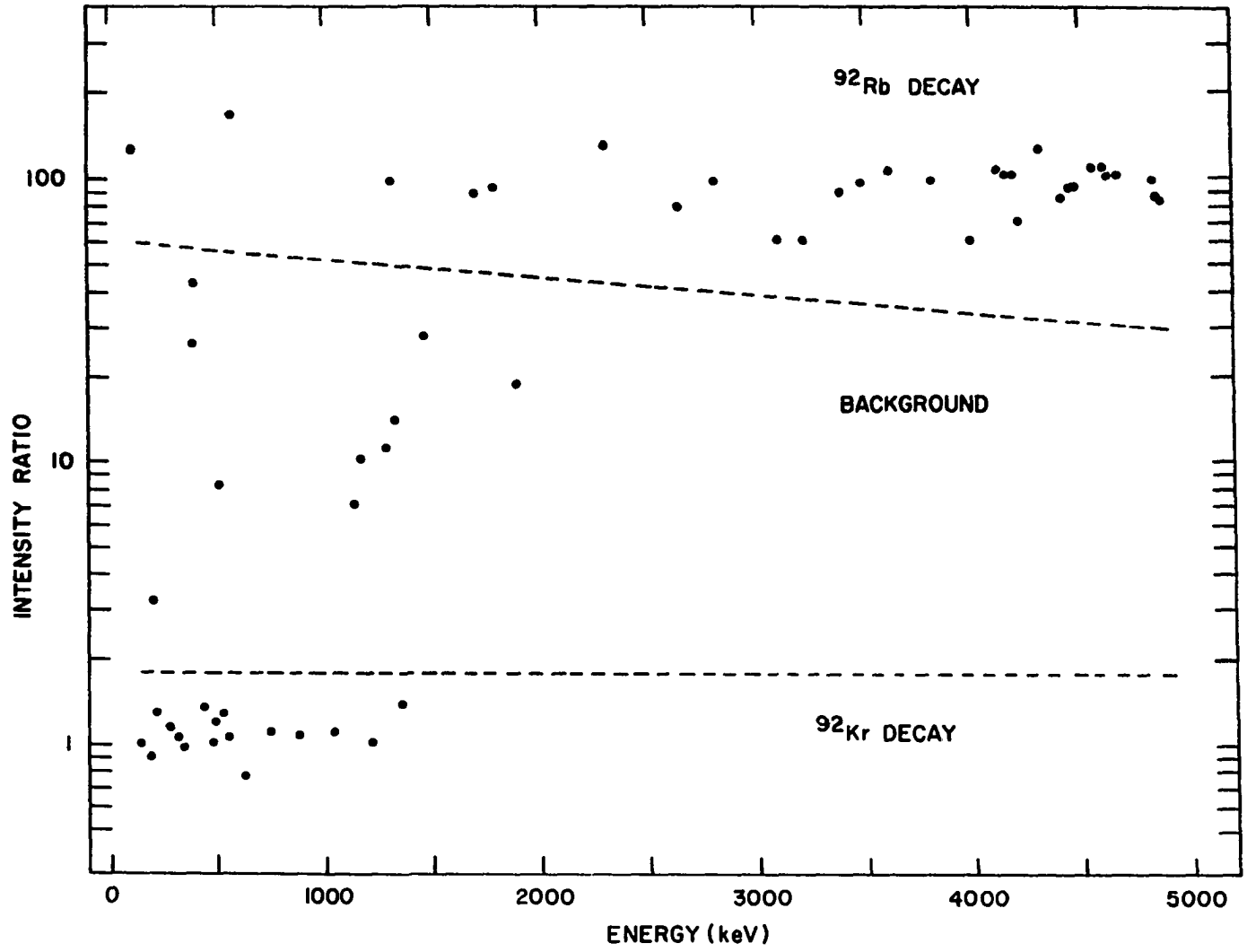

Figure 23. Intensity ratio map used to identify isobars and contamination transitions

F. Coincidence Data and Level Scheme Construction

Once lists of gamma rays had been prepared for the decays of ^{92}Kr, ^{92}Rb and ^{92}Sr, the work on the level schemes of ^{92}Rb, ^{92}Sr and ^{92}Y was begun. A computer program, ESUM, provided one of the most useful ways of placing gammas by combining all possible transitions with the crossover sum rule:

$$E_1 + E_2 = E_3 \, .$$

The program searched for and listed all gammas for which this relation was satisfied to within a certain error. If this error was less than the sum of the experimental errors of the three transitions involved, then this sum rule was taken to represent the possible placement:

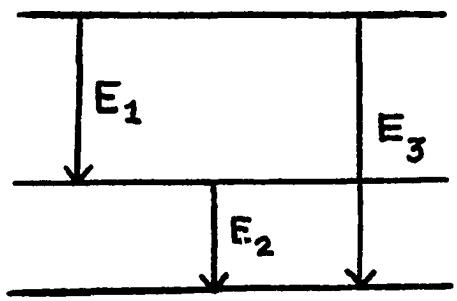

Additional help was obtained late in the level scheme construction by using ESUM to consider a more complex sum rule of the form:

$$E_1 + E_2 = E_3 + E_4 \, .$$

Before any two-parameter data were taken, the sum rules were used to construct tentative level schemes. Intensities of the transitions were considered insofar as it was desired to have the sum of the gamma intensity feeding a level to be less than or equal to the sum of the intensity of

gamma depopulation for that level, the inequality allowing for beta feeding. This relation was sought because internal conversion could be neglected in almost all the cases being considered.

These tentative level schemes were valuable in proposing coincidence gates in the early work when the band sorter was being used and only four gammas and their backgrounds could be investigated at one time. After the buffer tape system became available, this type of information was no longer so useful. Essentially all the possible coincidences could be tested if the statistics were good enough.

Most of the coincidence data was analyzed using computer plots to compare the spectrum resulting from a gate on a given transition with the spectrum resulting from an equal-width gate set on the Compton background above this peak. In some cases the statistics were good enough to permit computer fits to be made on the spectra to get the peak areas. In other cases, areas were obtained by summing the counts under the peaks by hand and subtracting the background. But the majority of the data was only good enough to provide a yes, no, or maybe answer to the question of possible coincidence and for this the plots were sufficient. One of the better pairs of coincidence slices is shown in Figure 24. The enhanced lines are labelled in the lower slice which is gated on the 191 keV gamma in ^{92}Kr decay.

The results of the coincidence runs, the output from ESUM and the relative intensity of the transitions were all combined to draw up the level schemes. The number of transitions observed for ^{92}Sr decay was small

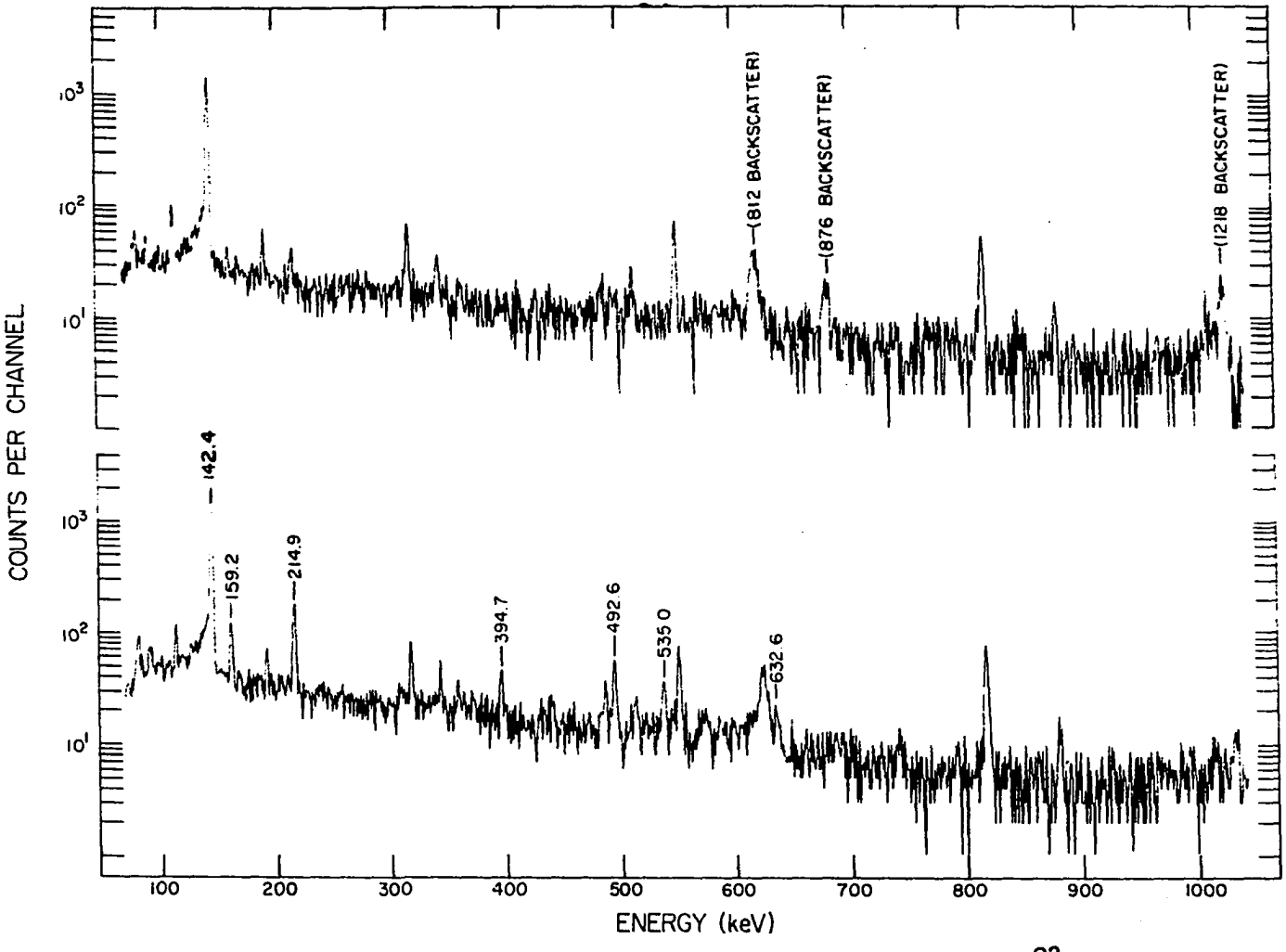

Figure 24. Coincidence gate and background slices for 191 keV gamma in ^{92}Kr decay

and it was possible to fit all of them into a level scheme for ^{92}Y. The numbers of transitions for ^{92}Kr and ^{92}Rb decay were much greater and there were several different alternative placements for many of these gammas.

The following rules were used for the levels in ^{92}Rb (for which there was a good deal of coincidence information):

1) The level was kept if it came from a coincidence relation with one of the gammas already placed.

2) The level was kept if there were at least 3 outgoing transitions or 2 outgoing and 2 or more incoming.

3) The level was kept if only 3 transitions exist for it or it is fed from another dotted level. In this case, the level was dotted.

4) If the level did not meet any of the above requirements, it was still kept if it did not involve the placement of any ambiguous gammas.

There were only two pieces of coincidence information for the ^{92}Sr level scheme. The rules in this case were:

1) There was a level if there were at least 2 gammas depopulating it. The level was dotted if there were only 2.

2) There was a firm level if 3 gammas fed or depopulated it.

3) There was a firm level if there existed a transition to the ground state.

After the transitions had been placed in the tentative level schemes, the percentage depopulation, D_{ij}, was determined for the $i^{\underline{th}}$ gamma de-exciting the $j^{\underline{th}}$ level. This gamma ray had energy E_{ij}. The final level energies, E_j, were then found using

$$E_j = \sum_i \frac{D_{ij}}{100} \times (E_{ij} + LE_{ij})$$

where LE_{ij} was the energy of the level fed by gamma ray E_{ij}. ΔE_j was found by weighting the errors contributed by the depopulating gammas in a similar manner.

G. Beta Feeding and Log Ft's

For the calculation of the log ft for a beta-branch to a particular level in a nucleus reached by beta decay, it is necessary to know the partial half-life of the branch decay or the percentage of the total beta feed which goes to that level. The only experimental beta evidence for the three decays studied for this work is a measurement by Heath (23) determining that 90 ± 10% of the ^{92}Sr beta decays are followed by the emission of the 1383.9 keV gamma. With this piece of information and with a complete level scheme incorporating all of the ^{92}Sr decay gamma lines observed, it was possible to calculate all of the beta-feeding percentages for the levels in ^{92}Y. In the same paper, Heath reported a value of 0.545 MeV for the beta group found to be in coincidence with the 1383.9 keV gamma ray. This beta endpoint energy gave a Q-value of 1.929 MeV for the ^{92}Sr beta decay. The energies for the beta decays to the excited levels of ^{92}Y were then determined using this Q-value and were combined with the beta feeding percentages to yield the log ft's of interest.

Experimental Q-values for ^{92}Kr or ^{92}Rb beta decay were not available at the time of this work. Instead, values were obtained from averages of

the predictions of the semi-empirical mass law of Seeger (50) and the recursion relation of Garvey and Kelson (51). The average results calculated were

$$Q_{Kr} = 5.01 \text{ MeV}$$

and

$$Q_{Rb} = 8.00 \text{ MeV}.$$

Experimental measurements of the absolute percentage of beta branching to levels in ^{92}Rb and ^{92}Sr have not been made yet. In such cases it is common to take the beta-feeding to the ground state to be zero as a first approximation. If the true ground state feeding is not large, this does not introduce a great error. (Of course, the log ft for beta decay to the ground state cannot be calculated at all in this instance.) During the course of these gamma measurements, a subjective observation had been made that there seemed to be much less gamma activity following the beta decay of ^{92}Rb than might be expected if the ground state beta branch were indeed small. This observation served as an incentive for the development of a method to determine the absolute beta feeding percentages for ^{92}Kr and ^{92}Rb decay indirectly from gamma-ray data and from the measured absolute percentages known for ^{92}Sr decay. The procedure described below provides a quantitative estimate of the percentage beta feeding to the ground state. In doing so, it also allows the calculation of the log ft for beta decay from the even-even ^{92}Kr ground state (probably 0^+) to the ground state of ^{92}Rb, and from the latter to the ground state of even-even ^{92}Sr (probably 0^+).

The procedure has three requirements for its use. First, there must

be simultaneous detection of the gamma activity from the decay of a nuclide (in the beta chain of the unknown) for which the absolute gamma intensity for one gamma or the percentage beta feeding for one excited state is known. (In the case under consideration, the absolute gamma intensity was known for the 1383.9 keV gamma following the decay of ^{92}Sr.) Second, most of the gamma intensity for the unknown nuclide should be placed in the level scheme for the decay of that nuclide and the relative beta feeding to the excited states of the daughter of that nuclide should be fairly well determined. (This was true for the level schemes following ^{92}Kr and ^{92}Rb in the cases studied here.) Finally, the parameters of the MTC run must be known for input to ISOBAR (except in the special case of an equilibrium run which would not require the use of ISOBAR).

The case of the beta feeding from ^{92}Rb to the ground state of ^{92}Sr will be considered as an illustrative example of the procedure used. ^{92}Sr decay lines and ^{92}Rb decay lines were simultaneously observed in a MTC run with parameters (30, 10, 30) sec. When these parameters were input to ISOBAR, the following integrated activity ratios were obtained (note that this run enhanced the observation of ^{92}Rb decay):

^{92}Kr:	0.027044
^{92}Rb:	0.946654
^{92}Sr:	0.026271
^{92}Y:	0.000031 .

Then the ratio of the number of betas for ^{92}Rb decay to the number of betas from ^{92}Sr decay was just

$$\frac{0.946654}{0.026271} = 36.0 \quad .$$

The intensity of the 1383.9 keV line from ^{92}Sr decay was determined in this case from the intensities measured for the four strongest gammas (including the 1383.9) from ^{92}Sr decay and the relative ^{92}Sr gamma intensities previously determined in another gamma run. The 1383.9 keV line was found to have a gamma intensity of $(1.89 \pm 0.09) \times 10^5$ (in relative units). Using Heath's determination that (90 ± 10) % of the ^{92}Sr decay betas are followed by a 1383.9 keV gamma, the amount of ^{92}Sr beta decay for this run was determined to be

$$\frac{(1.89 \pm 0.09) \times 10^5}{0.9 \pm 0.1} = (2.10 \pm 0.23) \times 10^5 .$$

Using the ratio found above, the amount of ^{92}Rb beta decay for this same run then had to be

$$(36.0) \times (2.10 \pm 0.23) \times 10^5 = (7.57 \pm 0.85) \times 10^6$$

in relative intensity units. The beta feed to the excited levels in ^{92}Sr for this run was calculated from the relative intensities of five ^{92}Rb decay lines and the knowledge of the level scheme for levels in ^{92}Sr reached by beta decay which had already been developed from the gamma spectroscopy work. The beta feed to these excited states was determined to be $(4.52 \pm 0.35) \times 10^5$ (in relative intensity units). The beta feed to the ground state of ^{92}Sr for this run was then found to be

$$(7.57 \pm 0.85) \times 10^6 - (4.52 \pm 0.35) \times 10^5 = (7.12 \pm 0.88) \times 10^6 .$$

The percentage beta feed to the ground state of ^{92}Sr was then easily

determined to be

$$\frac{(7.12 \pm 0.88) \times 10^6}{(7.57 \pm 0.85) \times 10^6} = 94\ (+6, -20)\ \% \ .$$

The percentage beta feeding to the rest of the excited levels of ^{92}Sr could also be determined since they must sum to the remaining 6%.

The ground state beta-feeding percentages were determined in two different runs each (different run parameters for both ^{92}Kr and ^{92}Rb beta decay). The following assignments were made for the ground state beta feedings:

^{92}Kr to ^{92}Rb: 50 ± 15 %

^{92}Rb to ^{92}Sr: 94 (+6, -20) % .

The calculated beta feeding percentages for ^{92}Kr and ^{92}Rb decay were then combined with the Q-values mentioned earlier to obtain the log ft's reported in the next section.

V. RESULTS

The results of the studies of the ^{92}Kr, ^{92}Rb and ^{92}Sr decay schemes are summarized in three forms for each of the decays observed. First, a "typical" gamma-ray spectrum is presented, with most of the observed transitions labelled with gamma-ray energy and also with identity for those peaks due to isobaric activity other than the one enhanced or due to contaminant and/or background sources. Secondly, tables are given which summarize the results of all spectra which have been taken for the isobaric decay. These tables list transition energies and uncertainties, E(ΔE), and intensities and uncertainties, I(ΔI), as determined by the computer program DRUDGE as described in the Data Analysis chapter. The tables also indicate the placement of the transition in the daughter nucleus level scheme, where applicable, and observed coincidences, if any (the symbol (?) indicating a weak coincidence or poor statistics and (??) standing for an uncertain coincidence observation). Gamma-ray peaks which have been identified as single- or double-escape events are also tabulated, along with their associated full-energy transitions. Beta branching and calculated log ft values are given for levels in the daughter nucleus which are fed by beta decay. Finally, level schemes are shown, as determined from considerations outlined in the chapter on Data Analysis. The discussion of the level schemes is the subject of the following chapter.

A. ^{92}Kr Decay

Figures 25a-f show the spectra of a moving tape collector run (from 0 to 5.2 MeV) with a tape speed of 1.87 cm/sec to enhance the decay of the

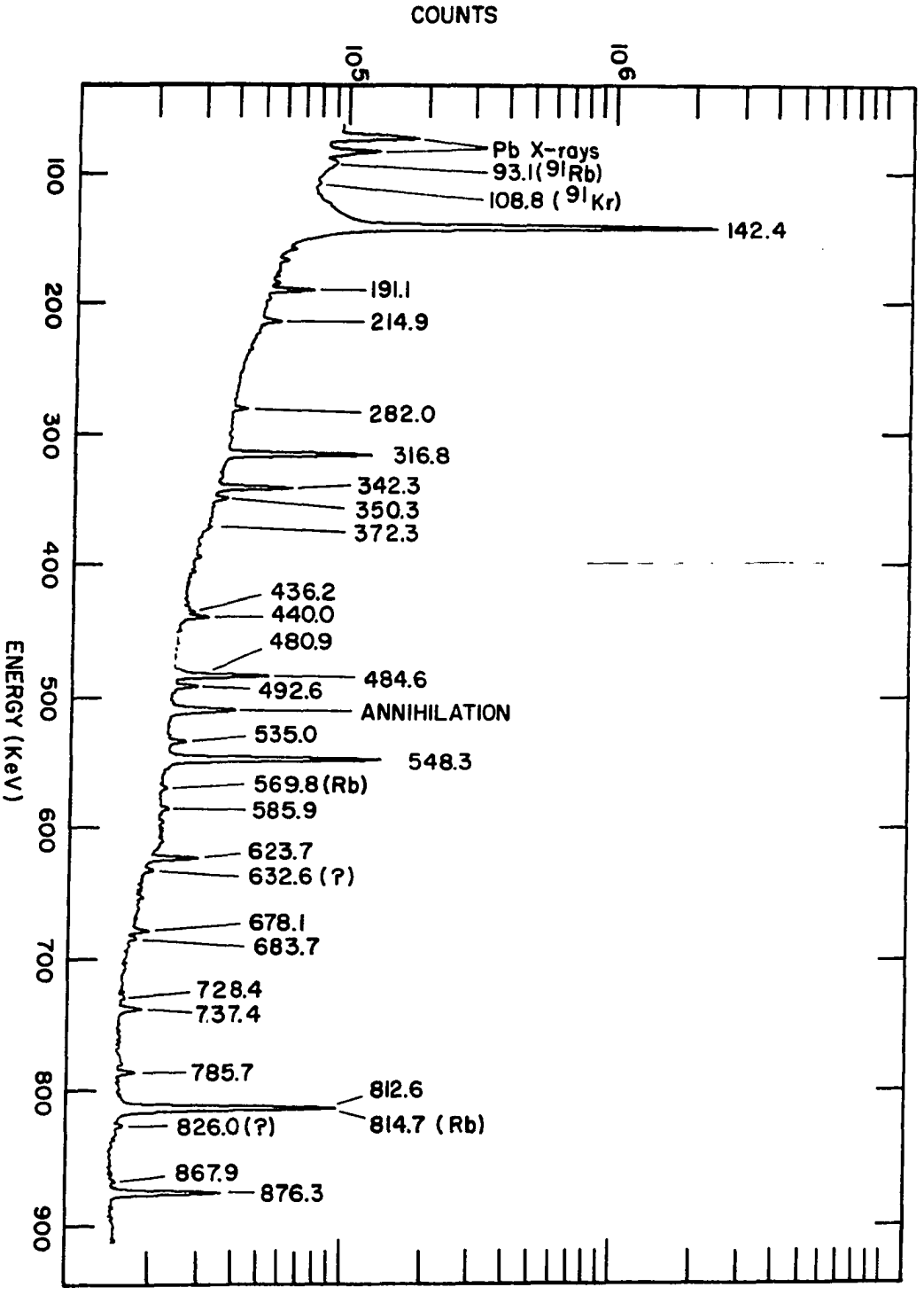

Figure 25a. Gamma ray spectrum of ^{92}Kr decay--60 keV to 915 keV

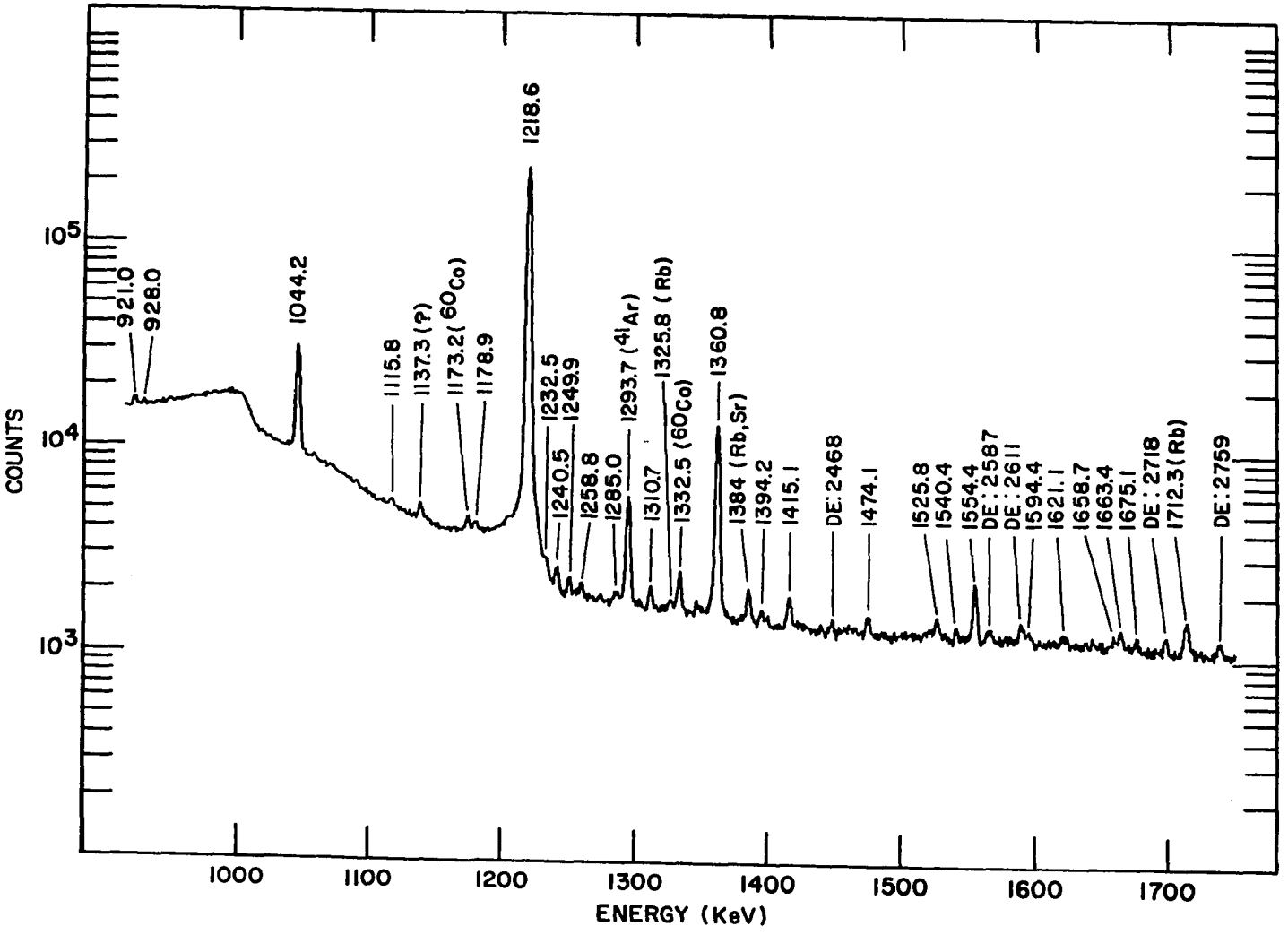

Figure 25b. Gamma ray spectrum of ^{92}Kr decay--915 keV to 1750 keV

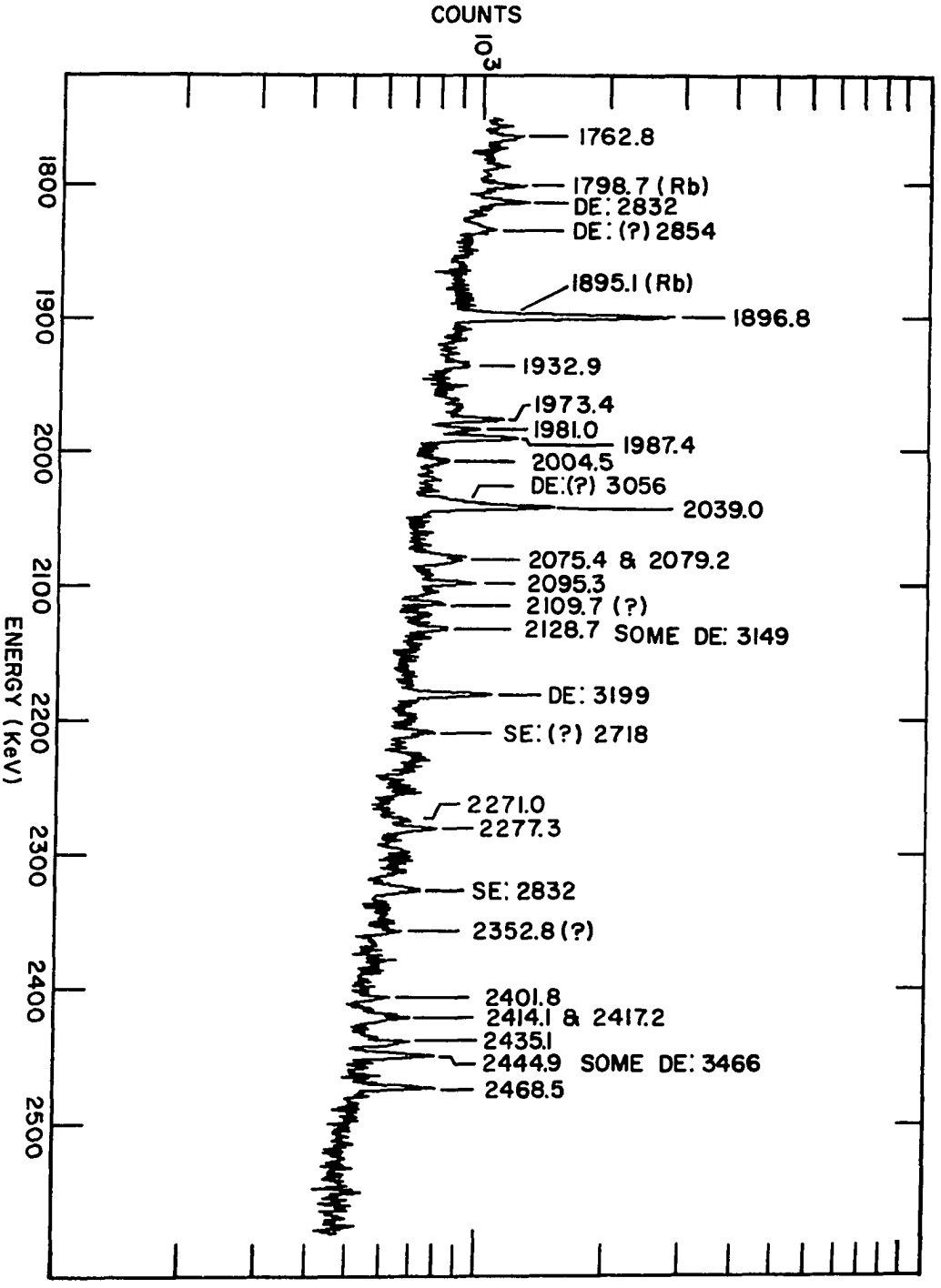

Figure 25c. Gamma ray spectrum of ^{92}Kr decay--1750 keV to 2580 keV

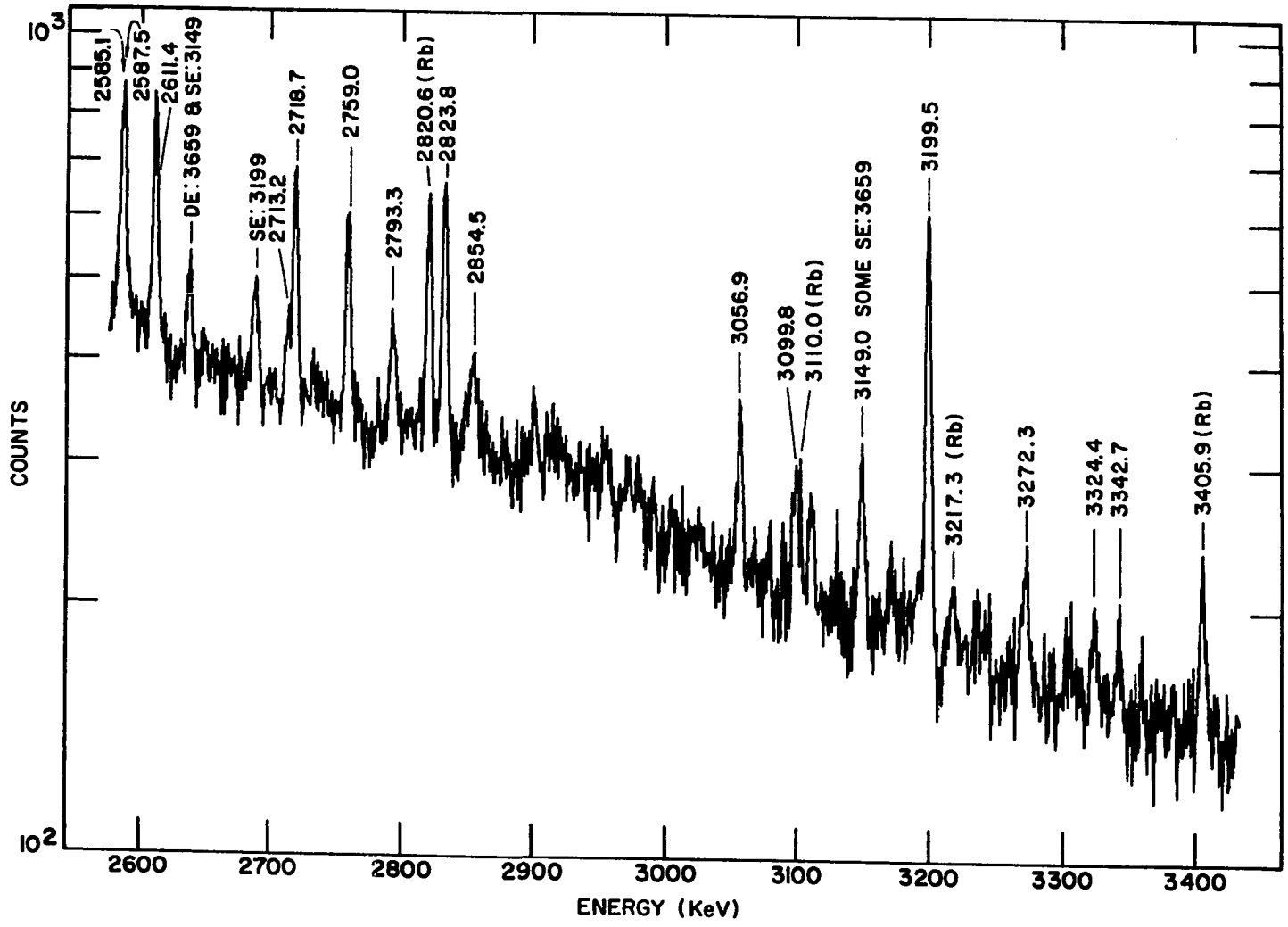

Figure 25d. Gamma ray spectrum of ^{92}Kr decay--2580 keV to 3440 keV

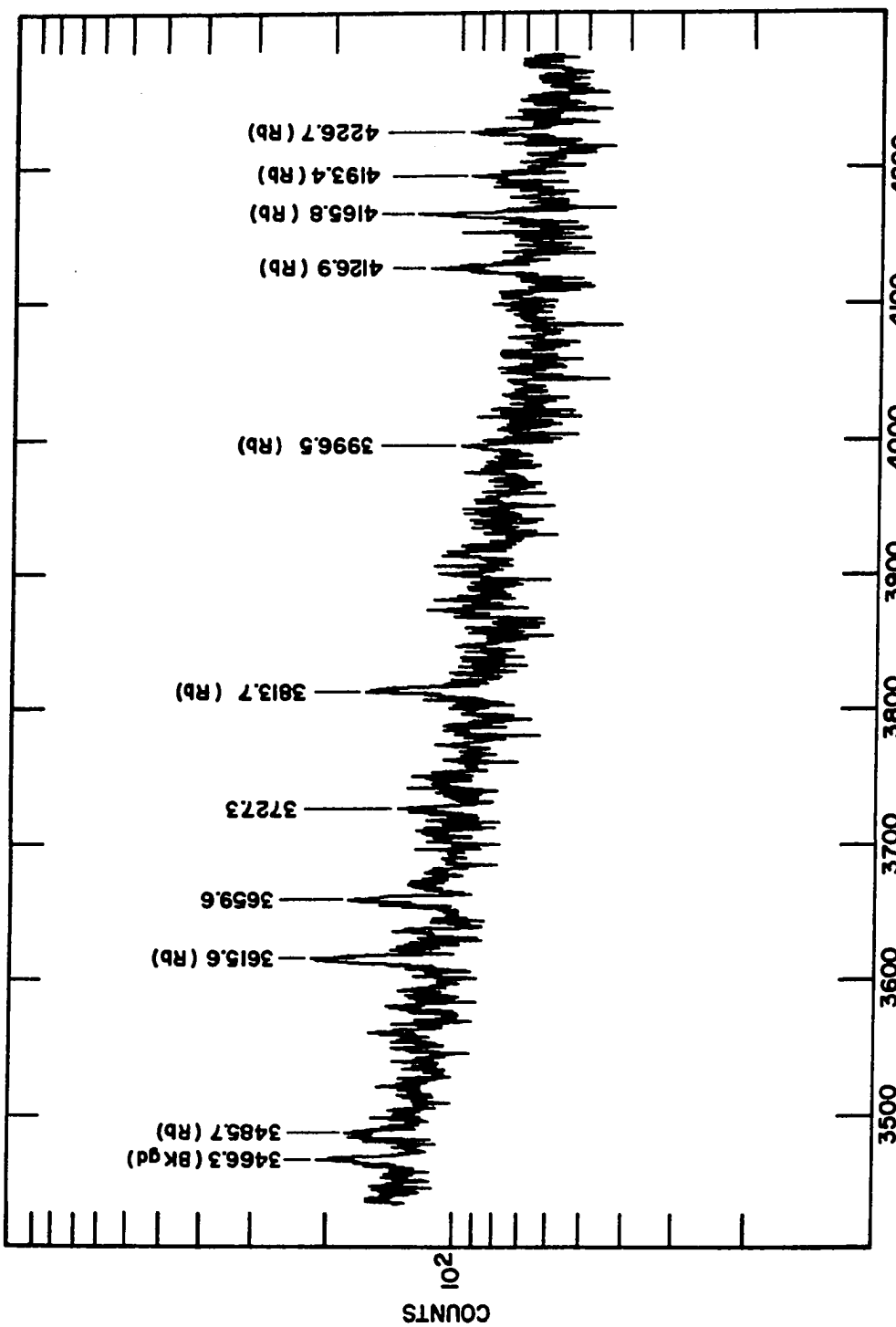

Figure 25e. Gamma ray spectrum of ^{92}Kr decay--3440 keV to 4280 keV

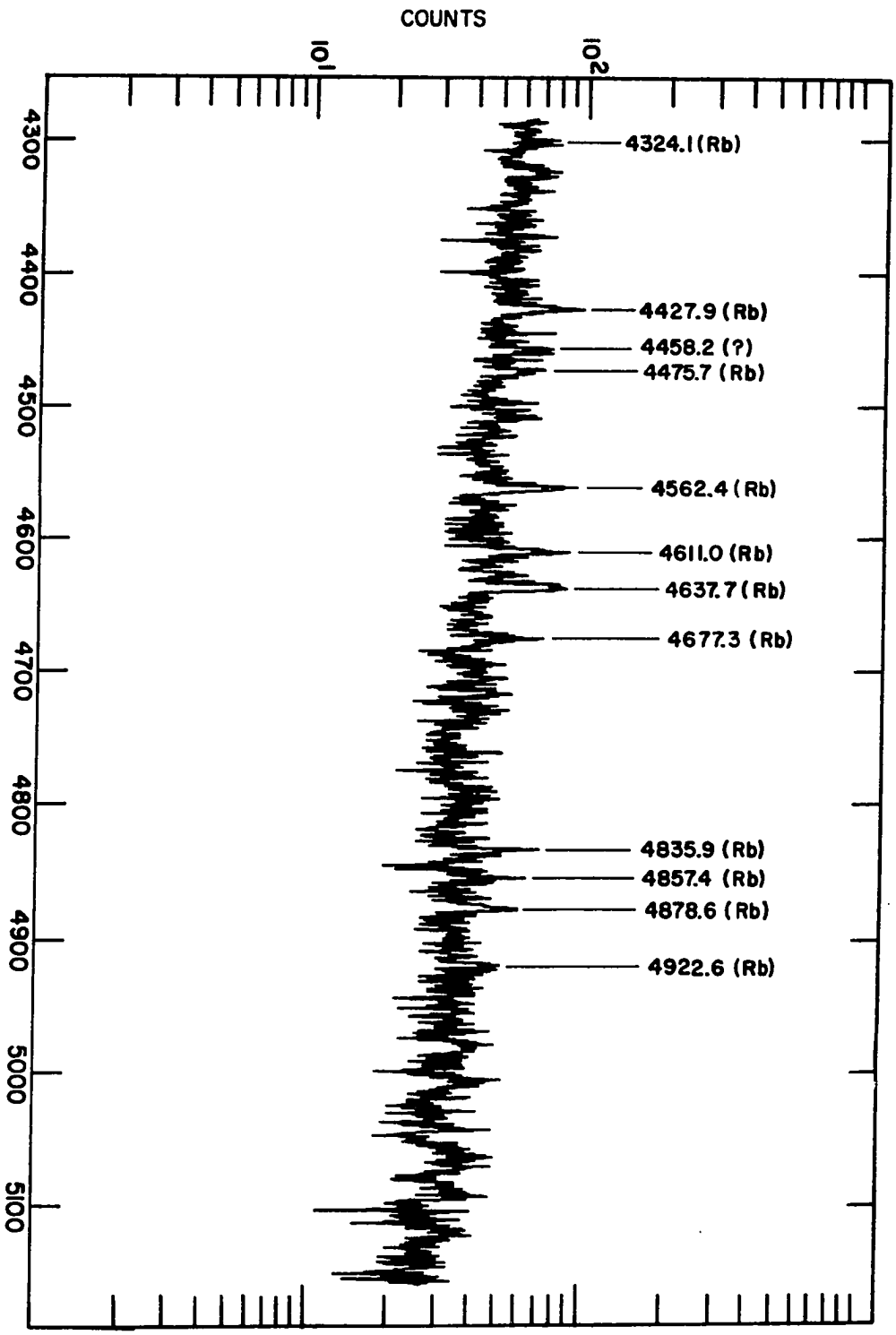

Figure 25f. Gamma ray spectrum of ^{92}Kr decay--4280 keV to 5160 keV

parent ^{92}Kr. All transitions above 3727 keV are identified as being due to the decay of the daughter ^{92}Rb.

Table 6 lists the transitions in ^{92}Rb following the beta decay of ^{92}Kr. For those transitions which have been placed in the ^{92}Rb level scheme, the placement is indicated in Table 6. In the four cases where there are two listings for a given transition, the gamma ray has been used twice in the level scheme. Present information does not allow unambiguous placement of these four gamma rays.

Table 7 lists those gamma-ray peaks from the decay of ^{92}Kr which have been identified as single- or double-escape peaks.

Table 8 summarizes the calculated log ft values for beta decay to ^{92}Rb levels. These calculations are based on an indirect measurement of 50% beta feeding to the ground state of ^{92}Rb (as discussed in the chapter on Data Analysis).

Figure 26 displays the tentative level scheme that has been constructed for the levels reached by beta decay in ^{92}Rb. This level scheme incorporates 84 of the 96 transitions identified as due to ^{92}Kr decay (or 99.4% of the measured total gamma-ray intensity). The four gamma rays which are used twice are identified by an asterisk (*). A solid circle at the head or tail of an arrow indicates a gamma ray placement by an observed coincidence, and an open circle represents the use of a "weak" coincidence.

B. ^{92}Rb Decay

Figures 27a-f show the spectra of a daughter analysis run (0 to 5.2 MeV) with moving tape collector operating in the (10.3, 10.3, 10.3)

Table 6. Gamma ray transitions in ^{92}Rb

Energy (keV)	Relative Intensity[a]	Level Scheme Placement	Observed Coincidences
142.37 (.1)	1000 (51)	142.4 to g.s.	191, 282(?), 342, 1218, 1896
159.2 (.3)	1.6 (.4)	492.6 to 333.5	191
167.9 (.2)	2.0 (.3)	484.6 to 316.8	316
185.6 (.2)	1.7 (.3)		
191.14 (.1)	13 (.8)	333.5 to 142.4	142, 159, 214, 394, 535, 492, 632
214.88 (.1)	5.6 (.5)	548.3 to 333.5	191
281.95 (.15)	4.2 (.4)	2321.1 to 2039.1	142(?), 1044(??)
316.76 (.1)	91 (4.8)	316.8 to g.s.	168, 1044, 2832(?)
333.4 (.5)	.7 (.3)	333.5 to g.s.	
342.28 (.1)	33 (1.8)	484.6 to 142.4	142,876
350.26 (.1)	4.2 (.4)	492.6 to 142.4	
372.3 (.3)	1.8 (.5)	920.9 to 548.3	
394.7 (.3)	1.8 (.4)	728.3 to 333.5	191
436.2 (.3)	3.3 (.6)	920.9 to 484.6	
440.04 (.1)	9.4 (.8)	1360.9 to 920.9	921
480.9 (.2)	2.8 (.4)	623.6 to 142.4	
484.65 (.1)	50 (2.6)	484.6 to g.s.	876
492.63 (.1)	8.8 (.7)	492.6 to g.s. 1360.9 to 868.4	191

[a]Normalized with 142.37 as 1000.

Table 6. (Continued)

Energy (keV)	Relative Intensity[a]	Level Scheme Placement	Observed Coincidences
534.98 (.1)	6.4 (.6)	868.4 to 333.5	191
548.30 (.1)	218 (12)	548.3 to g.s.	812
585.9 (.2)	3.5 (.6)	728.3 to 142.4	
623.66 (.1)	21 (1.3)	623.6 to g.s.	737(??)
632.6 (.3)	2.9 (.7)	1360.9 to 728.3	
678.07 (.1)	5.8 (.5)	2039.1 to 1360.9	
683.7 (.2)	2.6 (.5)		
728.4 (.4)	1.8 (.5)	728.3 to g.s.	
737.4 (.2)	8 (.8)	1360.9 to 623.6	623 (??)
785.66 (.1)	7 (.6)	928.0 to 142.4	
812.62 (.1)	227 (12)	1360.9 to 548.3	548
826.0 (.6)	2.0 (.9)		
867.9 (.8)	1.3 (.8)	868.4 to g.s.	
876.30 (.1)	66 (3.5)	1360.9 to 484.6	342, 484
921.0 (.2)	4.3 (.6)	920.9 to g.s.	440
928.0 (.4)	2.1 (.6)	928.0 to g.s.	
1044.18 (.1)	74 (4)	1360.9 to 316.8	316
1115.8 (.3)	1.6 (.3)	1663.5 to 548.3	
1178.9 (.3)	1.6 (.4)	1663.5 to 484.6	
1218.57 (.1)	934 (48)	1360.9 to 142.4	142
1232.5 (.6)	.8 (.4)		

Table 6. (Continued)

Energy (keV)	Relative Intensity[a]	Level Scheme Placement	Observed Coincidences
1240.5 (.2)	2.4 (.4)		
1249.9 (.3)	1.5 (.3)	2611.1 to 1360.9	
1258.8 (.4)	1.2 (.3)	3338.6 to 2079.3	
1285.0 (.5)	.8 (.3)		
1291.6 (.7)	1.4 (.7)	4193.0 to 2901.6	
1310.7 (.3)	1.8 (.3)	2039.1 to 728.3	
1345.5 (.7)	.7 (.3)	1663.5 to 316.8	
1360.83 (.1)	54 (3)	1360.9 to g.s.	
1394.2 (.5)	.8 (.3)	3057.5 to 1663.5	
1415.1 (.2)	2.6 (.3)	2039.1 to 623.6	
1474.1 (.3)	1.5 (.3)	4193.0 to 2718.8	
1525.8 (.3)	1.3 (.3)		
1540.4 (.7)	.7 (.4)	2901.6 to 1360.9	
1554.44 (.1)	6.0 (.5)	2039.1 to 484.6	
1594.4 (.6)	.8 (.3)	2079.3 to 484.6	
1621.1 (.8)	.6 (.3)	3659.7 to 2039.1	
1658.7 (.7)	.7 (.3)	2587.4 to 928.0	
1663.4 (.4)	1.4 (.3)	1663.5 to g.s.	
1675.1 (.5)	.9 (.3)	3338.6 to 1663.5	
1762.8 (.4)	1.1 (.3)	2079.3 to 316.8	
1896.8 (.2)	13 (1.9)	2039.1 to 142.4	142

Table 6. (Continued)

Energy (keV)	Relative Intensity[a]	Level Scheme Placement	Observed Coincidences
1932.9 (.5)	.9 (.3)		
1973.4 (.3)	2.2 (.4)	2901.6 to 928.0	
1981.0 (.4)	1.3 (.3)	2901.6 to 920.9	
1987.4 (.2)	3.8 (.4)	2611.1 to 623.6	
2004.5 (.6)	.8 (.3)	2321.1 to 316.8	
2039.0 (.2)	6.3 (.6)	2039.1 to g.s. 2587.4 to 548.3	
2075.4 (.4)	1.4 (.3)		
2079.2 (.4)	1.4 (.3)	2079.3 to g.s.	
2095.3 (.3)	2.0 (.4)	2587.4 to 492.6 2718.8 to 623.6	
2128.7 (.5)	1.3 (.4)	3057.5 to 928.0	
2271.0 (.5)	.8 (.3)	2587.4 to 316.8	
2277.3 (.3)	1.8 (.3)	2611.1 to 333.5	
2401.8 (.6)	.7 (.3)	2718.8 to 316.8	
2414.1 (.9)	.7 (.4)	3341.9 to 928.0	
2417.2 (.5)	1.4 (.4)	2901.6 to 484.6	
2435.1 (.6)	1.6 (.3)	3057.5 to 623.6	
2444.9 (.3)	2.7 (.4)	2587.4 to 142.4	
2468.5 (.3)	2.7 (.5)	2611.1 to 142.4	
2585.1 (.7)	1.9 (.9)	2901.6 to 316.8	
2587.5 (.4)	3.8 (.9)	2587.4 to g.s.	

Table 6. (Continued)

Energy (keV)	Relative Intensity[a]	Level Scheme Placement	Observed Coincidences
2611.4 (.2)	4.6 (.5)	2611.1 to g.s.	
2713.2 (.6)	.9 (.3)		
2718.7 (.2)	4.2 (.4)	2718.8 to g.s.	
2759.0 (.2)	3.3 (.4)	2901.6 to 142.4	
2793.3 (.4)	1.5 (.3)	3341.9 to 548.3	
2832.8 (.2)	4.7 (.5)	3149.4 to 316.8	316(?)
2854.5 (.7)	1.1 (.4)	3338.6 to 484.6	
3056.9 (.3)	2.0 (.4)	3057.5 to g.s.	
3099.8 (.5)	1.4 (.4)		
3149.0 (.4)	1.9 (.4)	3149.4 to g.s.	
3199.5 (.2)	6.8 (.5)	3341.9 to 142.4	
3272.3 (.5)	1.0 (.3)	4193.0 to 920.9	
3324.4 (.7)	.7 (.2)	4193.0 to 868.4	
3342.7 (.7)	.6 (.2)	3341.9 to g.s. 3659.7 to 316.8	
3659.6 (.5)	1.3 (.3)	3659.7 to g.s.	
3727.3 (.8)	.6 (.3)		

Table 7. Single- and double-escape peaks in ^{92}Rb

Energy (keV)	Relative Intensity[a]	Identity
1447.1 (.6)	.8 (.4)	2468 DE
1565.4 (.5)	.8 (.3)	2587 DE
1589.1 (.4)	1.5 (.3)	2611 DE
1696.8 (.5)	1.3 (.4)	2718 DE
1736.9 (.4)	1.2 (.3)	2759 DE
1811.0 (.3)	1.8 (.3)	2832 DE
2101.4 (1.1)	.5 (.4)	2611 SE
2177.7 (.2)	3.6 (.4)	3199 DE
2322.3 (.4)	1.5 (.3)	2832 SE
2637.9 (.4)	1.0 (.2) .5 (.2)	3659 DE 3149 SE
2688.4 (.4)	1.6 (.4)	3199 SE
3149.0 (.4)[b]	1.3 (.3)	3659 SE

[a]Normalized with 142.37 as 1000.

[b]Also a full energy peak at this energy.

Table 8. Calculated log ft values for beta decay to ^{92}Rb levels

^{92}Rb levels (keV)	Beta energy (MeV)	Percent beta branching	log ft
0	5.01	50	4.69
142.4 (.1)	4.87	~0	--
316.8 (.1)	4.69	~0	--
333.5 (.16)	4.68	~0	--
484.6 (.12)	4.53	~0	--
492.6 (.14)	4.52	0.41	6.57
548.3 (.11)	4.46	~0	--
623.6 (.12)	4.39	0.191	6.88
728.3 (.3)	4.28	0.079	7.22
868.4 (.3)	4.14	~0	--
920.9 (.27)	4.09	~0	--
928.0 (.2)	4.08	0.138	6.88
1360.9 (.15)	3.65	45	4.17
1663.5 (.4)	3.35	0.118	6.59
2039.1 (.22)	2.97	1.01	5.41
2079.3 (.5)	2.93	0.069	6.55
2321.1 (.3)	2.69	0.164	6.05
2587.4 (.3)	2.42	0.54	5.30
2611.1 (.3)	2.40	0.47	5.33
2718.8 (.3)	2.29	0.178	5.59
2901.6 (.5)	2.11	0.31	5.30

Table 8. (Continued)

^{92}Rb levels (keV)	Beta energy (MeV)	Percent beta branching	log ft
3057.5 (.6)	1.95	0.188	5.38
3149.4 (.3)	1.86	0.217	5.25
3338.6 (.7)	1.67	0.105	5.35
3341.9 (.4)	1.67	0.32	4.87
3659.7 (.7)	1.35	0.082	5.10
4193.0 (.7)	0.82	0.151	3.97

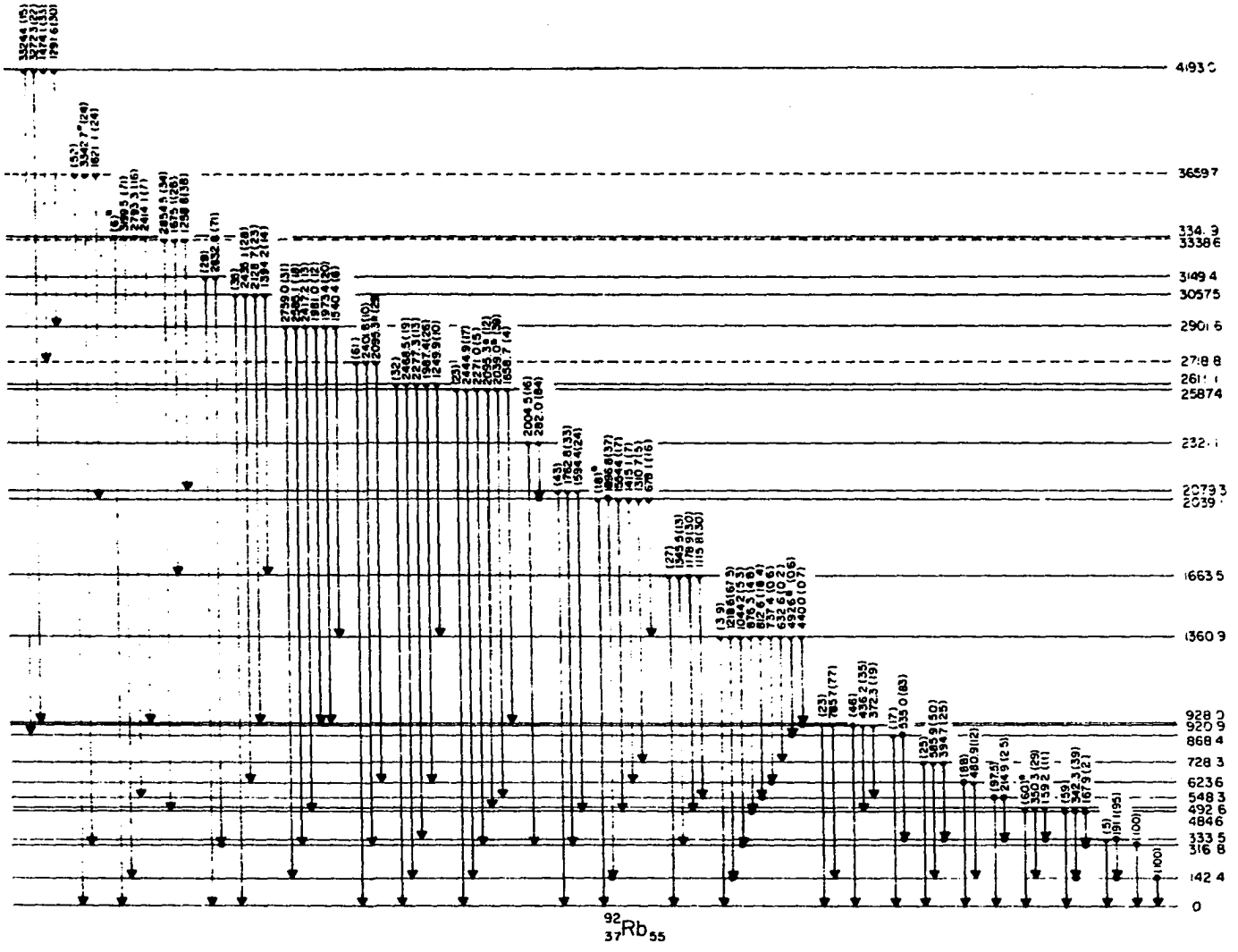

Figure 26. Level scheme of ^{92}Rb following the beta decay of ^{92}Kr

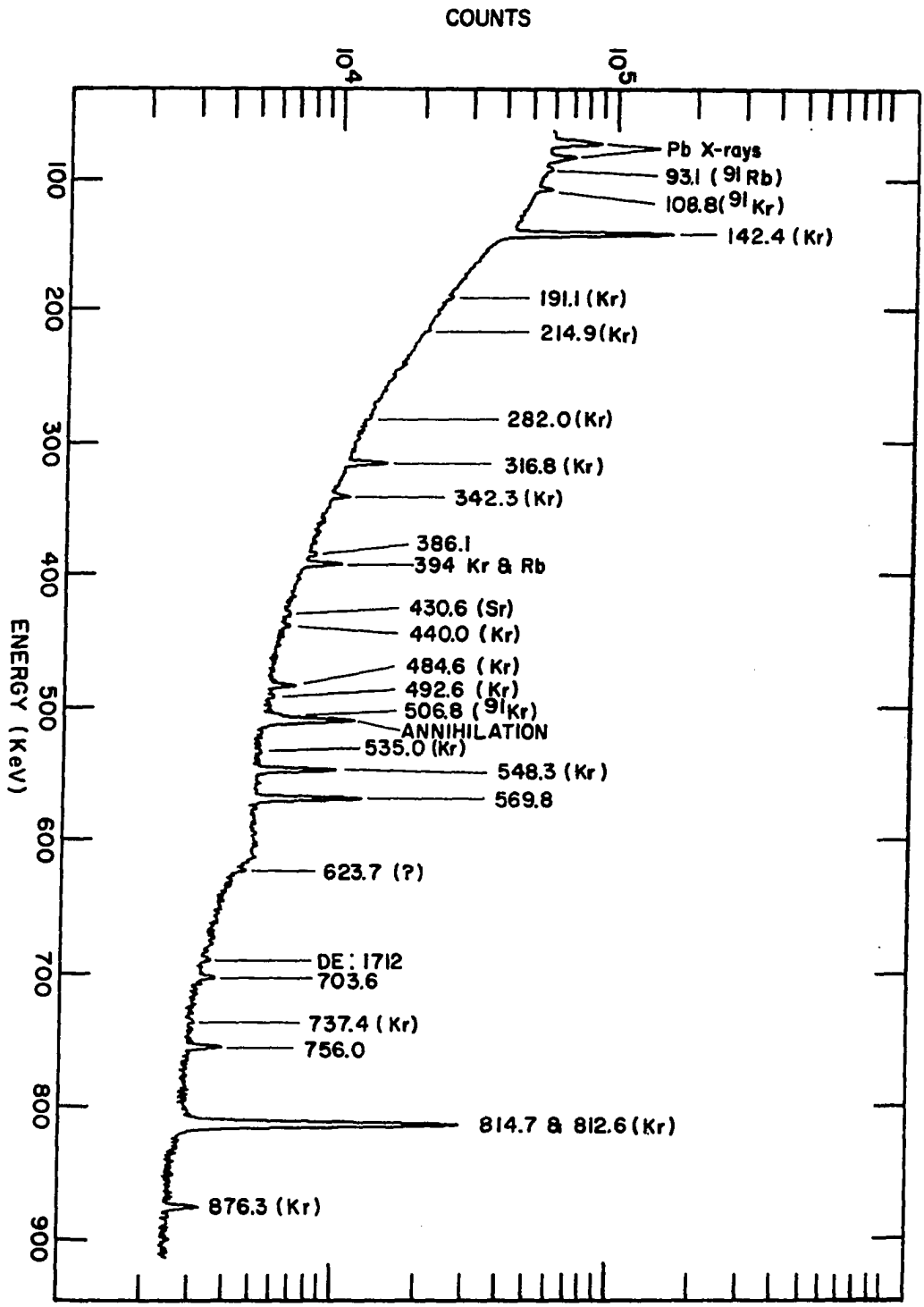

Figure 27a. Gamma ray spectrum of ^{92}Rb decay--60 keV to 915 keV

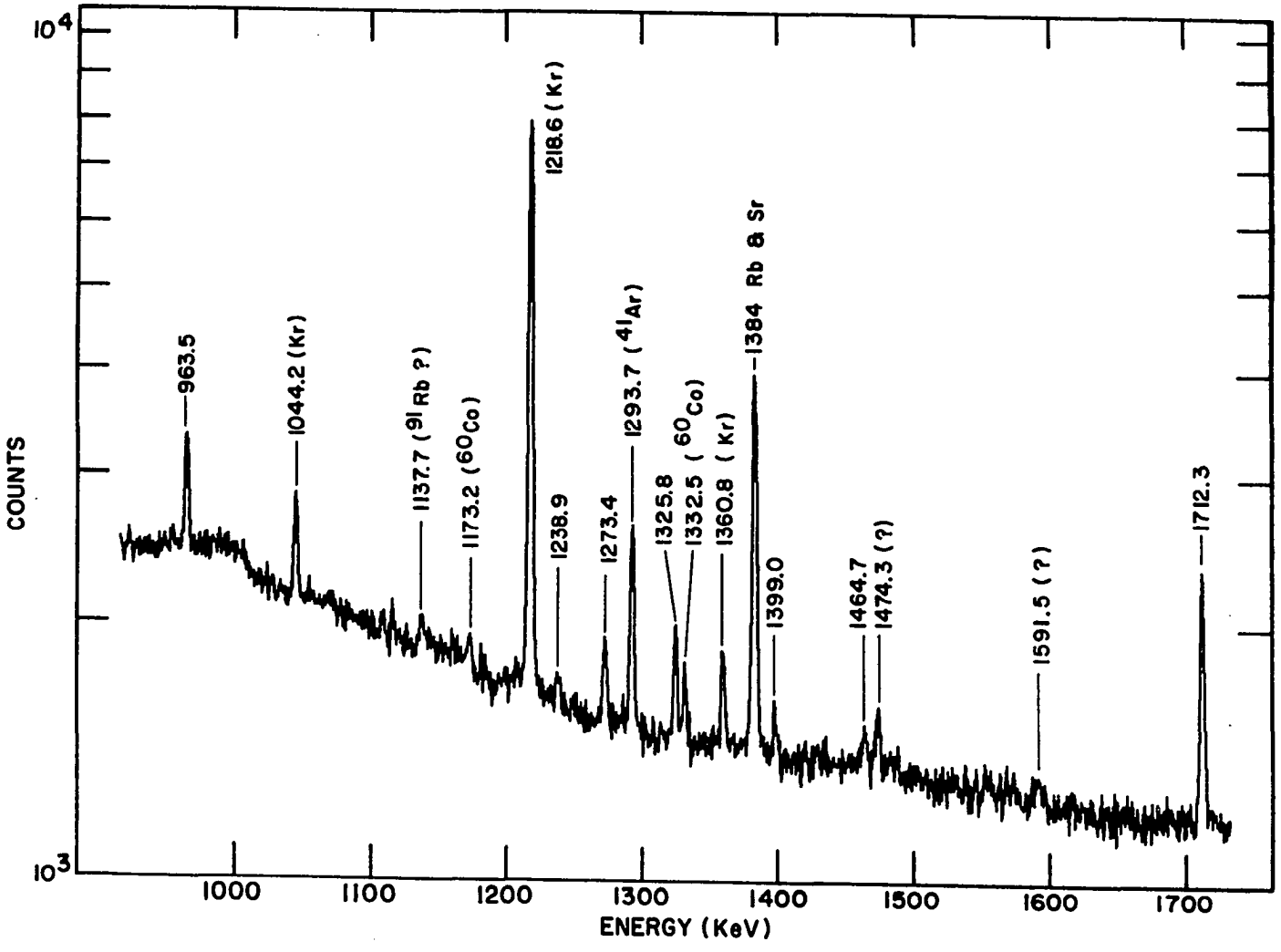

Figure 26b. Gamma ray spectrum of ^{92}Rb decay--915 keV to 1730 keV

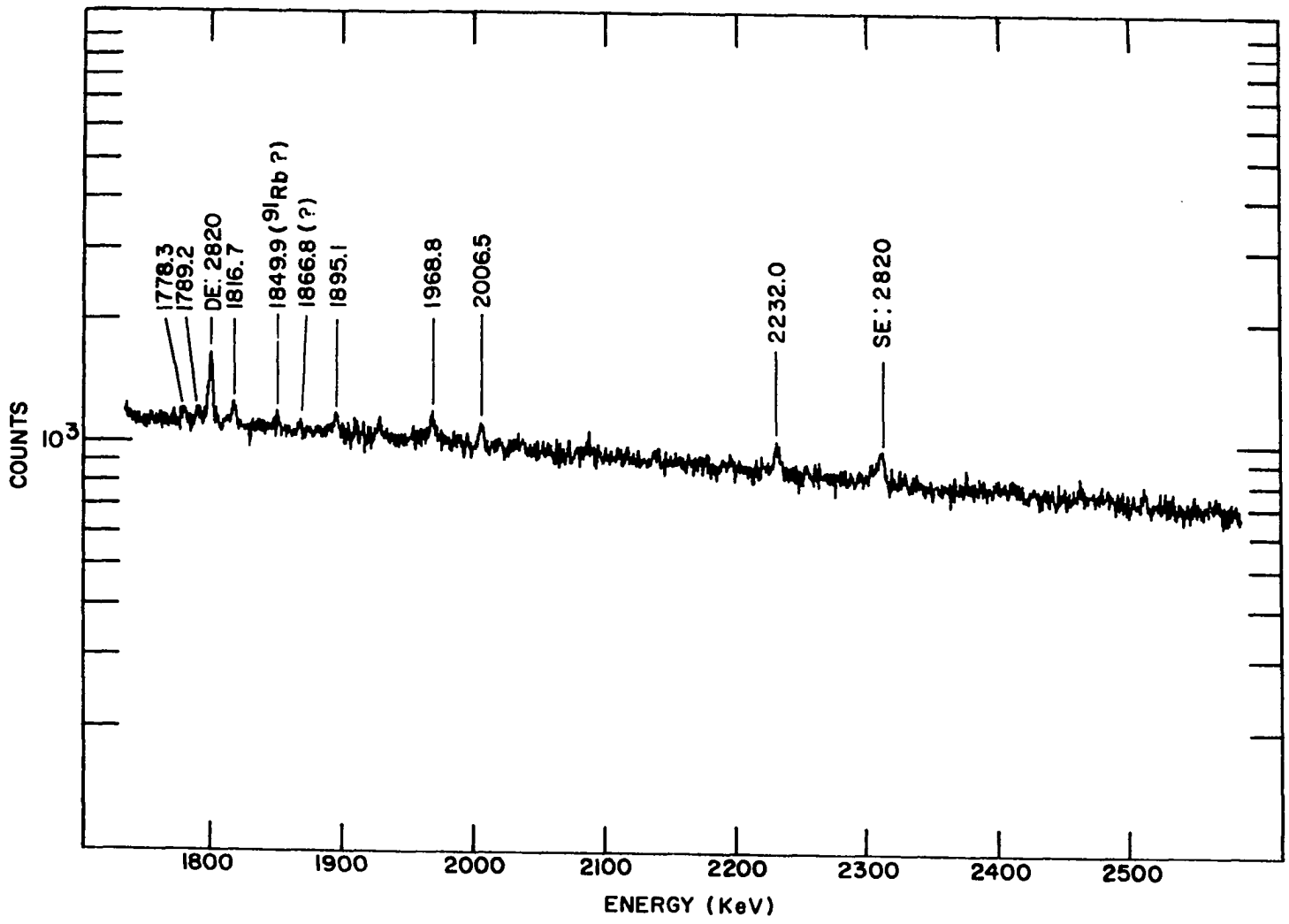

Figure 27c. Gamma ray spectrum of ^{92}Rb decay--1730 keV to 2580 keV

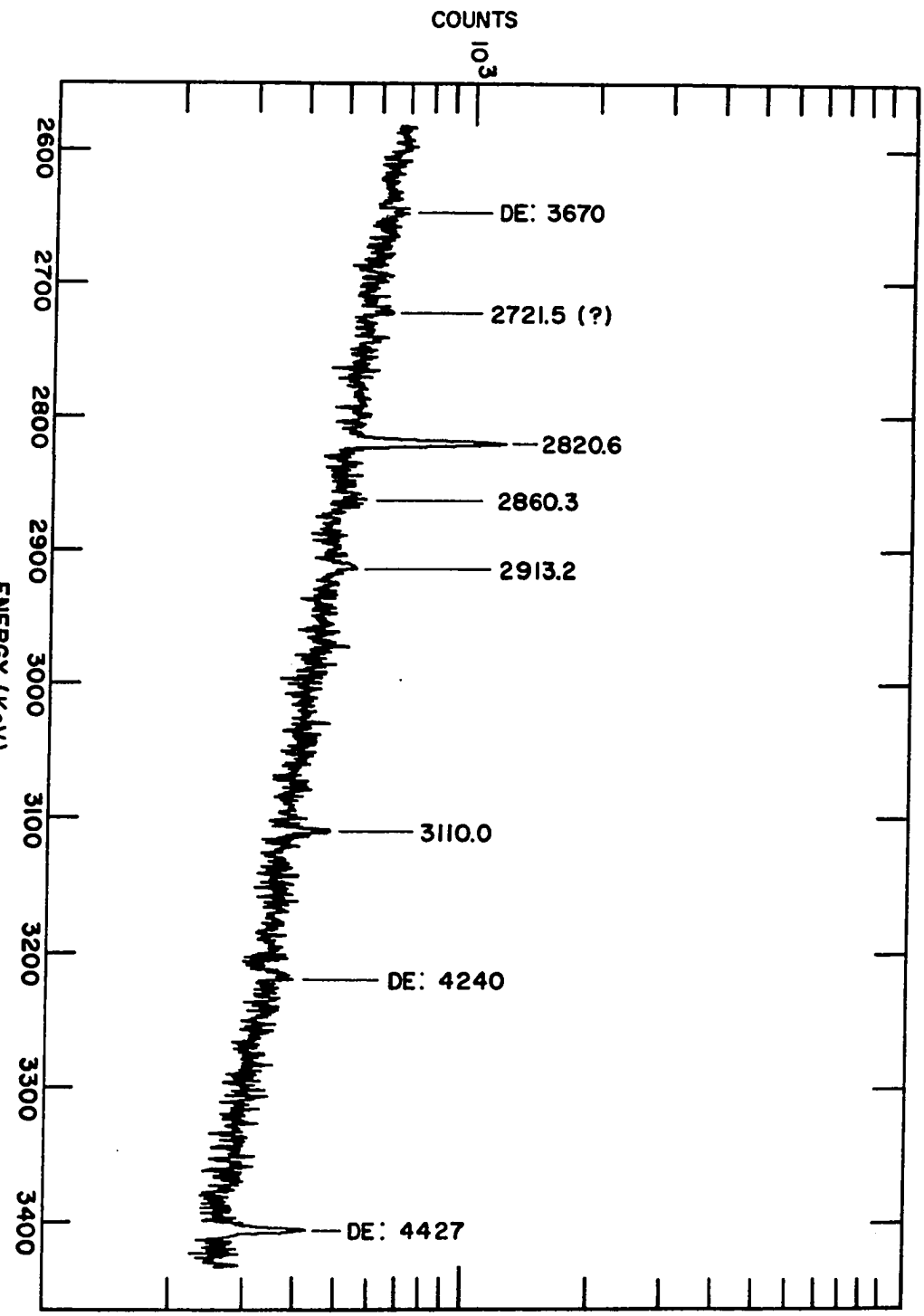

Figure 27d. Gamma ray spectrum of ^{92}Rb decay--2580 keV to 3430 keV

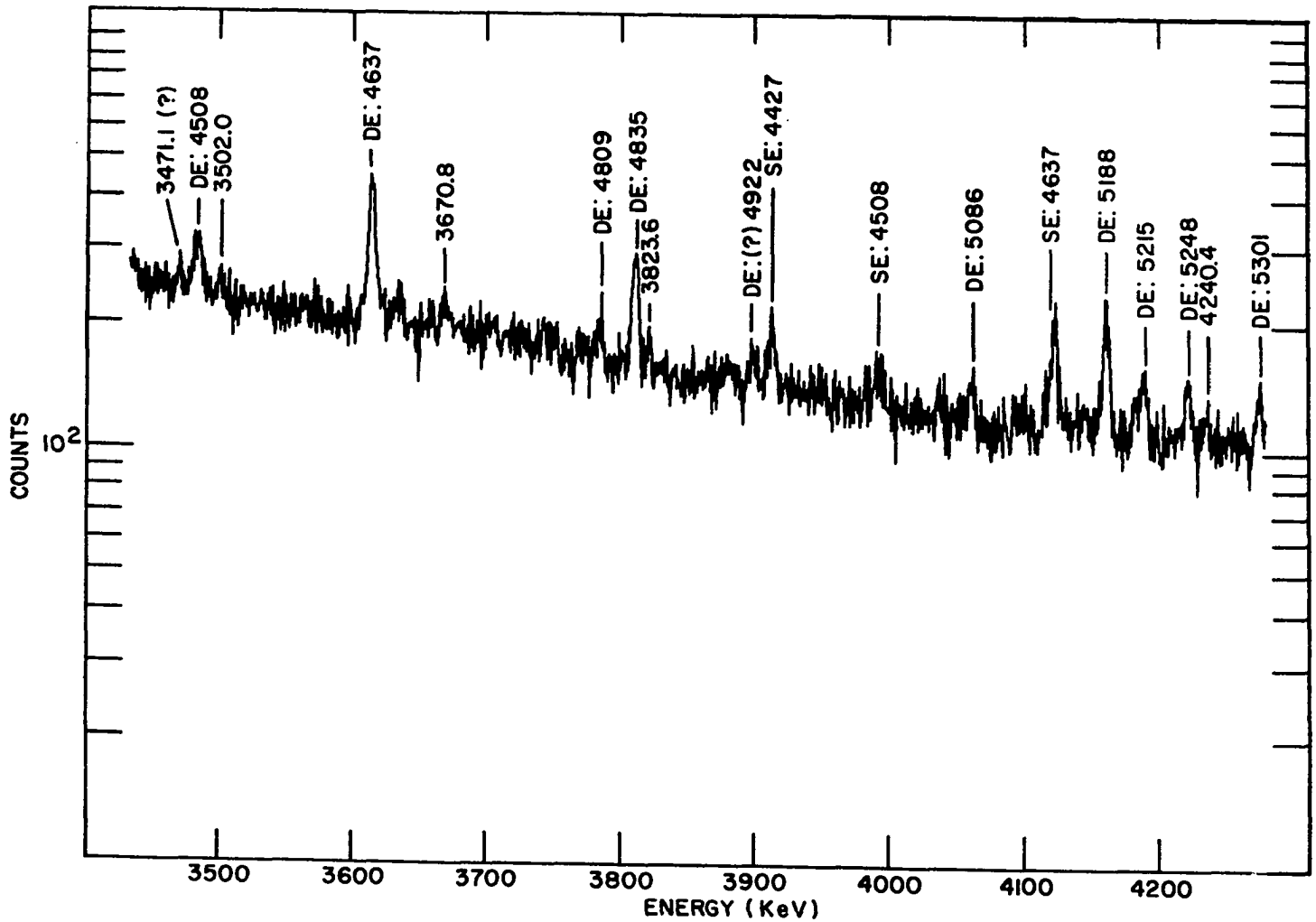

Figure 27e. Gamma ray spectrum of ^{92}Rb decay--3430 keV to 4280 keV

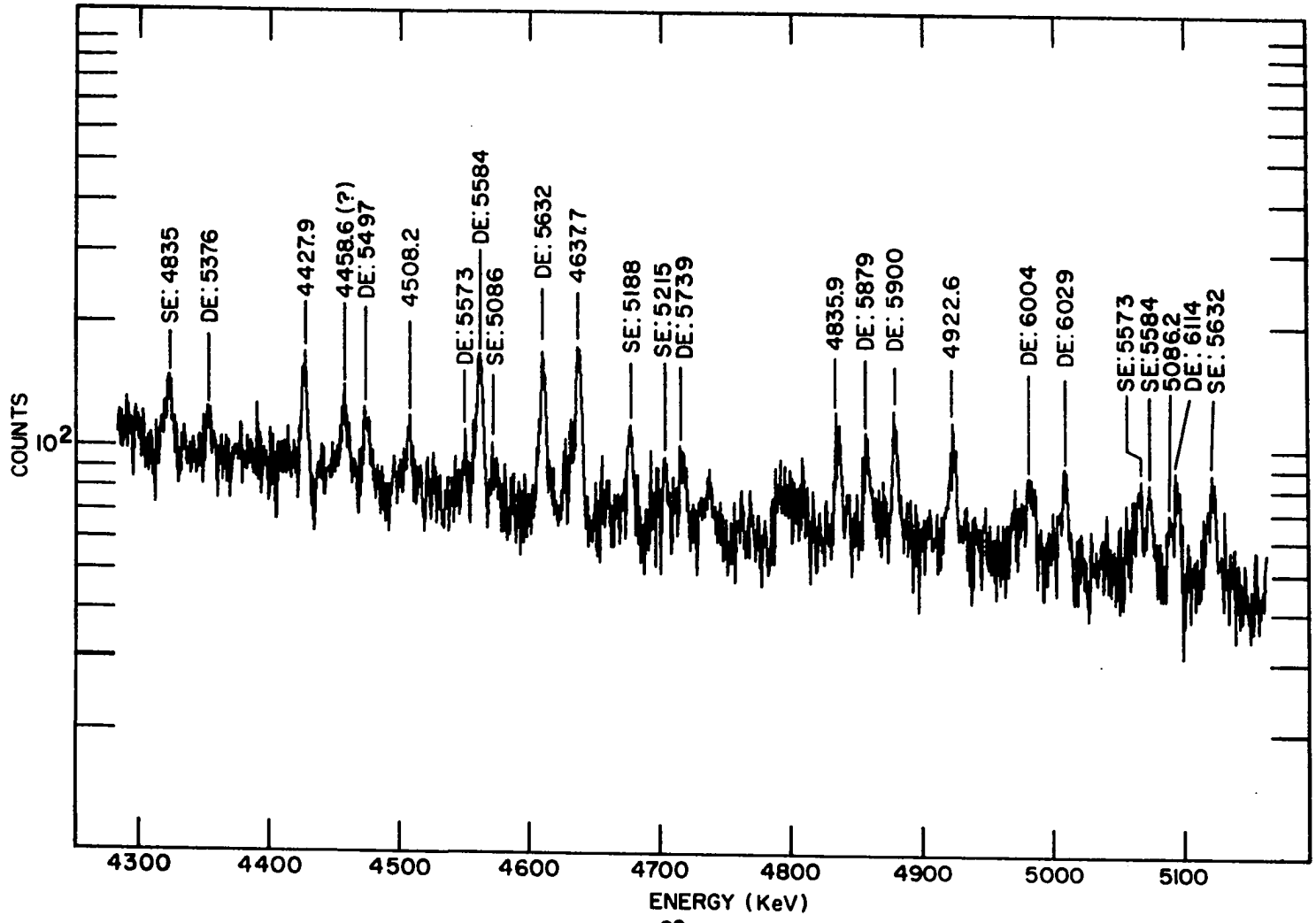

Figure 27f. Gamma ray spectrum of ^{92}Rb decay--4280 keV to 5160 keV

daughter analysis mode. For this decay, spectra were analyzed up to 8 MeV in energy, and gamma rays were observed up to 6.115 MeV.

Table 9 lists the transitions following the beta decay of ^{92}Rb, while Table 10 contains the single- and double-escape peaks.

Table 11 summarizes the calculated log ft values for beta decay to ^{92}Sr levels. As for the decay of ^{92}Kr, the ground-state beta branch to ^{92}Sr was measured indirectly as 94% (see the chapter on Data Analysis) and the calculations are based on this result.

Figure 28 shows the tentative level scheme for the levels in ^{92}Sr reached by beta decay of ^{92}Rb. Forty-four of the fifty-two observed transitions (or 91.7% of the measured total gamma-ray intensity) are placed in the level scheme.

C. ^{92}Sr Decay

Figures 29a-c show the spectra of an off-line run (0 to 2 MeV) using the chemical technique outlined in the chapter on Sample Production to enhance the ^{92}Sr decay. Table 12 lists the transitions identified as due to ^{92}Sr decay, and includes two lines identified as escape peaks. Table 13 contains the log ft values calculated for beta decay to ^{92}Y levels. Unlike the ^{92}Kr and ^{92}Rb decays, a previous measurement has been reported for the beta branching in this case (23), in which the 1384-keV transition is observed for 90% of the beta decays.

The beta decay properties for ^{92}Sr are illustrated in Figure 30.

The level scheme for levels reached in ^{92}Y by beta decay of ^{92}Sr is shown in Figure 31. All of the gamma transitions identified as due to ^{92}Sr are placed in this level scheme.

Table 9. ^{92}Sr transitions

Energy (keV)	Relative Intensity[a]	Level Scheme Placement	Observed Coincidences
96.7 (.6)	4.9 (2.3)	2623.5 to 2527.0	
386.1 (.3)	7.6 (1.3)	2527.0 to 2140.5	
393.5 (.1)	38 (2.4)	1778.1 to 1384.5	
569.8 (.1)	170 (10)	1384.5 to 814.7	814
703.6 (.3)	14 (2.7)	2088.1 to 1384.5	
756.0 (.15)	34 (3.3)	2140.5 to 1384.5	
814.7 (.1)	1000 (55)	8.417 to g.s.	569, 1712
963.5 (.15)	46 (4.0)	1778.1 to 814.7	
1238.9 (.6)	11 (3.6)	2623.5 to 1384.5	
1273.4 (.2)	30 (3.8)	2088.1 to 814.7	
1325.8 (.2)	42 (5)	2140.5 to 814.7	
1384.6 (.3)	110 (20)	1384.5 to g.s.	
1399.0 (.6)	16 (5)	2783.5 to 1384.5	
1464.7 (.6)	12.3 (4.4)	7362.9 to 5900.7	
1712.3 (.15)	131 (10)	2527.0 to 814.7	814
1778.3 (1.0)	11 (6)	1778.1 to g.s.	
1789.2 (.9)	12 (6)		
1816.7 (.5)	18 (4.4)	4637.8 to 2820.7	
1895.1 (.6)	17 (5.4)	6949.5 to 5053.9	

[a]Normalized with 814.7 as 1000.

Table 9. (Continued)

Energy (keV)	Relative Intensity[a]	Level Scheme Placement	Observed Coincidences
1968.8 (.6)	21 (6.4)	2783.5 to 814.7	
2006.5 (.5)	22 (6)	2820.7 to 814.7	
2232.0 (.5)	24 (6)	5053.9 to 2820.7	
2820.6 (.2)	188 (14)	2820.7 to g.s.	
2860.3 (2.1)	8.3 (7.8)	4637.8 to 1778.1	
2913.2 (.6)	22 (5.9)	5053.9 to 2140.5	
3110.0 (.7)	30 (8.5)	5893.2 to 2783.5	
3502.0 (1.6)	11 (7.2)	6029.7 to 2527.0	
3670.8 (1.2)	13 (6.1)	5053.9 to 1384.5	
3823.6 (1.6)	11 (6.6)	4637.8 to 814.7	
4240.4 (1.6)	10 (5.8)	5053.9 to 814.7	
4427.9 (.9)	39 (7.6)		
4508.2 (1.2)	19 (5.1)	5893.2 to 1384.5	
4637.7 (.9)	67 (8.8)	4637.8 to g.s.	
4809.3 (1.5)	32 (16)	6949.5 to 2140.5	
4835.9 (1.1)	31 (7.6)	7362.9 to 2527.0	
4922.6 (1.1)	33 (6.3)	5738.1 to 814.7	
5086.2 (1.2)	26 (12)	5900.7 to 814.7	
5188.1 (.8)	75 (13)	6003.0 to 814.7	
5215.1 (1.0)	33 (12)	6029.7 to 814.7	
5248.7 (1.2)	33 (8)		

Table 9. (Continued)

Energy (keV)	Relative Intensity[a]	Level Scheme Placement	Observed Coincidences
5301.7 (1.3)	25 (8)	6115.6 to 814.7	
5376.6 (1.5)	18 (8)		
5497.7 (1.3)	25 (7)		
5573.7 (1.7)	25 (15)		
5584.2 (1.1)	50 (10)	7362.9 to 1778.1	
5632.2 (1.0)	60 (10)		
5739.4 (1.4)	21 (8)	5738.1 to g.s.	
5879.4 (1.5)	21 (8)		
5900.6 (1.4)	28 (8)	5900.7 to g.s.	
6004.1 (1.5)	18 (6)	6003.0 to g.s.	
6030.0 (1.5)	24 (7)	6029.7 to g.s.	
6114.8 (1.5)	25 (8)	6115.6 to g.s.	

Table 10. Single- and double-escape peaks in ^{92}Sr

Energy (keV)	Relative Intensity[a]	Identity
690.1 (.5)	6.1 (2.3)	1712 DE
1798.7 (.2)	67 (7.4)	2820 DE
2310.2 (.5)	28 (7.1)	2820 DE
2648.9 (1.2)	13 (7.3)	3670 DE
3217.3 (1.1)	17 (7.6)	4240 DE
3405.9 (.4)	59 (7.4)	4427 DE
3485.7 (.6)	38 (7.3)	4508 DE
3615.6 (.5)	110 (11)	4637 DE
3787.3 (1.2)	19 (7.3)	4809 DE
3813.7 (.6)	69 (8.2)	4835 DE
3916.4 (.8)	30 (6)	4427 SE
3996.5 (1.6)	14 (7.2)	4508 SE
4064.7 (1.2)	17 (5.3)	5086 DE
4126.9 (.8)	50 (7.9)	4637 SE
4165.8 (.8)	60 (8.2)	5188 DE
4193.4 (1.0)	25 (6.8)	5215 DE
4226.7 (1.0)	25 (5.8)	5248 DE
4279.7 (1.1)	19.5 (5.9)	5301 DE
4324.1 (1.0)	28 (7.2)	4835 SE

[a]Normalized with 814.7 as 1000.

Table 10. (Continued)

Energy (keV)	Relative Intensity[a]	Identity
4354.6 (1.3)	14 (6)	5376 DE
4475.7 (1.1)	21.5 (5.2)	5497 DE
4549.8 (1.9)	10 (6.3)	5573 DE
4562.4 (.9)	58 (7.2)	5584 DE
4574.4 (1.7)	12 (6.7)	5086 SE
4611.0 (.9)	55 (7.2)	5632 DE
4677.3 (1.1)	30 (7)	5188 SE
4703.5 (1.6)	15 (6.8)	5215 SE
4717.4 (1.4)	20 (7)	5739 DE
4857.4 (1.3)	21 (7.5)	5879 DE
4878.6 (1.2)	28 (7.7)	5900 DE
4982.1 (1.4)	19 (6.2)	6004 DE
5008.0 (1.2)	25 (6.5)	6029 DE
5064.1 (1.5)	20 (6.4)	5573 SE
5072.8 (1.3)	22 (6.6)	5584 SE
5092.8 (1.2)	27 (6.6)	6114 DE
5120.1 (1.2)	26 (5.2)	5632 SE

Table 11. Calculated log ft values for beta decay to ^{92}Sr levels

^{92}Sr levels (keV)	Beta energy (MeV)	Percent beta branching	log ft
0	8.00	94	5.74
814.7 (.1)	7.19	1.33	7.39
1384.5 (.2)	6.62	0.55	7.61
1778.1 (.3)	6.22	0.151	8.05
2088.1 (.3)	5.91	0.179	7.87
2140.5 (.3)	5.86	~ 0	--
2527.0 (.2)	5.47	0.375	7.40
2623.5 (.7)	5.38	0.065	8.14
2783.5 (.7)	5.22	~ 0	--
2820.7 (.3)	5.18	0.685	7.03
4637.8 (1.1)	3.36	0.42	6.40
5053.9 (.9)	2.95	0.212	6.45
5738.1 (1.3)	2.26	0.220	5.94
5893.2 (1.1)	2.11	0.200	5.88
5900.7 (1.3)	2.10	0.171	5.95
6003.0 (1.0)	2.00	0.379	5.48
6029.7 (1.3)	1.97	0.277	5.59
6115.6 (1.4)	1.88	0.204	5.64
6949.5 (1.4)	1.05	0.200	4.67
7362.9 (1.2)	0.64	0.379	3.63

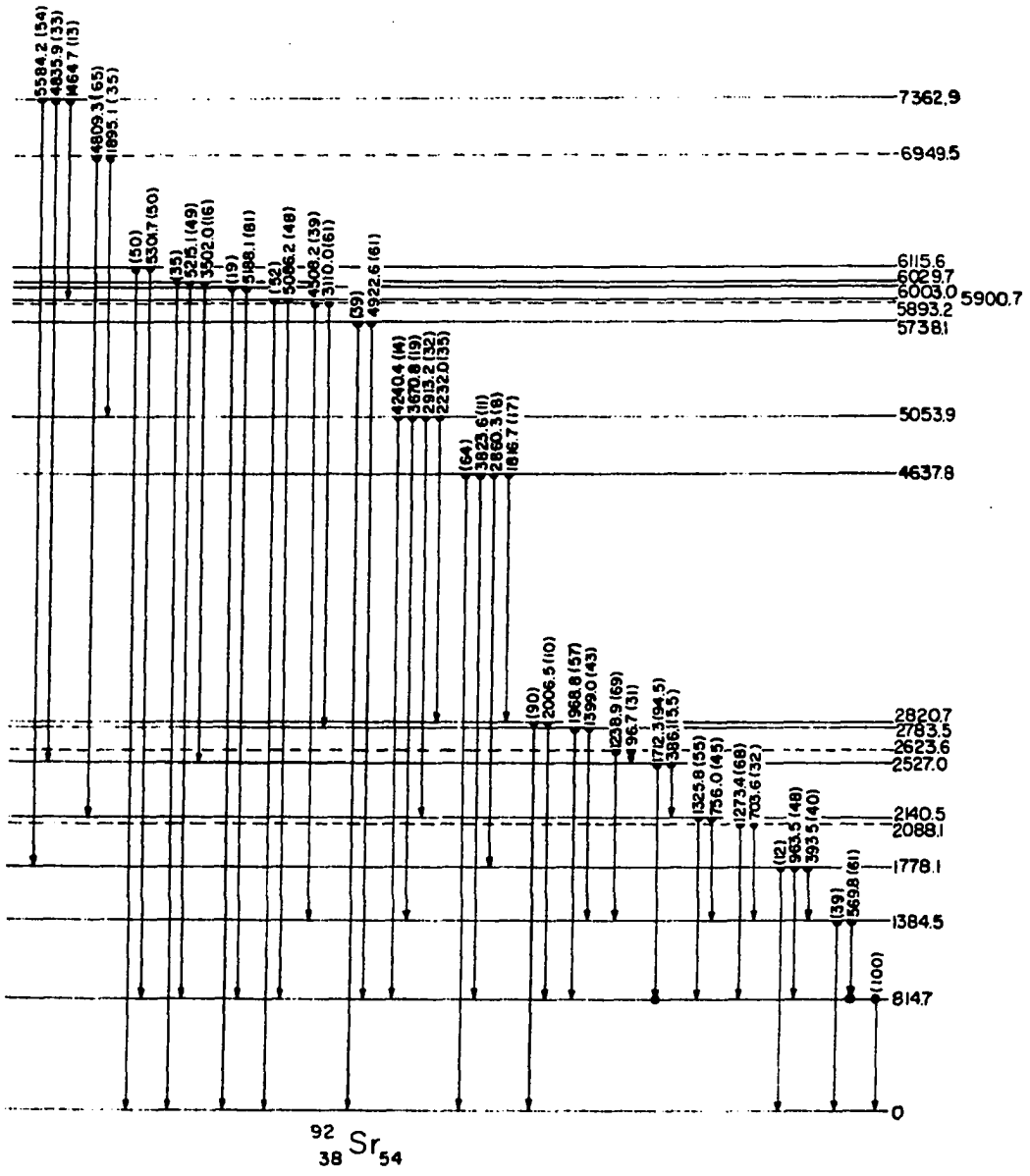

Figure 28. Level scheme of ^{92}Sr following the beta decay of ^{92}Rb

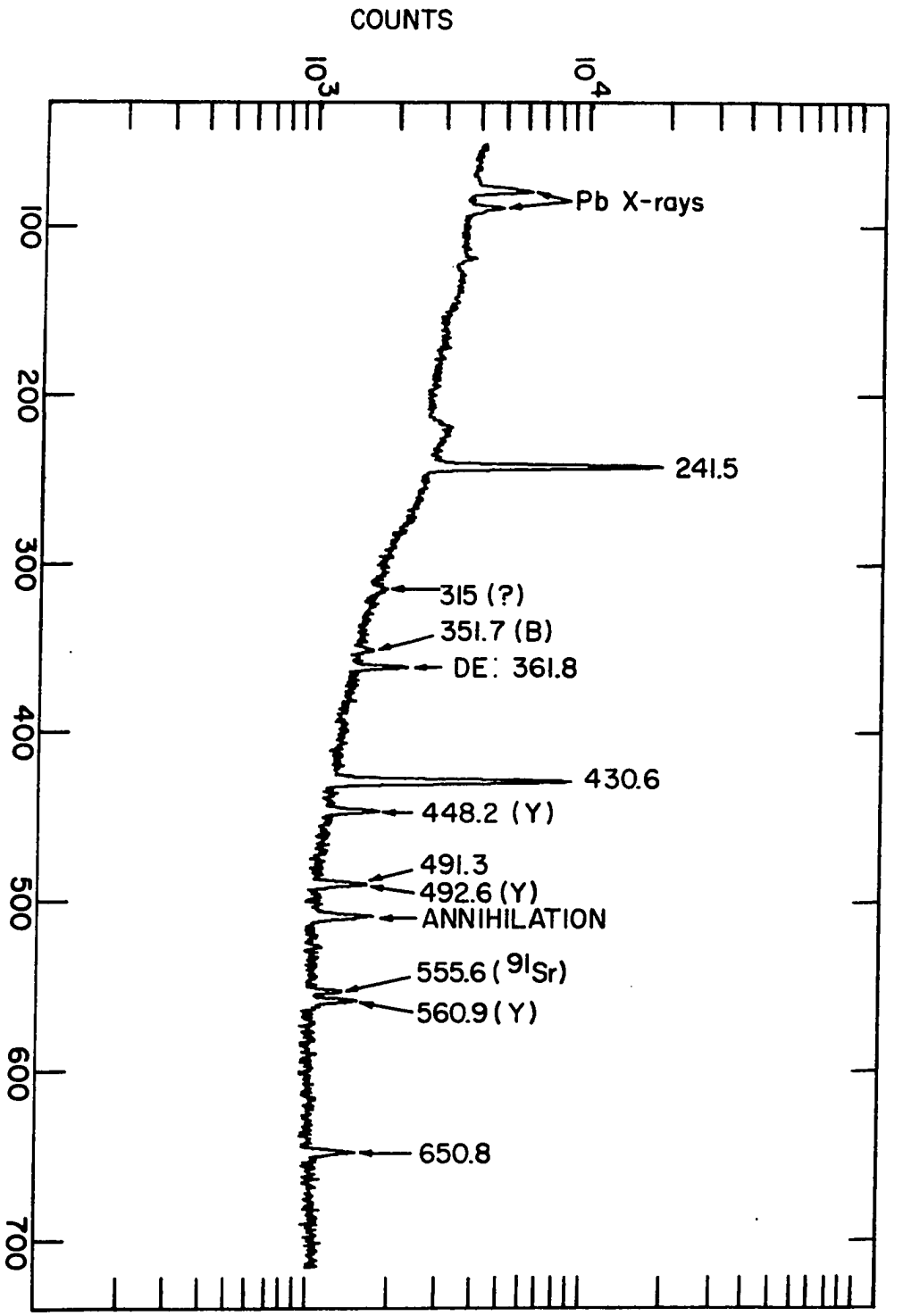

Figure 29a. Gamma ray spectrum of ^{92}Sr decay--50 keV to 725 keV

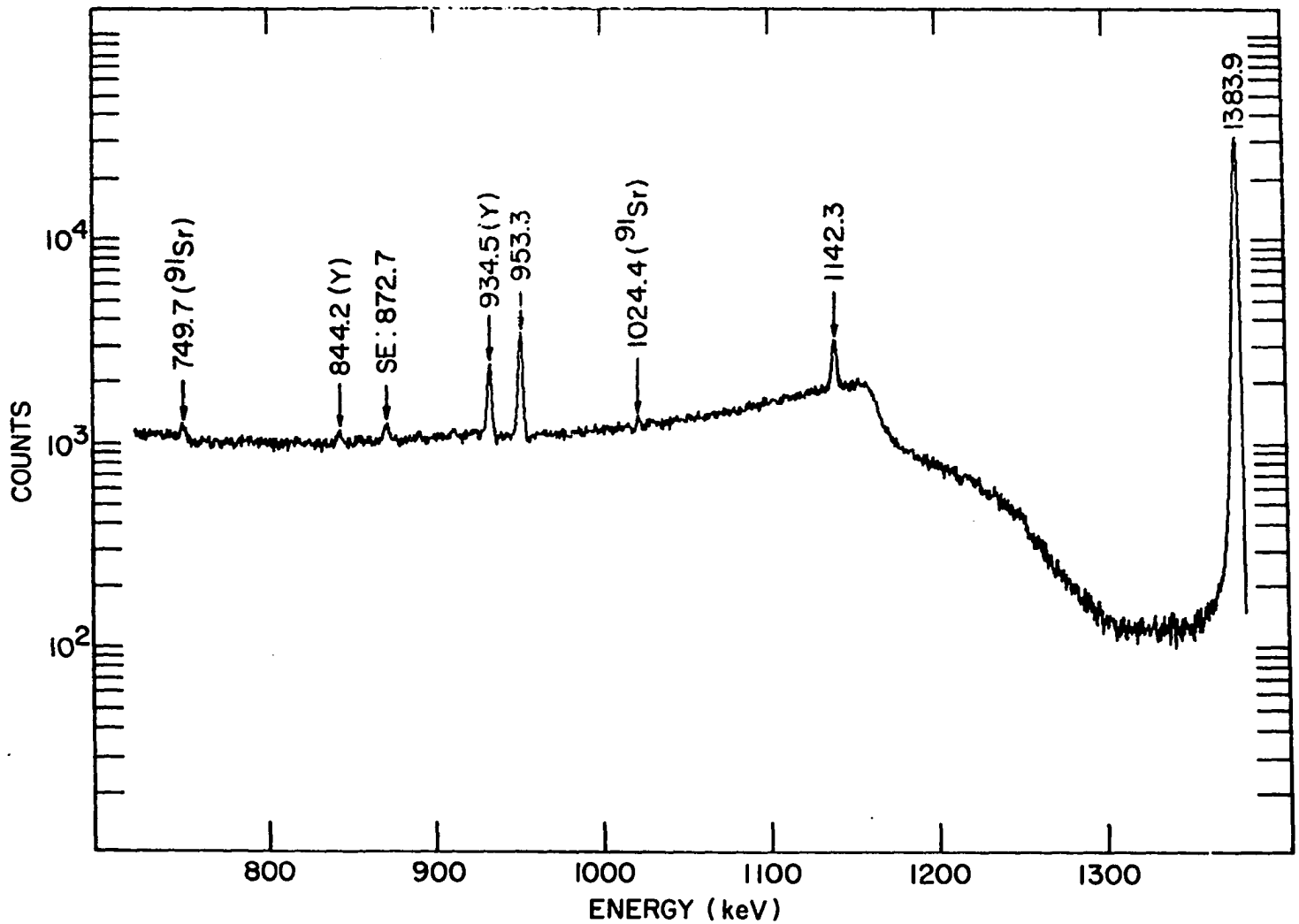

Figure 29b. Gamma ray spectrum of ^{92}Sr decay--725 keV to 1387 keV

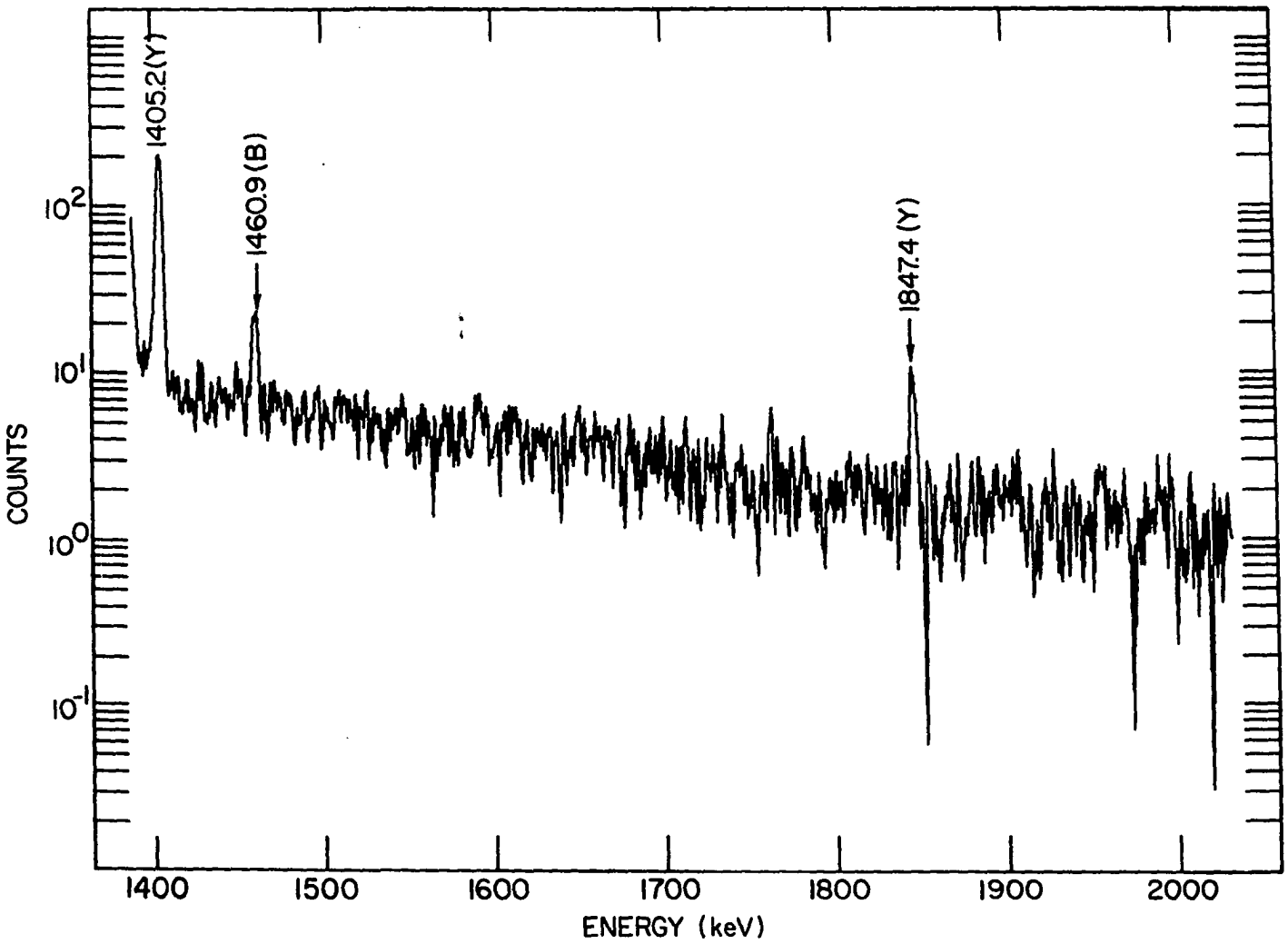

Figure 29c. Gamma ray spectrum of ^{92}Sr decay--1387 keV to 2040 keV

Table 12. Full-energy, single- and double-escape peaks in ^{92}Y

Energy (keV)	Relative Intensity[a]	Level Scheme Placement or Identity	Observed Coincidences
241.52 (.03)	33 (1)	241.5 to g.s.	491, 650, 1142
361.83 (.08)	2.89 (.18)	1383 DE	
430.56 (.05)	37 (2)	1383.9 to 953.3	953
491.3 (.2)	2.9 (.4)	1383.9 to 892.4	241, 650
650.8 (.1)	4.1 (.3)	892.4 to 241.5	241, 491
872.7 (.21)	2.7 (.4)	1383 SE	
892.2 (.4)	1.1 (.3)	892.4 to g.s.	
953.32 (.09)	40 (2)	953.3 to g.s.	430
1142.3 (.1)	32 (2)	1383.9 to 241.5	241
1383.94 (.06)	1000 (40)	1383.9 to g.s.	

[a]Normalized with 1383.94 as 1000.

Table 13. Calculated log ft values for beta decay to ^{92}Y levels

^{92}Y levels (keV)	Beta energy (MeV)	Percent beta branching	log ft
0	1.929	3.1	7.9
892.4 (.2)	1.037	0.2	8.0
953.3 (.1)	0.976	0.3	7.8
1383.93 (.05)	0.545	96.4	4.3

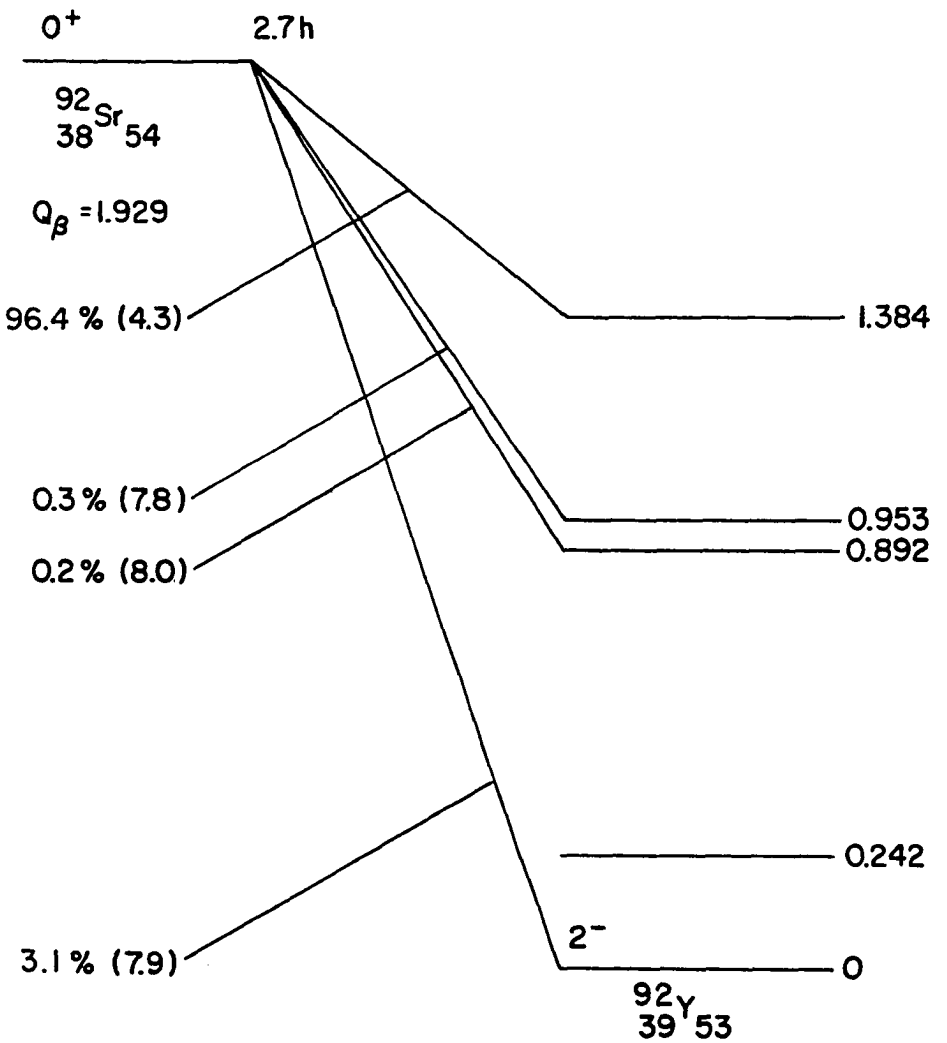

Figure 30. Beta feeding of ^{92}Y levels in ^{92}Sr decay

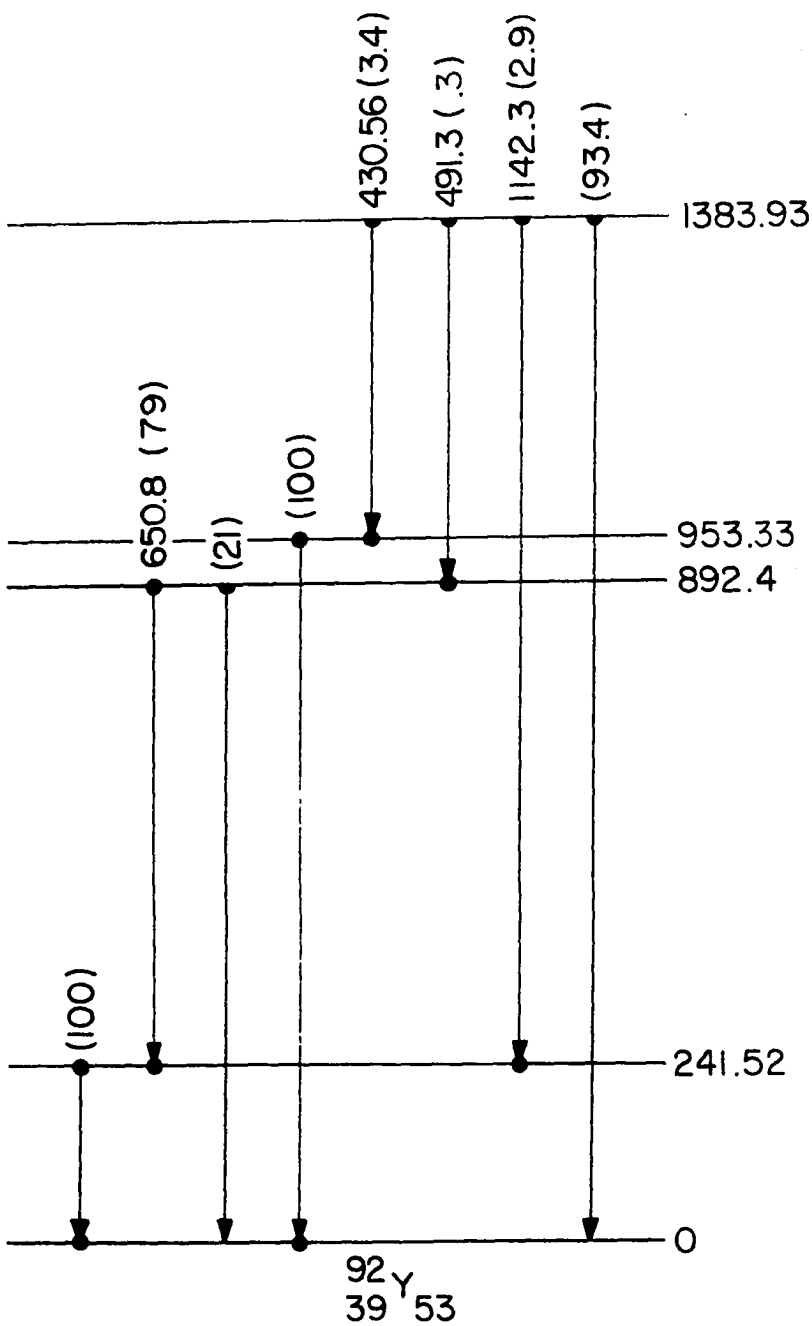

Figure 31. Level scheme of ^{92}Y following the beta decay of ^{92}Sr

VI. CONCLUSIONS

This section presents an interpretation of the level schemes which have been constructed for ^{92}Rb, ^{92}Sr, and ^{92}Y and a comparison of them with nearby nuclides and nuclides which might be expected to be similar on the basis of the independent particle shell model with jj-coupling. It should be noted that these level schemes are based solely on gamma ray spectroscopy with the exception of the measurement of the 2^- ground state spin and parity of ^{92}Y by Bunker et al. (52) (by an observation that the beta decay from the ^{92}Y ground state to the ^{92}Zr 0^+ ground state has a unique first-forbidden shape) and of the beta decay measurement by Heath (23) which suggests the 1384 keV level in ^{92}Y has a spin and parity of 1^+. These are the only actually accepted spins and parities in these three level schemes. Of course, the ground states of even-even ^{92}Sr and ^{92}Kr probably have $J^\pi = 0^+$ based on the systematics of even-even nuclei in general. Further, the 814 keV level in ^{92}Sr is most likely a 2^+ level, based upon the systematic occurrence of low-lying 2^+ states in even-even spherical nuclei (53). These pieces of information are very little upon which to base much interpretation of the level schemes reached by beta decay. Lacking further experimental measurements of spins and parities, the material which follows should be considered as tentative conjecture supported by what can be inferred from the known characteristics of the nuclides and the beta decays. Shell model explanations offered should be considered as suggestions of possible interpretations of the observed phenomena rather than as rigorous theoretical thoughts.

The consideration of level scheme systematics as a function of mass number A for these three nuclei is further limited in that this study marks the present limit of detailed spectroscopic studies of Kr, Rb, and Sr beta decay away from the valley of beta stability. Mass 93 is one of the next topics for investigation using the TRISTAN ISOL system with mass 94 as a possibility in the future. Studies of the beta decays of bromine activities which would give the levels of kryptons are also planned in the future for all cases where sufficient sample material can be collected to do nuclear spectroscopy. The material in this section is therefore necessarily limited to comparisons with Rb, Sr, and Y nuclei less neutron-enriched than mass 92 except in those rare cases where there exists an isolated piece of information (such as the energy of the first excited 2^+ level in both ^{94}Sr and ^{96}Sr). Comparisons with neighboring nuclei are not, however, limited to these three isotopes. For example, Zr nuclei are considered along with the Sr nuclei.

The following therefore represents a somewhat limited conjectural approach to the explanation of the level schemes constructed. It is hoped that the material will contribute eventually somewhat toward answering the question of the relation of the nuclear properties to the nuclear forces as studied in the two-body problem. It should be kept in mind, however, that level energies are not very sensitive to any but the gross features of the nuclear wave functions.

A. ^{92}Kr Decay to ^{92}Rb

Little is known about the ground state of ^{92}Kr from which the levels

observed in ^{92}Rb in this work are beta fed. As mentioned above, the ^{92}Kr ground state presumably has spin and parity 0^+. ^{92}Kr has 56 neutrons and 36 protons and probably has a ground state wave function comprised mainly of $\pi(p_{3/2})^2\ \nu(d_{5/2})^6$ and $\pi(f_{5/2})^{-2}\ \nu(d_{5/2})^6$. (In indicating shell model wave functions, the principal quantum numbers will be omitted. Proton configurations will be denoted by π and neutron configurations by ν. Closed subshells will generally not be indicated except for such cases as the one above where there is no partly-filled neutron subshell.)

The first nucleus for which the levels are considered, ^{92}Rb, has 55 neutrons and 37 protons and is thus an "odd-odd" nucleus. The energy levels of odd-odd nuclei are generally more difficult to interpret than those of even-even or odd A (even-odd) nuclei. The states of odd-odd nuclei will always consist of at least one unpaired proton particle or hole and one unpaired neutron particle or hole, which can sometimes couple strongly with each other.

It might be expected that the level scheme of ^{92}Rb would resemble that of ^{88}Rb on simple shell model grounds. The proton number is the same in both cases. ^{92}Rb has 55 neutrons and ^{88}Rb has 51. Since neutron number N = 50 is a magic number, ^{88}Rb then has one neutron outside a closed shell and ^{92}Rb has five. Since the next subshell to be filled for neutrons beyond N = 50 is the $2d_{5/2}$ which can hold a total of six particles, ^{92}Rb is one neutron short of closing this subshell. Thus ^{88}Rb has a $2d_{5/2}$ (neutron) particle and ^{92}Rb a $2d_{5/2}$ (neutron) hole. A single hole in a given nuclear subshell often has characteristics similar to those of a single particle in that same subshell. This suggests that ^{88}Rb and ^{92}Rb may have many features

of their level schemes in common.

A comparison of the ^{92}Rb level scheme constructed in this work with the ^{88}Rb level scheme found by Lycklama and Kennett (54) does not show much similarity. The main resemblance is an energy gap in the levels fed by beta decay which appears in both cases. ^{88}Rb is seen to have no states populated between the level at 1352 keV and the level at 2231 keV. ^{92}Rb was found to have a gap between 928 keV and 1361 keV. The only other point of strong similarity is the existence of one excited state in each case which receives the majority of the excited state beta feed. ^{88}Rb has a level at 2392 keV (above the gap) which receives 71% of the ^{88}Kr beta feeding while the ^{92}Rb level at 1361 keV (below the gap) is fed by 45% of the ^{92}Kr betas.

There is little else to compare besides these two points. The Q value for the ^{88}Kr beta decay is 2.9 MeV compared to the Q value of 5 MeV for ^{92}Kr, reflecting the difference in position of the two nuclei from the line of beta stability. The lowest beta-fed level seen in ^{92}Rb is 142 keV while a 28 keV level is postulated for ^{88}Rb. As a rule, the log ft's for ^{92}Kr beta decay are lower by about 2.0 than those for ^{88}Kr decay. The ground state of ^{88}Rb is 2^- while that for ^{92}Rb is probably 1^- (see the discussion later concerning coupling rules and log ft's). Finally, the levels in ^{92}Rb do not appear to "cluster" as much as do those for ^{88}Rb.

The lack of a great deal of similarity between these two level schemes may be understood, at least at lower energies, by considering the jj-coupling rules given for odd-odd nuclei by Brennan and Bernstein (55). The lower energy levels of ^{88}Rb should result from the quasi-particle

configurations $\pi(p_{3/2})^{-1}\ \nu(d_{5/2})$ and $\pi(f_{5/2})^{-1}\ \nu(d_{5/2})$. The measured spin and parity of 2^- for the ^{88}Rb ground state is in apparent contradiction with the lowest levels predicted by the coupling rules for these configurations. The lower energy levels of ^{92}Rb are probably due to the configurations $\pi(p_{3/2})^{-1}\ \nu(d_{5/2})^{-1}$ and $\pi(f_{5/2})^{-1}\ \nu(d_{5/2})^{-1}$. For the coupling rules of Brennan and Bernstein, there is a significant difference between the proton-hole, neutron-particle case of ^{88}Rb and the proton-hole, neutron-hole case of ^{92}Rb. Further, Freed and Rhodes (56) have noted that particle-particle (or hole-hole) spectra in the mass 90 region are in general strongly sensitive to core renormalization effects arising from realistic nuclear forces while particle-hole spectra appear to be less affected. But essentially, the particle vs. hole similarity fails in this case because odd-odd nuclei rather than odd-even nuclei are being considered here.

Since the level scheme of ^{90}Rb has appeared recently in the literature (57), a comparison was also made of it with the ^{92}Rb level scheme. ^{90}Rb should be somewhat similar to ^{92}Rb as far as the coupling is concerned since three neutrons in a $d_{5/2}$ subshell can be considered as either three particles or three holes. ^{90}Kr should also be somewhat similar to ^{92}Kr so that when the Q value for beta decay of the former (4.41 ± 0.03 MeV (57)) is noted to be almost the same as that for the latter (~5 MeV) it is surprising that the ^{90}Kr beta decay half-life should be a factor of 17.6 greater than that for ^{92}Kr (25).

The main points of similarity between ^{90}Rb and ^{92}Rb are found to be the same as between ^{88}Rb and ^{92}Rb. ^{90}Rb has an energy gap in the levels

fed by beta decay between 730 keV and 1240 keV. ^{90}Rb also has a strongly beta-fed level above this gap. Sixty-six percent of the beta decay intensity goes to a level at 1780 keV. In addition to these two features, ^{90}Rb probably has a ground state spin and parity of 1^- which would be the same as that postulated for ^{92}Rb.

Some general comments can be made concerning the levels reached by beta decay in ^{92}Rb in terms of quasi-particle states typical of this region. Although the $2p_{3/2}$ and $1f_{5/2}$ shells compete for the odd proton in this region, the ground state spins of the odd-mass Rb nuclei nearby lead one to believe that the ^{92}Rb ground state is largely composed of the $\pi(p_{3/2})^{-1}\ \nu(d_{5/2})^{-1}$ configuration. In this case, the Brennan and Bernstein coupling rules predict the spin and parity of the ground state will be either 1^- or 4^-. The log ft of 4.69 for beta decay from ^{92}Rb surely rules out the 4^- case. In fact, the log ft is low enough to be in the "allowed" category, which would indicate a positive parity state. This conflicts with the higher log ft of 5.74 observed for beta decay from the ^{92}Rb ground state to the ^{92}Sr ground state which has spin and parity 0^+. This latter log ft is more nearly in the region for first-forbidden non-unique beta decays expected for this region of the nuclidic chart (58). It is not understood exactly why the log ft for beta decay from ^{92}Kr to the ^{92}Rb ground state is so low. The indirect ground state beta feed determination may be in error for this case, causing the discrepancy. A direct measurement of the beta feed to the ground state of ^{92}Rb would possibly help to clear up this point.

Some of the lower lying ^{92}Rb levels which have first-forbidden log ft's

or no beta feeding observed at all are expected to result from the two quasi-particle configurations of $\pi(p_{3/2})^{-1}$ or $\pi(f_{5/2})^{-1}$ combined with the $\nu(d_{5/2})^{-1}$. Most of these levels have gamma transitions going to the 1^- ground state and thus are expected to have low spin ($\lesssim 3$). Some of the other levels below the 1361 keV state may be interpreted as belonging to a negative parity band due to the coupling of quadrupole vibrational states to the negative-parity low-lying states (a vibrational band built on quasi-particle states). Some possible seniority 4 states which could lie in this region result from the configurations:

$$\pi((f_{5/2})^{-2}\ (p_{1/2}))\ \nu(d_{5/2})^{-1}$$

$$\pi((f_{5/2})^{-2}\ (p_{1/2}))\ \nu(d_{5/2})^{4}\ (g_{7/2}))$$

$$\pi((p_{3/2})^{-2}\ (p_{1/2}))\ \nu(d_{5/2})^{-1}$$

$$\pi((p_{3/2})^{-2}\ (p_{1/2}))\ \nu(d_{5/2})^{4}\ (g_{7/2}))\ .$$

The allowed nature of the beta decay to the 1361 keV level (log ft = 4.17) indicates that the spin and parity of this state should be 0^+ or 1^+, with the 0^+ choice being ruled out by the isobaric spin selection rule. This allowed beta decay might be understood to occur in the following way. The 1361 keV level could have a configuration of $\pi(g_{9/2})\ \nu(g_{7/2})$ which then couples to a spin and parity of 1^+ by the Brennan and Bernstein rules. This state represents a two-particle transition from the ground state with

a $p_{3/2}$ proton lifted to a $g_{9/2}$ state and a $d_{5/2}$ neutron lifted to a $g_{7/2}$ state. On the surface, this would appear to require a great deal of energy but probably much of this energy would be returned from the pairing of the $g_{9/2}$ proton and the $g_{7/2}$ neutron together in the same orbit. For the beta decay to occur, the ground state of ^{92}Kr must also then contain an admixture of the configuration $\pi(p_{3/2})^2\ \nu((d_{5/2})^4(g_{7/2})^2)$. This would then allow the beta decay to be thought of as a $g_{7/2}$ neutron decaying into a $g_{9/2}$ proton. Such a Gamow-Teller beta decay with spin-flip only is then allowed, as is needed to explain the low log ft. The amount of admixture necessary can be calculated using the matrix element of the Gamow-Teller operator given the experimental log ft, although this has not been done. Since transition rates are much more sensitive to wave function details than are level energies, it is possible that not much admixture would be needed to get such a low log ft. There is no other experimental information on configurational mixing of $g_{7/2}$ neutron states into the ground state of ^{92}Kr (or of ^{90}Kr, either). However, a small fraction (9%) of the ^{92}Zr (N = 52) ground state has been found to be due to $(g_{7/2})^2$ admixture as will be discussed in the material on ^{92}Sr decay to ^{92}Y levels. This might suggest that postulation of similar configurational mixing in ^{92}Kr would not be unreasonable.

Another way of explaining the allowed beta decay from the ^{92}Kr ground state is to consider the 1361 keV configuration as $\pi(p_{3/2})^{-1}\ \nu((d_{5/2})^6(g_{9/2})^{10}(p_{1/2}))$, where here only one particle, a neutron, has been lifted all the way up from the $p_{1/2}$ subshell to the $d_{5/2}$ subshell (it is expected that the proton-neutron pairing interaction will not be as great for the

p shell as for the g shell case earlier). Now the allowed beta decay takes place as a $p_{1/2}$ neutron decaying into a $p_{3/2}$ proton (again a $\Delta\ell = 0$, spin-flip, allowed transition). Here, configuration mixing for the $p_{1/2}$ neutron in the ^{92}Kr ground state is involved. Finally, it could be possible that neither of these two cases occur and rather that the low log ft is caused by a strange case of coupling to a collective excitation.

Other allowed transitions may be occurring to the following experimental levels in ^{92}Rb (on the basis of log ft values) which would then also be expected to have low spins and positive parities: 2039, 2587, 2611, 2718, 2901, 3057, 3149, 3338, 3341, 3659, and 4193 keV. These allowed-type transitions to higher energy levels are also seen in ^{88}Rb and ^{90}Rb. They may be arising from a band due to the coupling of octupole vibrational states to the negative parity ground state band to give an overall positive parity band.

One final piece of experimental information has been obtained for the 142 keV level in ^{92}Rb (the first excited state). Its lifetime against gamma decay has been measured by Malmskog and McDonald (59) as $(0.75 \pm 0.03) \times 10^{-9}$ sec. This value was used to compute a photon transition probability for the 142 keV gamma and the result was compared with values predicted for photons of various multipolarities. With this half-life, the 142 keV transition was found to be mostly M1. Since the transition goes to the ground state which has a conjectured spin and parity 1^-, and the 142 keV level is not observed to be beta fed, the latter is probably a 2^- level. This assignment fits in with the quasi-particle configurations discussed earlier for this energy region in ^{92}Rb. It is perhaps the analog

of the ^{88}Rb 2^- ground state.

B. ^{92}Rb Decay to ^{92}Sr

The level structure of ^{92}Sr as fed by beta decay from ^{92}Rb is not as well-determined as the level scheme for ^{92}Rb discussed in the previous section, especially for higher energies. The reasons for this are several. Most importantly, the gamma counting rate obtained in the ^{92}Sr level scheme studies was not as high as in the ^{92}Rb level studies. The process of running in a mode to enhance the isobaric decay of ^{92}Rb over the other members in the mass 92 chain caused some of the low count rate problems. A trade-off had to be made between the enhancement of ^{92}Rb decay lines and the counting rate. Another significant reason for the low experimental count rate was the high percentage of beta feed to the ^{92}Sr ground state. The excited levels of ^{92}Sr were just not populated to the extent that the ^{92}Rb levels were and this cut down on the subsequent gamma emission observed.

The lower counting rate had an effect on both the singles and the coincidence data. The statistics for the singles data were not as good as for gammas from ^{92}Rb levels and this caused the errors to be greater for the gamma ray energies and intensities found. Any time the errors of a set of gamma ray transitions are increased, the use of crossover relations for the placement of gamma rays in a level scheme is made more difficult since more ambiguities (accidental crossover relations) will arise.

The effect on the coincidence results was much more serious since the coincidence counting rate for an experiment with two roughly equal Ge(Li)

detectors varies approximately quadratically with the singles counting rate. In fact, significant coincidence information was obtained only for a gate on the 814 keV transition (which was by far the strongest gamma ray seen) depopulating the first excited state. The rest of the ^{92}Sr level scheme then had to be determined from energy sum and intensity considerations.

The gamma transitions extended to much higher energies for the ^{92}Rb decay than for the decay of ^{92}Kr. Since the efficiency of the Ge(Li) detectors drops off rapidly with increasing energy above a few hundred keV, the counting rate for these gammas became quite small. Any coincidence work on these gammas was out of the question for the 30 cc detectors used.

For all these reasons, interpretation of the ^{92}Sr levels will be limited to those states at lower energies. Fortunately, there is one simplification for this nucleus. ^{92}Sr is an even-even nuclide, for which some properties are known in general. As has been mentioned earlier, the ground state and the 814 keV level are probably 0^+ and 2^+, respectively.

The log ft for beta decay to the ^{92}Sr ground state has been discussed earlier in connection with determining the spin and parity of the ground state of ^{92}Rb. This beta decay is expected to be first forbidden, 1^- to 0^+. If the ^{92}Rb ground state is indeed 1^-, then beta decay from it will feed only low spin excited states of ^{92}Sr. Since the ground state of ^{92}Rb is thought to be $\pi(p_{3/2})^{-1}\ \nu(d_{5/2})^{-1}$, with an admixture of $\pi(f_{5/2})^{-1}\ \nu(d_{5/2})^{-1}$, the beta decay to the ground state of ^{92}Sr may be interpreted as a $d_{5/2}$ neutron decaying to a $p_{3/2}$ or $f_{5/2}$ proton ($\Delta\ell = 1$, parity change,

first-forbidden non-unique). The ground state of ^{92}Sr is then probably mainly comprised of the configuration $\pi((p_{3/2})^4(f_{5/2})^6)\nu(d_{5/2})^{-2}$. (It will be seen in the next section that some $\nu(g_{7/2})^2$ contribution may be mixed in.)

Using shell model considerations, ^{92}Sr can be related to ^{94}Zr. Both nuclei have 54 neutrons, of which the first 50 are assumed to comprise a closed core and the last four are expected to be in a $(d_{5/2})^{-2}$, or equivalently a $(d_{5/2})^4$, configuration. ^{92}Sr has 38 protons which presumably closes the $2p_{3/2}$ and $1f_{5/2}$ subshells, irrespective of whichever lies higher. ^{94}Zr has two additional protons with Z = 40, which then closes the next subshell, $2p_{1/2}$. Since proton subshells would seem to be closed in either case, the two nuclei should be similar for those levels determined solely by the $(d_{5/2})^4$ neutron configuration.

It is thought that the single-particle $2p_{1/2}$ proton level lies from 1.5 MeV (60) to 1.85 MeV (61) above the $p_{3/2}$-$f_{5/2}$ level complex in this mass region. Also for this mass region, the $1g_{9/2}$ single-particle proton level is estimated to be about 0.9 MeV above the $2p_{1/2}$ (62). While these level separations are not comparable with those associated with magic number shell closures, they may be significant enough for their effects to be observed in level schemes in this mass region.

On the other hand, neutrons beyond N = 50 occupy primarily the $2d_{5/2}$ orbit. Preston et al. (63) determined that the increases in single-particle energies above that for the $2d_{5/2}$ neutron level in this region were 1.215 MeV for the $3s_{1/2}$, 2.07 MeV for the $2d_{3/2}$, and 2.19 MeV for the

$1g_{7/2}$. Cohen (64) used stripping reactions to determine the spacings in ^{92}Zr as 1.7 MeV, 2.6 MeV, and 2.6 MeV for the $3s_{1/2}$, $2d_{3/2}$, and $1g_{7/2}$ states, respectively, and in ^{94}Zr as 2.1 MeV, 3.3 MeV, and 3.3 MeV. Using an angular distribution measurement on a stripping reaction, Cohen and Price (65) found that the ^{92}Zr 2^+ level at 0.93 MeV was a rather pure $(d_{5/2})^2$ configuration.

A comparison of ^{92}Sr with the ^{94}Zr level scheme populated by beta decay (66), with spins and parities for the latter provided by recent (p,t) reaction studies by Ball et al. (67), shows a first excited state of spin and parity 2^+ at 814 keV in the former and at 920 keV in the latter. Above this energy range, the agreement abruptly ceases. The next levels in ^{94}Zr are a 0^+ state at about 1300 keV and a 4^+ state at 1470 keV. The next two levels in ^{92}Sr are the 2^+ level (by beta decay log ft and the existence of a strong gamma de-excitation to the 0^+ ground state) at 1384 keV and a level at 1778 keV for which no conjecture on spin and parity is made at this point. The ^{94}Zr level scheme was determined in the beta decay from ^{94}Y only up to 2058 keV so no further comparison can be made (there is no more agreement up to that energy).

To investigate further the comparison between the Sr and Zr nuclei in this mass region, the predictions of the method of "effective interactions" will be discussed because it works well for the $(d_{5/2})^n$ states proposed for the Zr. With the similarities pointed out above for configurations of ^{92}Sr and ^{94}Zr which should hold in general between ^{A}Sr and $^{(A+2)}Zr$ for $90 \leq A \leq 94$, the method should also have application for the

Sr nuclei.

Basically, the method of effective interactions as explained by Talmi and Unna in an excellent review article (68) assumes that the potential energy of a nucleus is due to two-body interactions between nucleons. Instead of constructing specific wave functions for the states involved or assuming a specific form for the two-body nuclear interaction, they use experimental data from nuclear level separations to evaluate the nuclear matrix elements. Underlying this type of calculation is the assumption that the matrix elements are the same for neighboring nuclei so that the number of matrix parameters is less than the number of experimental points available.

For the case where only states arising from $(d_{5/2})^n$ configurations in a jj-coupling scheme are considered, there are only three constants to be determined which can be related to the matrix elements

$$\langle (d_{5/2})^2 \; J=0 \; |V| \; (d_{5/2})^2 \; J=0 \rangle \equiv V_0$$

$$\langle (d_{5/2})^2 \; J=2 \; |V| \; (d_{5/2})^2 \; J=2 \rangle \equiv V_2$$

$$\langle (d_{5/2})^2 \; J=4 \; |V| \; (d_{5/2})^2 \; J=4 \rangle \equiv V_4 \; .$$

These constants are related to the level energies of the 0^+, 2^+, and 4^+ states arising from the $(d_{5/2})^2$ configuration, and can be used to predict level energies for other $(d_{5/2})^n$ configurations with $n \neq 2$ by the use of relations which are derived purely from angular momentum considerations

(Racah algebra).

The effective interaction concept was applied by Talmi to the Zr nuclei (69). Identifying the 0^+, 2^+, and 4^+ levels due to $\nu(d_{5/2})^2$ in ^{92}Zr as the ground state, the 930 keV level, and the 1490 keV level, respectively, Talmi predicted the $\nu(d_{5/2})^3$ configuration in ^{93}Zr would have a 3/2+ state (seniority = 3) at 260 keV and a 9/2+ state (seniority = 3) at about 1100 keV above the 5/2+ state (seniority =1) ground state. The 3/2+ level is seen at 267 keV and there is a possible 9/2+ level at 1168 keV (70). This last level is very tentative, however.

The effective interaction model further predicts that the $0^+ - 2^+$ and $0^+ - 4^+$ level spacings will be the same for ^{94}Zr as for ^{92}Zr (basically because $(d_{5/2})^4 \equiv (d_{5/2})^{-2}$ is equivalent to $(d_{5/2})^2$). Experimentally, the 2^+ level in ^{94}Zr lies at 920 keV and the 4^+ level lies at 1470 keV (71). This is in quite good agreement with the ^{92}Zr levels.

The effective interaction approach has been used by Malmskog and McDonald (72) to calculate the energies of the first excited 3/2+ and 9/2+ states due to the $\nu\ (d_{5/2})^3$ configuration in ^{91}Sr using the parameters as obtained from the 0^+, 2^+, and 4^+ levels due to $(d_{5/2})^2$ in ^{90}Sr. The 1655 keV level in ^{90}Sr (57) is assumed to be the 4^+ level (this gives the closest results). The calculations predict that the 3/2+ level in ^{91}Sr should lie 25 keV above the 5/2+ ground state whereas experimentally the energy difference is found to be 93.54 keV. The 9/2+ level was calculated to lie at 1260 keV above the ground state which agrees well with a level found recently at 1230 keV (spin and parity unknown) by Mason and Johns (73).

The effective interaction predicts the same $0^+ - 2^+$ and $0^+ - 4^+$ level spacings for ^{92}Sr and for ^{90}Sr ($(d_{5/2})^4$ vs. $(d_{5/2})^2$). The 2^+ state in ^{90}Sr is at 831 keV (57) while ^{92}Sr is in good agreement with its first excited 2^+ state at 814 keV. Unfortunately, there is no level seen in this work near 1665 keV in ^{92}Sr, which is the energy of the 4^+ state in ^{90}Sr.

Since the effective interaction method does not work for ^{92}Sr as well as for ^{94}Zr, two other methods were tried for determining the effective interaction parameters to be used to find the 4^+ state. In the first try, the energy difference between the 3/2+ and 5/2+ and the 9/2+ and 5/2+ levels in ^{91}Sr were used to find the constants in the hope that these parameters might be more valid for use with ^{92}Sr, having been determined from levels in a nucleus one mass number closer to ^{92}Sr. With these parameters, the 2^+ level in ^{92}Sr was predicted to lie at 871 keV and the 4^+ level at 1629 keV. These results do not represent any improvement.

A second try was made to find the parameters using the 3/2+ to 5/2+ level spacing in ^{91}Sr and the 2^+ to 0^+ level spacing in ^{92}Sr itself. It was hoped that these values would be better since they were determined using lower energy levels than the first two cases and also because the 3/2+ state in ^{91}Sr and the 2^+ state in ^{92}Sr were identified reasonably well (cf. the tentative 4^+ state in ^{90}Sr and the tentative 9/2+ state in ^{91}Sr). However, this set of parameters predicted the 4^+ level at 1514 keV which still could not be identified with an experimental level.

It thus appears that the use of the effective interaction method and/or the conjecture of the purity of the $\nu(d_{5/2})^n$ configurations is not valid

for the Sr nuclei. That is, a study of ^{92}Sr has produced some information on the question of possible shell closures at Z = 38 and Z = 40. It appears that Z = 38 is not a good shell closure and further that the change in proton number from 38 to 40 could be affecting the neutron single-particle levels. Reaction work done by Hardy et al. (74) also suggests the failure of the closed shell at ^{88}Sr. More levels at low energies in ^{91}Y were seen in this work than would be expected from shell model considerations if ^{88}Sr were a closed core.

A significant difference between proton numbers Z = 38 and Z = 40 can be seen when the dependence of the energy of the first excited 2^+ level for even-even nuclei is charted versus neutron number. This has been done in Figure 32 for the Kr (Z = 36) nuclei (75,76), the Sr nuclei (15,57,76-79), the Zr nuclei (15,26,71,80-83), and the Mo (Z = 42) nuclei (15,84-88) for which experimental evidence was available. All four cases show a large increase in the band-gap energy for N = 50, the magic number. For N = 56, however, only Zr shows evidence of the closure of the $2d_{5/2}$ subshell. It is thus not surprising that the effective interaction applied to $(d_{5/2})^n$ configurations is more successful for the Zr nuclei than for the Sr nuclei. The effect of two additional protons in going from Z = 38 to Z = 40 or from Z = 40 to Z = 42 is seen to be significant in this region.

Figure 32 also shows for the Zr and Mo nuclei an indication of the onset of stable deformation. The approximate limit for the energy of the first excited 2^+ state below which nuclei in this mass region are probably stably deformed is about 300 keV (10). This borderline is crossed by both Zr and Mo for N = 60. For Zr, the change from ^{98}Zr (1223 keV) to ^{100}Zr

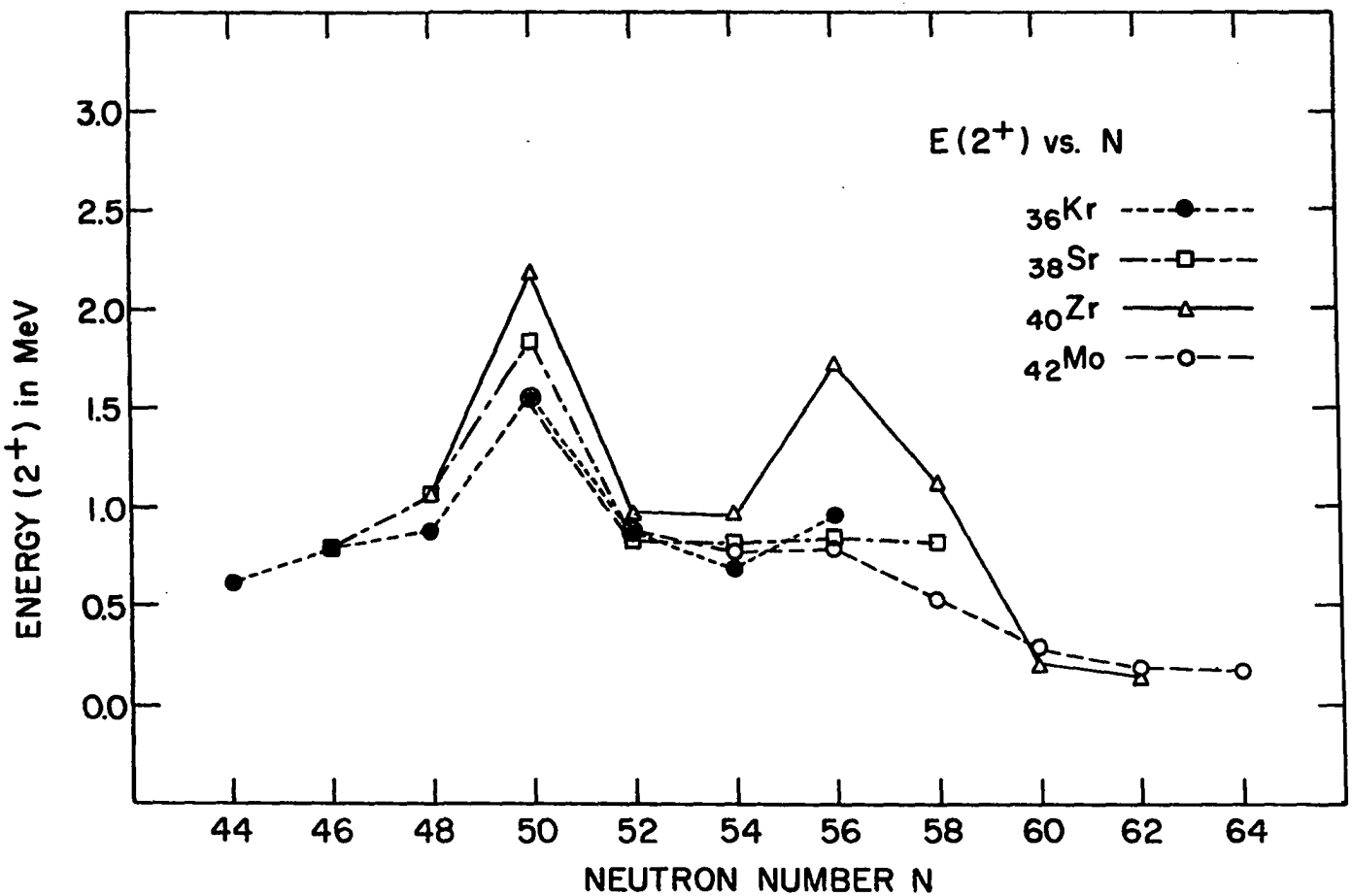

Figure 32. Experimental energies of the first excited 2+ level in even-even nuclei versus neutron number for Kr, Sr, Zr, and Mo

(212.7 keV) is very abrupt, indicating that the stable deformation develops suddenly for a change in neutron number of only two.

The collective vibrational model was considered as an explanation for some of the low-lying levels in ^{92}Sr. With the most reasonable choice for the states in the two-phonon 0^+, 2^+, 4^+ band, the ratio of the energy of the center of gravity of this triplet to the energy of what would be assumed to be the one-phonon 2^+ level (814 keV) turns out to be 2.47, too large for a nucleus this close to shell closure. This picture was discarded in favor of a model of two-quasi-particle states provided by the shell model.

Before discussing the shell model configurations considered for the low-lying levels in ^{92}Sr, the evidence for tentative spin and parity assignments obtained from relative photon transition probability considerations (89) for these levels will be presented. Only the levels up to the gap at 2820.7 keV will be covered.

The ground state and the 814 keV level are assumed known as 0^+ and 2^+, respectively, as discussed previously. All levels between 1384 keV and 2820 keV, which are beta-fed, have log ft's between 7.03 and 8.14. These beta transitions are considered first-forbidden (parity change, $\Delta J = 0,1,2$) which then limits each of these levels to spins and parities of 0^+, 1^+, 2^+, and 3^+ since they are fed from the 1^- ground state of ^{92}Rb. The two levels for which no beta-feeding is seen (2140 keV and 2783 keV) are assumed to have possible second- or third-forbidden beta transitions to them since the upper limits on the assumption of zero feeding are not known. This requires these two levels to have spins and parities of 3^-, 4^-, 4^+,

or 5^+. Relative photon transition probability considerations and the levels with known spins and parities are then used to further limit the possible spins and parities for each level.

1384 keV level: This cannot be a 0^+ state since a strong gamma transition is seen to the 0^+ ground state and 0^+ to 0^+ gamma transitions (of type E0) are not allowed. The 3^+ assignment is also ruled out by the presence of a ground state gamma. Depopulation branching intensities do not differentiate between the 1^+ and 2^+ possibilities. However, the 756 keV transition from the 2140 keV level suggests the 1384 keV level as having spin and parity of 2^+.

1778 keV level: The 0^+ and the 3^+ possibilities are ruled out by the ground state gamma. Depopulation branching suggests that a 2^+ assignment is best for this level.

2088 keV level: This level is suggested to have spin and parity of 2^+, from consideration of depopulation branching intensities and the lack of an observed ground state gamma transition. (A transition from the 2088 keV level (assumed to be 2^+) to the ground state (0^+) would have multipolarity E2. Calculated branching for such a transition in competition with the other two (M1) transitions depopulating this state suggests that this transition would be too weak to be seen in this work.)

2140 keV level: 3^-, 4^-, or 4^+ possibilities are indicated by the transitions to the 1384 keV and 814 keV levels. The 386 keV transition from the 2527 keV level points to 4^+ as the most likely spin and parity.

2527 keV level: The most likely spin-parity assignment is 3^+ from

depopulation branching intensities and the lack of a ground state transition.

2623 keV level: To fit this level in, it is necessary to assume a spin and parity of either 2^+ or 3^+ and that the 96 keV gamma is M1 and the 1238 keV gamma is E2. The conversion coefficient for an M1 96 keV gamma is about 0.2 from the tables of Sliv and Band (90). With these assumptions, the depopulation intensity ratio can be predicted to within a factor of 3.

2783 keV level: Depopulation considerations rule out the 5^+ possibility, and do not allow a distinction between the 3^-, 4^-, and 4^+ possibilities.

2820 keV level: This level has a ground state gamma transition ruling out 0^+ and 3^+ assignments. The best fit for branching intensities is obtained for both gammas being M1 which yields a 1^+ spin and parity.

Of the ten levels considered here (including the ground state), the most probable spins and parities are thus 0^+ for the ground state, 2^+ for 814 keV, 2^+ for 1384 keV, 2^+ for 1778 keV, 2^+ for 2088 keV, 4^+ (3^-, 4^-) for 2140 keV, 3^+ (2^+) for 2527 keV, 2^+ or 3^+ for 2623 keV, 3^- or 4^- or 4^+ for 2783 keV, and 1^+ for 2820 keV.

From shell-model considerations, the neutron configuration $(d_{5/2})^4$ is still considered to give levels of spin-parity 0^+, 2^+, and 4^+. Two other possible lower-energy proton quasi-particle configurations are $\pi((p_{3/2})^{-1}(p_{1/2}))\ \nu(d_{5/2})^4$ and $\pi((f_{5/2})^{-1}(p_{1/2}))\ \nu(d_{5/2})^4$ which will give levels with spins and parities of 1^+ and 2^+ for the former and 2^+ and 3^+ for the latter. The next most likely configuration is the neutron two-quasi-particle one $\pi((p_{3/2})^4(f_{5/2})^6)\ \nu((d_{5/2})^3(s_{1/2}))$ (the $3s_{1/2}$ is

considered to be the next single-particle level above the $2d_{5/2}$ for this mass region (63,64)). This configuration forms states with level spins and parities of 2^+ and 3^+.

Summarizing these quasi-particle levels considered so far yields 0^+, 2^+, 2^+, 2^+, 2^+, 4^+, 3^+, 3^+, and 1^+. These values have been arranged to show the obvious similarity to the experimentally determined spins and parities listed earlier. There is a one-to-one correspondence between the lists except for the 2783 keV (3^-, 4^-, 4^+) level. A negative parity state (non-collective) is not easy to obtain at low energies from the shell model for ^{92}Sr. If the level has spin-parity of 4^+, it could be associated with the configuration $\pi((f_{7/2})^{-1}(p_{1/2}))\ \nu(d_{5/2})^4$.

These shell model quasi-particle states listed here should not be considered as rigorous explanations of the levels observed (the experimental spins and parities are not determined all that well). Rather, the configurations suggested are an indication that the shell model can provide enough of the right kinds of states to explain the experimental details observed. The use of such a model would seem to be justified for ^{92}Sr. More precise application of the model must await further experimental data on spins and parities and transition multipolarities.

Spins and parities of levels above the energy gap at 2820 keV in levels fed by beta decay are not considered here. However, it may be noted that the log ft's tend to decrease with increasing energy. This would suggest the existence of negative parity states (allowed beta transitions) at these higher energies. This is in agreement with the shell

model since it is possible to create negative parity states given sufficient energy (by lifting a neutron from the $2p_{1/2}$ subshell across the closed shell to the $2d_{5/2}$ subshell, for example), and could also indicate the presence of small admixtures of the isobaric analog state in the higher energy levels.

C. ^{92}Sr Decay to ^{92}Y

In terms of the shell model, ^{92}Y does not offer any golden opportunities for comparison with similar nuclei. The protons should have a $(p_{1/2})^1$ ground state configuration, which is a half-filled subshell. The neutrons are in a $(d_{5/2})^3$ configuration, which is also a half-filled subshell. When one thus changes particles into holes for either protons or neutrons, the original nucleus is retained. Probably the best comparisons to be made are to keep the proton number fixed and vary the neutron number up (^{94}Y) or down (^{90}Y) by a pair. Only in the latter case does this prove useful as little is known about the former.

The most striking feature of this beta decay is the allowed nature of the transition to the 1383 keV level (log ft = 4.3). Since the ground state spin-parity of ^{92}Sr is 0^+, this limits the spin and parity of the 1383 keV level to 1^+. This case is similar to the beta decay of ^{92}Kr to the 1361 keV level in ^{92}Rb. It is suggested that this occurs because the 1383 keV level has the configuration $\pi(g_{9/2})\ \nu((d_{5/2})^2(g_{7/2}))$ and because the ^{92}Sr ground state has an admixture of $\pi((p_{3/2})^4(f_{5/2})^6)\ \nu((d_{5/2})^2(g_{7/2})^2)$. The beta decay is then a $g_{7/2}$ neutron decaying into a $g_{9/2}$ proton (Gamow-Teller decay as discussed in the ^{92}Kr Decay to ^{92}Rb section).

As mentioned earlier, transition rates are much more sensitive than level energies to wave function details so that a small amount of admixture may give enough overlap of the wave function for allowed beta decay to occur. Information on ^{92}Zr (91) indicates an admixture of 9% $\nu(g_{7/2})^2$ for its ground state. It is thus reasonable to expect also some $\nu(d_{5/2})^2(g_{7/2})^2$ admixture in the ^{92}Sr ground state.

Explanation of this allowed beta decay as a $p_{1/2}$ neutron decaying into a $p_{3/2}$ proton, which was the alternative suggestion for the ^{92}Kr decay to the 1361 keV level in ^{92}Rb, is not as valid in this case since the $p_{3/2}$ single-particle subshell is "blocked" by being full. Of course, to the extent that Z = 38 does not close the $p_{3/2}$ subshell completely (that is, to the extent that there exists some probability for $p_{3/2}$ holes) then this $p_{1/2}$ to $p_{3/2}$ decay could occur. But only the $g_{7/2}$ to $g_{9/2}$ decay mechanism will be considered here for simplicity.

The ground state of ^{92}Y has been measured to have spin and parity 2^-, as mentioned earlier. The simplest explanation for this is to consider the configuration as $\pi(p_{1/2})\ \nu(d_{5/2})^3$. Besides the spin-parity of 2^-, this configuration also yields a level of spin and parity 3^- which should lie low in energy. A comparison with ^{90}Y is valuable at this point because it reveals a 2^- ground state and a 3^- level at 203 keV, both of which have been determined to result from the configuration $\pi(p_{1/2})\ \nu(d_{5/2})(92)$. This is good evidence for considering the 241 keV level in ^{92}Y to be the 3^- level arising from the configuration $\pi(p_{1/2})\ \nu(d_{5/2})^3$. This spin and parity also fits in well with the absence of beta feeding from the ^{92}Sr 0^+ ground state.

Further comparison with ^{90}Y does not produce any further information. Instead, log ft's and transition intensities can be used to determine the following:

892 keV level: Assuming first-forbidden beta decay, this level must have spin and parity 0^-, 1^-, or 2^-. The gamma depopulation branching intensities rule out the 0^-.

953 keV level: Assuming first-forbidden beta decay, this level has spin and parity 0^-, 1^-, or 2^-.

These two levels can be explained by postulating the following configurations: $\pi((p_{3/2})^{-1}(p_{1/2})^2)\ \nu(d_{5/2})^3$ which should have spin-parity 1^- for the lowest level by the coupling rules of Brennan and Bernstein (55), and $\pi((f_{5/2})^{-1}(p_{1/2})^2)\ \nu(d_{5/2})^3$ (which should lie slightly higher since the $p_{3/2}$ appears slightly above the $f_{5/2}$ near A = 90) which should have spin-parity 0^- for its lowest level.

With these choices for spins and parities, the relative photon transition probabilities are all well-satisfied except for the 1142 keV transition from the 1383 keV 1^+ state to the 241 keV 3^- state. This is expected to be an M2 (or E3) transition but, if so, it is much too strong in relation to the other E1 transitions depopulating the 1383. Since the 1383 keV 1^+ state and the ground state 2^- assignments are well-determined, and the 241 keV 3^- spin-parity is well-indicated, this depopulation remains the biggest problem in this level scheme. Further information such as an internal conversion measurement is needed here.

D. Future Work

Some difficulties and specific areas for improvement have been pointed out throughout the Conclusions. This subsection will cover future work which could be done in general.

Detection equipment available and sample production by TRISTAN have continued to improve since most of these measurements were made. The better Ge(Li) detector efficiencies and greater sample activities now available would be useful mainly for coincidence studies (particularly for the ^{92}Rb decay). There is probably not a great deal of value in using higher counting rates to continue to probe for weaker gamma transitions not seen in this work. The physical understandings presented here come mainly from the placement of the stronger gamma rays.

If sample production and chemical separation improve to the point where it becomes possible to study the decay of ^{92}Br, this would be helpful to extend the mass 92 chain knowledge one step further from the valley of beta stability.

The greatest experimental opportunity probably lies in the area of beta measurements. For example, shape measurements could distinguish between different types of beta decay. Moving Tape Collector studies with a plastic scintillator (for beta spectra) are now being made, with silicon detector studies (for conversion electrons) planned for the near future. Beta-gamma coincidence measurements have begun and should help to unravel the decays studied here. Such beta-gamma work would give experimental Q values for the beta decays, for example. The beta-ray spectrometer should

soon be used for studying neutron-enriched nuclei and will be useful in examining beta spectra shapes. Any internal conversion coefficients which could be measured would be helpful. Finally, it is desirable to measure directly ground state beta transition intensities to replace the indrect measurements reported here for the ^{92}Kr and ^{92}Rb decays. (For example, the 50% beta feed to the ^{92}Rb ground state is hard to understand.) The Heath measurement for beta decay to the 1384 keV level of ^{92}Y should be checked to see if it is in fact 90 $\pm$ 10%.

Information on multipolarities of observed gamma transitions could be obtained from gamma-gamma angular correlation studies which will be possible on-line in the future with TRISTAN. Level lifetime information would be useful in the same manner. Knowledge of the electromagnetic character of those transitions in mass 92 decays which can be studied would help to determine further spins and parities of levels.

In short, except for possibly some more coincidence work on the ^{92}Rb decay, the purely gamma-spectroscopic work on the levels of ^{92}Rb, ^{92}Sr, and ^{92}Y is as complete as is necessary. Other measurement techniques must supply the further characteristics needed to allow a more detailed comparison of the various physical models which might explain the properties of these nuclei and perhaps eventually yield information which can be used to deduce properties of the nuclear force.

VII. LITERATURE CITED

1. Kofoed-Hansen, O. and Nielsen, K. O. Measurements on shortlived radioactive krypton isotopes from fission after isotopic separation. Kgl. Danske Videnskab. Selskab, Mat.-Fys. Medd. 26, No. 7. 1951.

2. Borg, S., Fägerquist, U., Holm, G., and Kropff, F. Experiences of on-line isotope separation of short-lived isotopes. Nucl. Instr. Methods 38: 296. 1965.

3. Holm, G., Borg., S., Fägerquist, U., and Kropff, F. Isotope separator on-line studies of gaseous fission products. Arkiv Fysik 36: 91. 1967.

4. Talbert, W. L., Jr. Experimental techniques using ISOL systems. Int. Conf. on Properties of Nuclei far from the Region of Beta-Stability Proc. 1: 109. 1970.

5. Weizsäcker, C. F. Zur Theorie der Kernmassen. Z. Physik 96: 431. 1935.

6. Mayer, M. G. On closed shells in nuclei. II. Phys. Rev. 75: 1969. 1949.

7. Haxel, O., Jensen, J. H. D., and Suess, H. E. On the "magic numbers" in nuclear structure. Phys. Rev. 75: 1766. 1949.

8. Bohr, A. The coupling of nuclear surface oscillations to the motion of individual nucleons. Kgl. Danske Videnskab. Selskab, Mat.-Fys. Medd. 26, No. 14. 1952.

9. Bohr, A. and Mottelson, B. Collective and individual-particle aspects of nuclear structure. Kgl. Danske Videnskab. Selskab, Mat.-Fys. Medd. 27, No. 16. 1953.

10. Johansson, S. A. E. Gamma de-excitation of fission fragments. Nucl. Phys. 64: 147. 1965.

11. Maienschein, F. C., Peelle, R. W., Zobel, W., and Love, T. A. Paper P/670. United Nations Int. Conf. on Peaceful Uses of Atomic Energy Proc. 15: 366. 1958.

12. Mottelson, B. R. and Nilsson, S. G. The intrinsic states of odd-A nuclei having ellipsoidal equilibrium shape. Kgl. Danske Videnskab. Selskab, Mat. Fys. Skr. 1, No. 8. 1959.

13. Arseniev, D. A., Sobiczewski, A., and Soloviev, V. G. Equilibrium deformations of neutron-rich nuclei in the A ≈ 100 region. Nucl. Phys. A139: 269. 1969.

14. Ragnarsson, I. "Extrapolations" to the Z = 40 - 60 region of elements. Int. Conf. on Properties of Nuclei far from the Region of Beta-Stability Proc. 2: 847. 1970.

15. Cheifetz, E., Jared, R. C., Thompson, S. G., and Wilhelmy, J. B. Excited state in even-even fission products. Int. Conf. on Properties of Nuclei far from the Region of Beta-Stability Proc. 2: 883. 1970.

16. Lustman, B. Irradiation effects in uranium dioxide. In Belle, J., ed. Uranium dioxide: properties and nuclear applications. p. 431. Washington, D. C., U.S. Govt. Print. Off. 1961.

17. Wahl, A. C. Private communication to W. L. Talbert, Jr. 1969.

18. Hahn, O. and Strassmann, F. Über den Nachweis und das Verhalten der bei der Bestrahlung des Urans mittels Neutronen entstehenden Erdalkalimettale. Naturwiss. 27: 11. 1939.

19. Hahn, O. and Strassmann, F. Nachweis der Entstehen aktiver Nachweis weiterer aktiver Bruchstücke bei der Uranspaltung. Naturwiss. 27: 89. 1939.

20. Hahn, O. and Strassmann, F. Getrennte Abscheidung der bei der Uranspaltung entstehenden Krypton- und Xenon-Isotope. Naturwiss. 29: 455. 1940.

21. Götte, H. Neue bei der Uranspaltung auftretende Strontium- und Yttrium-Isotope. Naturwiss. 29: 496. 1941.

22. Herrmann, G. and Strassmann, F. Über einige Strontium- und Yttrium-Isotope bei der Uranspaltung. Z. Naturforsch. 11a: 946. 1956.

23. Heath, R. L. Decay of 2.7 hr ^{92}Sr. Phys. Rev. 105: 1011. 1957.

24. Clifford, J. R. Private communication. 1971.

25. Carlson, G. C., Schick, W. C., Jr., Talbert, W. L., Jr., and Wohn, F. K. Half-lives of some short-lived mass-separated gaseous fission products and their daughters. Nucl. Phys. A125: 267. 1969.

26. Talbert, W. L., Jr., Wohn, F. K., Hsu, H. H., and Hsue, S. T. Gamma-ray studies of the decay of mass-separated ^{92}Y. Nucl. Phys. A146: 149. 1970.

27. Talbert, W. L., Jr. and McConnell, J. R. Preparation for on-line studies of short-lived nuclei produced by a reactor. Arkiv Fysik 36: 99. 1967.

28. Alväger, T. and Uhler, J. Electromagnetic isotope separators for laboratory purposes. In Farley, F. J. M., ed. Progress in Nuclear Techniques and Instrumentation. Vol. 3. p. 159. New York, John Wiley & Sons, Inc. 1968.

29. Kozhina, I. I., Shiryaeva, L. V., and Tolmachev, Yu. M. Thermal decomposition of uranium oxides in a vacuum. Ser. Fiz. Khim. 22: 133. 1967.

30. Booth, A. H. and Rymer, G. T. Determination of the diffusion constant of fission xenon in UO_2 crystals and sintered compacts. Atomic Energy of Canada Limited Report AECL-692 (Chalk River, Ontario) 1968.

31. Linder, R. and Matzke, H. J. Diffusion of radioactive noble gases in uranium oxides and uranium monocarbide. Z. Naturforsch. 14A: 1074. 1959.

32. Amiel, S. Modern rapid radiochemical separations. In Yaffe, L., ed. Nuclear Chemistry. Vol. 2. p. 241. New York, Academic Press. 1968.

33. Hahn, O. The emanation method. J. Chem. Soc. Suppl. No. 2: S259. 1949.

34. Wahl, A. C., Ferguson, R. L., Nethway, D. R., Troutner, D. E., and Wolfsberg, Z. K. Nuclear-charge distribution in low-energy fission. Phys. Rev. 126: 1112. 1962.

35. Brown, F. Electromagnetic separator and associated techniques. In Yaffe, L., ed. Nuclear Chemistry. Vol. 2. p. 295. New York, Academic Press. 1968.

36. Uhler, J. Investigation of contamination properties with emphasis on broad range isotope collection in an electromagnetic separator of the 90° sector type. Arkiv Fysik 24: 329. 1963.

37. Knight, J. D., Johnson, O. E., Tucker, A. B., and Solecki, J. E. The levels of ^{91}Y from the decay of ^{91}Sr. Nucl. Phys. A130: 433. 1969.

38. Norman, J. H., Talbert, W. L., and Roberts, D. M. Optimizing activity separation in fission product decay chains. U.S. Atomic Energy Commission Report IS-1893 (Iowa State Univ., Ames) 1968.

39. Sidenius, G., Gammon, R. M., Naumann, R. A., and Thomas, T. D. On-line separation of short-lived products from ^{252}Cf spontaneous fission. Nucl. Instr. Methods 38: 299. 1965.

40. Goulding, F. S. Semiconductor detectors for nuclear spectrometry, I. Nucl. Instr. Methods 43: 1. 1966.

41. Tavendale, A. J. Semiconductor nuclear radiation detectors. Ann. Rev. Nucl. Sci. 17: 73. 1967.

42. Büker, H. High-resolution gamma-spectroscopy with lithium-drifted germanium detectors, Part 1. Kerntechnik 10: 687. 1968.

43. Büker, H. High-resolution gamma-spectroscopy with lithium-drifted germanium detectors, Part 2. Kerntechnik 11: 39. 1969.

44. Mariscotti, M. A. A method for automatic identification of peaks in the presence of background and its application to spectrum analysis. Nucl. Instr. Methods 50: 309. 1967.

45. Lietzke, M. H. A generalized least squares program for the IBM 7090 computer. U.S. Atomic Energy Commission Report ORNL-3259 (Oak Ridge National Lab., Tennessee) 1962.

46. Morrison, D. Computers applied to nuclear chemistry. In Yaffe, L., ed. Nuclear Chemistry. Vol. 2. p. 335. New York, Academic Press. 1968.

47. Grodstein, G. W. X-ray attenuation coefficients from 10 keV to 100 MeV. National Bureau of Standards Circular 583. 1957.

48. McGinnies, R. T. X-ray attenuation coefficients from 10 keV to 100 MeV. National Bureau of Standards Supplement to Circular 583. 1959.

49. Nielsen, K. B. and Duke, C. L. Private communication. 1969.

50. Seeger, P. A. and Perisho, R. C. Model-based mass law and a table of binding energies. U.S. Atomic Energy Commission Report LA-3751 (Los Alamos Scientific Lab., New Mexico) 1967.

51. Garvey, G. T., Gerace, W. J., Jaffe, R. L., Talmi, I., and Kelson, I. Set of nuclear-mass relations and a resultant mass table. Rev. Mod. Phys. 41: S1. 1969.

52. Bunker, M. E., Dropesky, B. J., Knight, J. D., and Starner, J. W. Decay of Y^{92} and Nb^{92}. Phys. Rev. 127: 844. 1962.

53. Scharff-Goldhaber, G. and Weneser, J. System of even-even nuclei. Phys. Rev. 98: 212. 1955.

54. Lycklama, H. and Kennett, T. J. Level structure of ^{88}Rb. Can. J. Phys. 48: 753. 1970.

55. Brennan, M. H. and Bernstein, A. M. jj coupling model in odd-odd nuclei. Phys. Rev. 120: 927. 1960.

56. Freed, N. and Rhodes, W. Particle-hole and particle-particle interactions in the mass-90 region. Phys. Letters 31B: 45. 1970.

57. Mason, J. F. and Johns, M. W. Decay of ^{90}Kr and ^{90}Rb. Can. J. Phys. 48: 2056. 1970.

58. Gove, N. B. Beta and gamma transition probabilities. In Gove, N. B. and Robinson, R. L., eds. Nuclear spin-parity assignments. p. 83. New York, Academic Press. 1966.

59. Malmskog, S. and McDonald, J. Private communication to W. L. Talbert, Jr. 1970.

60. Bayman, B. F., Reiner, A. S., and Sheline, R. K. Levels in Zr^{90}: theoretical. Phys. Rev. 115: 1627. 1959.

61. Bjørnholm, S., Nielsen, O. B., and Sheline, R. K. Levels in Zr^{90}: experimental. Phys. Rev. 115: 1613. 1959.

62. Ford, K. W. Predicted 0^+ level in $_{40}Zr^{90}$. Phys. Rev. 98: 1516. 1955.

63. Preston, R. L., Martin, H. J., Jr., and Sampson, M. B. Energy levels in Zr^{91} excited by the (d,p) reaction. Phys. Rev. 121: 1741. 1961.

64. Cohen, B. L. Nuclear structure studies in the zirconium region with stripping reactions. Phys. Rev. 125: 1358. 1962.

65. Cohen, B. L. and Price, R. E. Studies of low-lying levels of even-even nuclei with (d,p) and (d,t) reactions. Phys. Rev. 118: 1582. 1960.

66. Fiedler, H. J., and Kennett, T.J. Gamma-ray transitions associated with the decay of ^{94}Y and ^{95}Y. J. Inorg. Nucl. Chem. 28: 1129. 1966.

67. Ball, J. B., Auble, R. L., and Roos, P. G. Study of the zirconium isotopes with the (p,t) reaction. Phys. Rev. C4: 196. 1971.

68. Talmi, I. and Unna, I. Theoretical interpretation of energy levels in light nuclei. Ann. Rev. Nucl. Sci. 10: 353. 1960.

69. Talmi, I. Neutron $d_{5/2}^{n}$ configurations in Zr isotopes. Phys. Rev. 126: 2116. 1962.

70. Arad, B., Boulter, J., Prestwich, W. V., and Fritze, K. Level scheme of ^{93}Zr. Nucl. Phys. A131: 137. 1969.

71. Dickens, J. K., Eichler, E., and Satchler, G. R. ^{90,92,94}Zr(p,p') reactions at 12.7 MeV. Phys. Rev. 168: 1355. 1968.

72. Malmskog, S. G. and McDonald, J. The 93.54 keV level in ^{91}Sr. Nucl. Phys. A142: 263. 1970.

73. Mason, J. F. and Johns, M. W. Level structures of ^{91}Rb and ^{91}Sr as populated in beta decay. Can. J. Phys. 48: 2895. 1970.

74. Hardy, J.C., Davies, W. G., and Darcey, W. ^{91}Y and the failure of the closed shell at ^{88}Sr. Nucl. Phys. A121: 103. 1968.

75. Nolte, E., Kutschera, W., Shida, Y., and Morinaga, H. On- and off-beam gamma spectroscopy on neutron deficient isotopes of Ge, Se, Br and Kr. Int. Conf. on Properties of Nuclei far from the Region of Beta-Stability Proc. 2: 911. 1970.

76. Horsh, F. Prompt gamma transitions in primary fragments from neutron-induced fission. Int. Conf. on Properties of Nuclei far from the Region of Beta-Stability Proc. 2: 917. 1970.

77. Auble, R. L. Nuclear data sheets for A = 84. Nuclear Data Sheets B5: 109. 1971.

78. Auble, R. L. Nuclear data sheets for A = 86. Nuclear Data Sheets B5: 151. 1971.

79. Bunting, R. L. Private communication. 1971.

80. Ball, J. B., Auble, R. L., and Drisko, R. M. Level structure of ^{88}Zr studied with the ^{90}Zr(p,t) reaction. Phys. Rev. 177: 1699. 1969.

81. Lieb, K. P., Kent, J. J., and Moore, C. F. Isobaric-analog study of ^{90}Zr. Phys. Rev. 175: 1482. 1968.

82. Flynn, E. R., Armstrong, D. D., and Beery, J. G. Inelastic triton scattering from $^{92,94,96}Zr$. Phys. Rev. C1: 703. 1970.

83. Blair, A. G., Beery, J. G., and Flynn, E. R. Nuclear states of ^{98}Zr. Phys. Rev. Letters 22: 470. 1969.

84. Jaklevic, J. M., Lederer, C. M., and Hollander, J. M. A study of levels in ^{92}Mo and ^{94}Ru by in-beam gamma-ray spectroscopy. Phys. Letters 29B: 179. 1969.

85. Aras, N. K., Eichler, E., and Chilosi, G. G. Decay of ^{94}Tc isomers into the levels of ^{94}Mo. Nucl. Phys. A112: 609. 1968.

86. Antman, S., Grunditz, Y., Johansson, A., Nyman, B., Pettersson, H., and Svahn, B. Internal conversion studies of transitions in ^{96}Mo. Z. Physik 233: 275. 1970.

87. Hübenthal, K., Monnand, E., and Moussa, A. Excited states of ^{98}Mo in the radioactive decay of ^{98}Nb isomers. Nucl. Phys. A128: 577. 1969.

88. Eidens, J., Roeckl, E., and Armbruster, P. On-line separation and identification of several short-lived fission products: decay of ^{84}Se, ^{91}Kr, ^{97}Y, ^{99}Nb, ^{99}Zr, $^{100,101}Nb$ and ^{101}Zr. Nucl. Phys. A141: 289. 1970.

89. Moszkowski, S. A. Theory of multipole radiation. In Siegbahn, K., ed. Alpha-, beta-, and gamma-ray spectroscopy. Vol. 2. p. 863.. Amsterdam, North Holland Publishing Co. 1965.

90. Sliv, L. A. and Band, I. M. Tables of internal conversion coefficients. In Siegbahn, K., ed. Alpha-, beta-, and gamma-ray spectroscopy. Vol. 2. p. 1639. Amsterdam, North Holland Publishing Co. 1965.

91. Ball, J. B. and Fulmer, C. B. Neutron hole states in Z = 40 nuclei studied with the (p,d) reaction on ^{90}Zr, ^{91}Zr, and ^{92}Zr. Phys. Rev. 172: 1199. 1968.

92. Yamaya, T., Nakagome, Y., Hiratate, Y., Lee, S. M., Iwasaki, S., Tohei, T., and Morita, S. Coulomb stripping in the reaction $^{89}Y(d,p)^{90}Y$ at 4 MeV bombarding energy. Nucl. Phys. A126: 449. 1969.

VIII. ACKNOWLEDGMENTS

The author wishes to express his sincere thanks to the following people for their invaluable assistance in the completion of this project:

Dr. Willard L. Talbert, Jr., who, as major professor, suggested the topic for this investigation and skillfully continued to provide encouragement and guidance until its completion. He is responsible for developing the TRISTAN system which enabled these measurements to be made and for setting my feet back on the right path at times as I attempted to relate my results to physical pictures. I am boundlessly grateful to him for his counseling and assistance throughout this work.

John McConnell, who also has labored long and hard to bring TRISTAN into being and to keep it in operation. A special note of thanks is due him for patiently introducing me to the details of construction and principles of operation of the TRISTAN system and for instructing me in beam tuning methods.

Drs. B. S. Cooper, W. C. Schick, Jr., and F. K. Wohn for many fruitful discussions concerning interpretation of my data.

Ken Malaby, who performed the necessary chemical separations.

Jay Norman, who developed the ISOBAR routine.

Harold Skank for his help in repairing electronics.

Roger Bunting and Eugene Henry for computational help.

In addition to these and others whose help was directly related to this work, I would like to thank:

Dr. Daniel Zaffarano, who served as occasional major professor during

my graduate career and provided stimulation and encouragement in great supply.

The National Science Foundation, for providing financial support for part of my graduate training.

My parents, Mr. and Mrs. Ernest Olson, for their encouragement and assistance throughout my entire education.

Finally, I would like to dedicate this thesis to my wife, Susan, for providing me with an environment conducive to the successful completion of this work. Her many sacrifices, endless patience, and constant encouragement have been appreciated much more than my words can ever express.